

# The Unusual Properties of Nanobubbles

*A Thesis Submitted*

*in Partial Fulfilment of the Requirements*

*for the Degree of*

## DOCTOR OF PHILOSOPHY

*by*

**Kalyani Agarwal**

**(2017CHZ0003)**



DEPARTMENT OF CHEMICAL ENGINEERING  
INDIAN INSTITUTE OF TECHNOLOGY ROPAR

June 2023

Kalyani Agarwal: *The Unusual Properties of Nanobubbles*  
Copyright ©2023, Indian Institute of Technology Ropar  
All Rights Reserved

*This thesis is dedicated to*

*Almighty who gave me knowledge, wisdom, and perseverance and showed path  
during my doctoral research and indeed, throughout my life.*

## Declaration of Originality

I hereby declare that the work which is being presented in the thesis entitled **The Unusual Properties of Nanobubbles** has been solely authored by me. It presents the result of my own independent investigation/research conducted during the time period from January 2018 of joining the Ph.D. program to February 2023 of Ph.D. thesis submission under the supervision of **Dr. Neelkanth Nirmalkar**, Assistant Professor in the Department of Chemical Engineering, IIT Ropar, India. To the best of my knowledge, it is an original work, both in terms of research content and narrative, and has not been submitted or accepted elsewhere, in part or in full, for the award of any degree, diploma, fellowship, associateship, or similar title of any university or institution. Further, due credit has been attributed to the relevant state-of-the-art and collaborations (if any) with appropriate citations and acknowledgments, in line with established ethical norms and practices. I also declare that any idea/data/fact/source stated in my thesis has not been fabricated/falsified/ misrepresented. All the principles of academic honesty and integrity have been followed. I fully understand that if the thesis is found to be unoriginal, fabricated, or plagiarized, the Institute reserves the right to withdraw the thesis from its archive and revoke the associated Degree conferred. Additionally, the Institute also reserves the right to appraise all concerned sections of society of the matter for their information and necessary action (if any). If accepted, I hereby consent for my thesis to be available online in the Institute's Open Access repository, inter-library loan, and the title & abstract to be made available to outside organizations.



Name: Kalyani Agarwal

Entry Number: 2017CHZ0003

Program: Ph.D.

Department: Chemical Engineering

Indian Institute of Technology Ropar

Rupnagar, Punjab 140001

Date: 22.02.2023



---

## Acknowledgement

It transcends all the written word barriers to owe a deep sense of gratitude and express my profound indebtedness to my supervisor **Dr. Neelkanth Nirmalkar** for his support and guidance throughout my dissertation work. Without his timely monitoring of the progress of research work, efforts to arrange comprehensive research facilities, and constructive criticism, it would have been impossible to shape this thesis in its present form. He played multiple roles, from being a guide to a mentor to a senior who was always there whenever I was stuck with work and at times of failure. His diligence and perseverance are the backbone for turning this work into a reality. Thank you for helping to guide me through the many pitfalls of research, towards a project I really enjoyed digging into.

A deep sense of gratitude is to acknowledge the support of the Doctoral Committee members, **Dr. Tarak Mondal**, **Dr. Chandi Sasmal** and chairperson **Dr. Vishwajeet Mehandia** and former chairperson **Prof Raj P. Chhabra**, Department of Chemical Engineering, IIT Ropar, and, **Dr. Lipika Kabiraj**, Department of Mechanical Engineering, IIT Ropar. Their inspiring suggestions greatly helped to improvise this dissertation. I would like to extend my acknowledgment to all the faculty members in the Department of Chemical Engineering, IIT Ropar.

I am thankful to the **Indian Institute of Technology Ropar** for providing the necessary infrastructure and financial support. My sincere thanks to the **Ministry of Education**, Government of India, for providing a scholarship to conduct this research work. A deep sense of gratitude is acknowledged to **Prof. S. K. Das**, former Director, and **Prof. Rajeev Ahuja**, Director, IIT Ropar, for providing access to different academic and non-academic facilities, equipment for experimentation, and making life healthy and enjoyable in the IIT Ropar campus.

I sincerely thank **Dr. Rajneesh Kumar Prajapati**, Center for Nanosciences & Advanced Imaging Center, Indian Institute of Technology Kanpur for allowing me to use the Cryo -TEM facility.

I greatly appreciate all the various funding sources that helped me to carry-out this research work. The funding sources include the **DST Inspire scheme** (DST/INSPIRE/04/2016/001163) under the Department of Science & Technology (DST), and **TIF-AWaDH** (Technology Innovation Hub-Agriculture and Water Technology Development Hub), DST, IIT Ropar, India.

I appreciate the support provided by **Ms. Sunpreet Kaur** and all the office personnel in the Department of Chemical Engineering.

I can't thank enough all my fellow, which were like a family away from my home, and who helped in all possible ways to get this work completed especially **Dr. Mohit Trivedi**, **Priya Koundle**, **Harsh Sharma**, **Nilanjan Dutta**,

**Aakriti Sharma, Gaurav Yadav, Alok Das, Shivi Garg, Saurabh Maurya, Avinash, G Nandkumar Goud, Md Jawed Alam, Pargat, Sumit and Arghya Roy.**

Also, I would like to sincerely thank all my friends for their constant support in this endeavor. They stood by me through thick and thin and helped me maintain normality. Thanks for sharing so many laughs that helped me keep a semblance of sanity.

A mere acknowledgment in a few sentences would definitely not suffice for the efforts and support given by my family members all through my life, especially in this undertaking. I dedicate this effort to the prayers and good wishes of my parents, elder brother, little **Ivaan** and **Tiya**, and all other family members who have made me what I am today in every possible way. They have inspired me and taught me to go for excellence in everything. Finally, I kneel in front of the almighty to give the wisdom and perseverance bestowed upon me during my doctoral research, and indeed, throughout my life.

Kalyani Agarwal

## Certificate

This is to certify that the thesis entitled **The Unusual Properties of Nanobubbles**, submitted by **Kalyani Agarwal (2017CHZ0003)** for the award of the degree of **Doctor of Philosophy** of Indian Institute of Technology Ropar, is a record of bonafide research work carried out under my guidance and supervision. To the best of my knowledge and belief, the work presented in this thesis is original and has not been submitted, either in part or full, for the award of any other degree, diploma, fellowship, associate, or similar title of any university or institution. In my opinion, the thesis has reached the standard of fulfilling the requirements of the regulations relating to the Degree.



Dr. Neelkanth Nirmalkar  
Department Chemical Engineering  
Indian Institute of Technology Ropar  
Rupnagar, Punjab 140001  
Date: 22.02.2023

## Lay Summary

Nanobubbles or ultrafine bubbles are invisible to the naked eye, with an average size typically in the range of 100 - 200 nanometres which is approximately 100 times smaller than a human hair. Ordinary bubbles (diameter  $> 1\mu\text{m}$ ) quickly rise to the liquid surface and collapse but these nanoscale bubbles are neutrally buoyant and survived for several weeks and even months. They act as an oxygen carrier sustaining the level of dissolved oxygen during wastewater treatment and promoting the growth of animals and plants which is inhibited by anaerobic bacteria. These tiny bubbles are distinct owing to their peculiar properties which have magnetized a wide spectrum of applications. The following objectives have been addressed during my Ph.D. work:

- The decrease in gas solubility in an aqueous salt solution is termed the “salting-out effect”. Does this parameter play an important role in nanobubble dynamics?
- To investigate the long-term stability of nanobubbles in the presence of strong surface charge.
- To differentiate between a bubble and a particle by estimating the refractive index.
- To unravel the effect of physicochemical properties on nanobubble formation during fluctuating pressure field.
- The presence of detergents and nanoscale particles governs how these nanoscale bubbles behave.
- To examine the role of these small bubbles causing a drop in surface tension in the presence of salt solution.

## Abstract

Nanobubbles are nanoscale bubble swarms with several peculiar properties that have been demonstrated to have a widespread application in the engineering and medical sectors. Surface nanobubbles are bubbles that are confined on a solid surface, whereas bulk nanobubbles are bubbles that are dispersed in the bulk liquid. Bulk nanobubbles have gained more attention in recent years owing to their long-term stability. Despite the several overwhelming applications, the fundamental research questions, for instance, driving force for nanobubble nucleation, interfacial properties in the presence of nanobubble, bubble dynamics under ultrasound and oscillating pressure field, differentiating nanobubbles and nanoparticles, etc. are still unanswered. The present work aims to fill the gap in the literature and thus delineates to understand the nanobubble nucleation during salting-out effect, nanobubble dynamics under oscillating pressure fields, the effect of nanobubbles on Ray-Jones effect, etc.

Based on the refractive index calculation, the excess dissolved gas does definitely nucleate in the form of nanobubbles during the salting-out process. As a result, we intend to present evidence of nanobubbles that were supported by the freezing and thawing process. Based on Mie theory calculations, a novel approach for estimating the refractive index of nanobubbles is presented. When the salt concentration increases, so does the differential in solubility, and bubble number density exhibits a positive correlation with the salt concentration .

The influence of an oscillating pressure field on nanobubble dynamics during salting-out effects has been extensively discussed. The refractive index calculation and the electrical conductivity confirmed the evidence for the gas-filled nanobubbles. The screening of the electric double layer decreases the surface potential of the nanobubbles depending on the valency of the salt. Therefore, the equilibrium size of nanobubbles was observed to be higher in the presence of salts. The mean diameter of nanobubbles exhibits the inverse dependence on the surface potential. Our experimental findings agree well with the theoretical prediction based on the mechanical stability model.

Altogether, this thesis presents a novel mechanical stability model for nanobubbles which has been constructed by considering the ion cloud pressure, and it is shown to be twice the electrostatic pressure. The present nanobubble stability model not only predicts the existence of stable nanobubbles but is also in line with the experimental results obtained in this work. We also aim to explore further the surface tension of the salt solution that exhibits minima in the low salt concentration regime, which is widely known as the Jones-Ray effect. The nanobubble may be one of the contributing factors to the Jones-Ray effects. The size of the nanobubbles in the low salt regime is smaller than that in the

high salt concentration regime, and therefore, the activity of the nanobubbles is expected more in the low salt concentration regime. In a further study, the coupling effect of nanobubbles and nanoparticles determines the refractive index and behavior of the suspension, concluding the existence of bulk nanobubbles.

**Keywords:** Nanobubbles; Refractive index; Zeta potential; Jones-Ray effect; Oscillating pressure field; Surfactants; Nanoparticle tracking analysis; Surfactant

---

## List of Publications

### Published Papers

1. **Agarwal, K.**, Trivedi, M., & Nirmalkar, N. (2022). Does salting-out effect nucleate nanobubbles in water: Spontaneous nucleation?. *Ultrasonics sonochemistry*, 82, 105860.
2. **Agarwal, K.**, Trivedi, M., Ohl, C. D., & Nirmalkar, N. (2023). On Nanobubble Dynamics under an Oscillating Pressure Field during Salting-out Effects and Its DLVO Potential. *Langmuir*, 39(15), 5250-5262.

### Publication under peer review process

1. **Agarwal, K.**, Trivedi, M., & Nirmalkar, N. (2023). Surface tension reduction by nanobubbles generated during salting-out effects and oscillating pressure fields. *International Journal of Multiphase Flow (IJMF-D-23-00274R1)*
2. **Agarwal, K.**, & Nirmalkar, N. (2023). On nanobubble dynamics during surfactant adsorption at the gas-liquid interface and its refractive index estimation. *Colloids and Surfaces A: Physicochemical and Engineering Aspects (COLSUA-D-23-02571)*

### Conference Proceeding

1. **Agarwal, K.**, Trivedi, M., & Nirmalkar, N. (2022). Bulk nanobubbles in aqueous salt solution. *Materials Today: Proceedings*, 57, 1789-1792.
2. **Agarwal, K.**, & Nirmalkar, N. (2022). Fundamentals and Theory of Nanobubbles. *Nanobubble production* 7, 30.
3. **Agarwal, K.**, Nirmalkar, N., & Kabiraj, L. (2022). Influence of nanobubbles on the surface tension and atomization characteristics of water. *Bulletin of the American Physical Society*.

### Patent

1. IN Patent Application No. 202111005491. Inventors: **Kalyani AGARWAL**, Neelkanth NIRMALKAR. Date of Filing: 9/02/2021. Title: Plate and Frame type unit for nanobubble generation.

# Contents

---

Declaration	iv
Acknowledgement	v
Certificate	vii
Lay Summary	viii
Abstract	ix
List of Publications	xi
List of Figures	xv
List of Tables	xviii
<b>1 Introduction</b>	<b>1</b>
1.1 What are nanobubbles? . . . . .	1
1.2 Surface nanobubbles . . . . .	1
1.3 Introduction to bulk nanobubbles . . . . .	3
1.3.1 Milestones of bulk nanobubbles . . . . .	3
1.3.2 Generation techniques . . . . .	3
1.3.3 Peculiar properties . . . . .	5
1.3.4 Characterization . . . . .	6
1.4 Applications . . . . .	8
1.4.1 Water treatment technologies . . . . .	9
1.4.2 Flotation technique . . . . .	9
1.4.3 Surface cleaning . . . . .	10
1.4.4 Agriculture . . . . .	10
1.4.5 Aquaculture . . . . .	10
1.4.6 Biomedical . . . . .	10
1.5 Research Objectives . . . . .	11
1.6 Organization of the Dissertation . . . . .	11
<b>2 Does Salting-out Effect Nucleate Nanobubbles in Water: Spontaneous Nucleation?</b>	<b>13</b>
2.1 Introduction . . . . .	13
2.2 Experimental methods . . . . .	17
2.2.1 Materials . . . . .	17



2.2.2	Preparation of nanobubble sample . . . . .	17
2.2.3	Refractive index estimation . . . . .	18
2.2.4	Sample preparation for Cryo-TEM imaging . . . . .	18
2.3	Results and discussion . . . . .	19
2.3.1	Physical perturbation of nanobubbles . . . . .	19
2.3.2	Refractive index of nanobubbles . . . . .	21
2.3.3	Influence of salt valency . . . . .	22
2.3.4	Temporal stability of nanobubbles in salt solution . . . . .	24
2.3.5	Nanobubbles in acidic and alkaline medium . . . . .	25
2.4	Conclusion . . . . .	26
<b>3</b>	<b>On Nanobubble Dynamics under an Oscillating Pressure Field during Salting-out Effects and its DLVO Potential</b>	<b>29</b>
3.1	Introduction . . . . .	29
3.2	Experimental methods . . . . .	32
3.2.1	Oscillating pressure field setup . . . . .	32
3.2.2	Ultrasound irradiation . . . . .	33
3.3	Results and Discussion . . . . .	33
3.3.1	Salting-out effects and oscillatory pressure fluctuation on nanobubble dynamics . . . . .	33
3.3.2	Light scattering and electrical conductivity of nanobubbles . . . . .	36
3.3.3	Nanobubble dynamics in the presence of charged ions . . . . .	38
3.3.4	Nanobubble charging by ultrasound waves . . . . .	40
3.3.5	Single nanobubble stability theory . . . . .	42
3.3.6	DLVO interaction potential of nanobubbles . . . . .	45
3.4	Conclusion . . . . .	47
<b>4</b>	<b>Does nanobubble contribute to Jones-Ray effects in aqueous salt solution?</b>	<b>49</b>
4.1	Introduction . . . . .	49
4.2	Experimental methods . . . . .	52
4.2.1	Materials . . . . .	52
4.2.2	Nanobubble characterization by particle tracking and dynamic light scattering method . . . . .	53
4.2.3	Surface tension measurement . . . . .	53
4.3	Results and discussion . . . . .	54
4.3.1	Evidence of nanobubbles . . . . .	54
4.3.2	Nanobubbles by salting-out effects . . . . .	55
4.3.3	Nanobubble temporal stability . . . . .	58
4.3.4	Role of nanobubbles in Jones-Ray effects . . . . .	59
4.4	Conclusions . . . . .	61

<b>5</b>	<b>Nanobubble Dynamics in the Presence of Surfactant Molecules and its Interaction with Nanoparticles</b>	<b>63</b>
5.1	Introduction . . . . .	63
5.2	Experimental methods . . . . .	65
5.2.1	Materials . . . . .	65
5.2.2	Generation of bulk nanobubbles . . . . .	66
5.2.3	Characterization of bulk nanobubble suspensions . . . . .	66
5.2.4	Refractive index determination . . . . .	67
5.3	Results and discussion . . . . .	68
5.3.1	Nanobubble dynamics in surfactant solutions . . . . .	68
5.3.2	Differentiating nanobubbles and nanoparticles in the presence of surfactant molecule . . . . .	71
5.3.3	Effect of ultrasound field on nanobubbles in surfactant solution	73
5.3.4	Surface tension in the presence of nanobubbles . . . . .	75
5.4	Conclusions . . . . .	76
<b>6</b>	<b>Conclusions, Implications, and Recommendations</b>	<b>78</b>
6.1	Conclusions . . . . .	78
6.2	Implications and Recommendations . . . . .	80
	<b>References</b>	<b>81</b>
<b>A</b>	<b>Appendix</b>	<b>106</b>
A.1	Zeta potential measurement by DLS . . . . .	106
A.2	Characterization of nanobubble sample by NTA . . . . .	106
A.3	Mie theory . . . . .	107
A.4	Steps to estimate refractive index . . . . .	108
	<b>Curriculum vitae</b>	<b>109</b>

## List of Figures

---

1.1	Schematic illustration of the formation of nanobubbles [1]. . . . .	2
1.2	Generation of nanobubbles using hydrodynamic cavitation [2]. . . . .	4
1.3	Working principle of nanoparticle tracking analysis (NTA) [3]. . . . .	6
1.4	Water treatment processes enhanced by nanobubble technology [4]. . . . .	8
1.5	Nanobubbles capacity for fouling prevention [5]. . . . .	9
2.1	Schematic illustration of the generation of nanobubble suspension. . . . .	15
2.2	(a) Cryo-TEM micrograph of nanobubbles in 1 mM of NaCl solution (b) 3D histogram of bubble count, size, and light scattering intensity in nanobubble sample of 1 mM NaCl. . . . .	16
2.3	Freezing and thawing experiments on nanobubble sample generated by dissolution of NaCl (a) bubble size distribution before freezing and after thawing (b) bubble number density before freezing and after thawing (c) NTA micrograph before freezing (d) NTA micrograph after thawing. . . . .	19
2.4	Effect of ultrasound amplitude on (a) zeta potential (b) bubble size distribution (c) mean bubble diameter of nanobubble sample generated by dissolution of NaCl. . . . .	20
2.5	(a) Representative scattering cross-section for nanobubbles in NaCl, CaCl <sub>2</sub> , Na <sub>2</sub> SO <sub>4</sub> , and AlCl <sub>3</sub> solution versus mean bubble diameter (b) Refractive index of nanobubble sample of 0.001 mM and 1 mM of NaCl. . . . .	21
2.6	Nanobubbles in NaCl solution of varying concentration (a) zeta potential (b) mean bubble diameter (c) bubble number density. The pure water is analyzed using NTA before adding the salt, and no nano-entities were observed. . . . .	22
2.7	Nanobubbles in Na <sub>2</sub> SO <sub>4</sub> solution of varying concentration (a) zeta potential (b) mean bubble diameter (c) bubble number density. . . . .	23
2.8	Nanobubbles in salt solution (1 mM) of different valency (a) zeta potential (b) mean bubble diameter (c) bubble number density. . . . .	25
2.9	Effect of a storage container on the long-term stability of nanobubbles generated in NaCl (a) bubble size distribution (b) bubble number density and mean bubble diameter. . . . .	26
2.10	Effect of pH on nanobubbles in NaCl solution (a) zeta potential (b) mean bubble diameter (c) bubble number density. . . . .	27
3.1	Schematic of the experimental setup and applied pressure wave. . . . .	32

3.2	Effect of cycle time on nanobubble generation by oscillating pressure method (a) bubble size distribution (1 mM NaCl) (b) mean diameter and zeta potential. . . . .	33
3.3	Cryo-TEM micrographs for nanobubble suspension generated in (a) 1 mM NaCl (b) 0 mM NaCl (c) nanobubble size distribution (1 mM NaCl) (d) nanobubble size distribution (0 mM NaCl). . . . .	35
3.4	(a) Numerical comparison of the scattered electric field ( $E$ ) and (b) comparison of the Scattering intensities of 100 nm mono-dispersed Polystyrene Latex beads and the NBs generated by Salting-out effect using $NaCl$ and $AlCl_3$ measured by $NTA$ . . . . .	36
3.5	Refractive index estimation (a) The variation of scattering cross-section with the size of polystyrene nanoparticle (b) Refractive index of different salt valency. . . . .	37
3.6	Nanobubbles dynamics in aqueous solutions of NaCl, $CaCl_2$ , and $AlCl_3$ of varying concentration (a) mean bubble diameter and (b) bubble number density. . . . .	38
3.7	The DLS measurement of the Zeta Potentials of NBs aqueous solutions of $NaCl$ , $CaCl_2$ , and $AlCl_3$ of varying salt concentration. .	39
3.8	Nanobubble dynamics in terms of (a) zeta potential (b) mean bubble diameter under the effect of ultrasound amplitude. . . . .	41
3.9	The nanobubble mechanical stability map comprising the contour value of $\phi$ obtained from the <b>Eq. 3.12</b> for various values of $\beta$ and $\xi$ and for a fixed $\alpha = 1$ . The values obtained using the experiment are shown with the solid lines, and the corresponding theoretical values of $\beta$ and $\xi$ are estimated from the relation <b>Eq. 3.13</b> . . . . .	42
3.10	DLVO interaction potentials of bulk nanobubbles generated in aqueous salt solution of varying concentration. . . . .	47
4.1	(a) Optical configuration of the NS-300. (b) The reference frame and variables used to determine the scattering intensity of a laser-illuminated spherical particle. . . . .	49
4.2	Light Scattering intensities of 100 nm mono-dispersed Polystyrene latex beads and NBs generated by the salting-out effect. . . . .	51
4.3	Nanobubbles during salting-out effects in NaCl solution (a) bubble size distribution (b) zeta potential. . . . .	53
4.4	Nanobubbles during salting-out effects in NaCl solution (a) bubble number density (b) mean bubble diameter. . . . .	54
4.5	Effect of oscillating pressure on nanobubble generation in $Na_2SO_4$ (a) bubble size distribution (b) zeta potential. . . . .	55

4.6	Mean bubble diameter of nanobubble suspension measured by DLS (a) mono- and trivalent salts (b) divalent salts. . . . .	56
4.7	Cryo-TEM micrograph for nanobubble suspension generated in (a) 0 mM NaCl (b) nanobubble size distribution (0 mM NaCl). . . . .	57
4.8	Effect of ultrasound amplitude on nanobubble solution in NaCl (a) bubble size distribution (b) bubble number density (c) mean bubble diameter. . . . .	57
4.9	Effect of ultrasound amplitude on nanobubble stability (a) mean bubble diameter (b) bubble number density. . . . .	58
4.10	Surface tension difference ( $\Delta\gamma$ ) measured with salt concentration for nanobubble suspension (a) salting-out effect in aqueous NaCl and nanobubbles generated by pressure fluctuation in aqueous (b) NaCl (c) $\text{AlCl}_3$ . . . . .	60
4.11	Surface tension difference ( $\Delta\gamma$ ) measured with salt concentration for nanobubbles generated by pressure fluctuation in aqueous (a) $\text{Na}_2\text{SO}_4$ (b) $\text{CaCl}_2$ . . . . .	61
5.1	Schematic diagram of the nanobubble generation in surfactant solution.	65
5.2	Effect of cationic surfactant (CTAB) on nanobubble generation (a) bubble size distribution (b) zeta potential (c) mean bubble diameter (d) bubble number density. . . . .	67
5.3	Bulk Nanobubbles evolution in anionic surfactant (SDS) (a) bubble size distribution (b) zeta potential (c) mean bubble diameter (d) bubble number density. . . . .	68
5.4	Bulk Nanobubbles evolution in non-ionic surfactant (Triton X-100) (a) bubble size distribution (b) zeta potential (c) mean bubble diameter (d) bubble number density. . . . .	69
5.5	Comparison of light scattering intensities of 100 nm aqueous silver nanoparticle dispersion and NBs suspension in (a) CTAB (b) SDS. .	70
5.6	Differentiating bulk nanobubbles and nanoparticles based on refractive index (a) Tween 20 (b) CTAB (c) Triton X-100 (d) SDS. .	71
5.7	Dynamics of bulk nanobubbles in 100 nm aqueous silver nanoparticle dispersion (a) bubble size distribution in CTAB (b) bubble size distribution in CTAB and nanoparticle (c) mean bubble diameter (d) bubble number density. . . . .	73
5.8	Effect of ultrasound amplitude on nanobubble suspension of Triton X-100 (2 cmc) (a) bubble size distribution (b) zeta potential (c) mean bubble diameter (d) bubble number density. . . . .	74
5.9	Surface tension measurements using the Wilhelmy plate method (a) CTAB (b) SDS (c) Tween 20 (d) Triton X-100. . . . .	75

## List of Tables

---

2.1	Salting out parameters of electrolytes for oxygen at 298.2 K . . . . .	24
3.1	Refractive index variation with ultrasound amplitude. . . . .	37
A.1	List of parameters for Mie Scattering . . . . .	108

# Chapter 1

## Introduction

---

### 1.1 What are nanobubbles?

Nanobubbles are gas-filled pockets in the liquid phase with diameters ranging from 50 to 200 nm. Simply described, these tiny bubbles are approximately 2,500 times smaller than a grain of salt. Their macro and micron-scale counterparts have sizes in the range from 100 to 2500  $\mu\text{m}$  [6]. Besides this, the term micro and nanobubble alludes to a fine bubble with a mean size of less than 100  $\mu\text{m}$  that appears milky in solution [7, 8]. It is perceived that nanoscale gas bubbles primarily consist of surface nanobubbles and bulk nanobubbles [9]. Surface nanobubbles (SNBs) [10] and bulk nanobubbles (BNBs) [11], as well as nano pancakes [12] and multilayer structures, are now categorized based on whether they are adhered to a surface or dispersed in the bulk liquid as shown in **Figure. 1.1**. Both the research background and the approaches employed to examine the two types of nanobubbles are rather distinct systems. Why do nanobubbles magnetize interest? There are primarily two grounds for this. First, they are prospective contenders in the study of micro and nanofluidics, explaining multiple phenomena associated with the liquid-solid interface, including the anomalous attraction of hydrophobic surfaces or the stability of colloidal systems [13, 14]. Second, and more significantly, according to the Epstein-Plesset hypothesis [15], nanobubbles should not exist; these bubbles have a radius of curvature lower than 1 $\mu\text{m}$  and should dissolve on a timeframe considerably below microseconds due to high laplace pressure inside the bubbles. In contrast, the investigations show that nanobubbles can remain stable for several hours or even days and months [16, 17, 18, 19]. Presently, science and technology involving nano-scale materials have emerged coupled with tremendous potential to deliver numerous benefits, giving substantial contributions in real-life applications including various sectors, such as food [20, 21], agricultural [22, 23], wastewater treatment [24, 25], and medicinal domains [26, 27, 28].

### 1.2 Surface nanobubbles

As per research findings on the interactions involving hydrophobic surfaces and aqueous solutions, spherical cap-shaped bubbles develop and adhere to the hydrophobic surface at the solid-liquid interface [29, 30]. These nanoscale bubbles are termed surface nanobubbles, which have drawn intensive attention. The studies roughly 20 years ago, were based on stepwise patterns in force curves

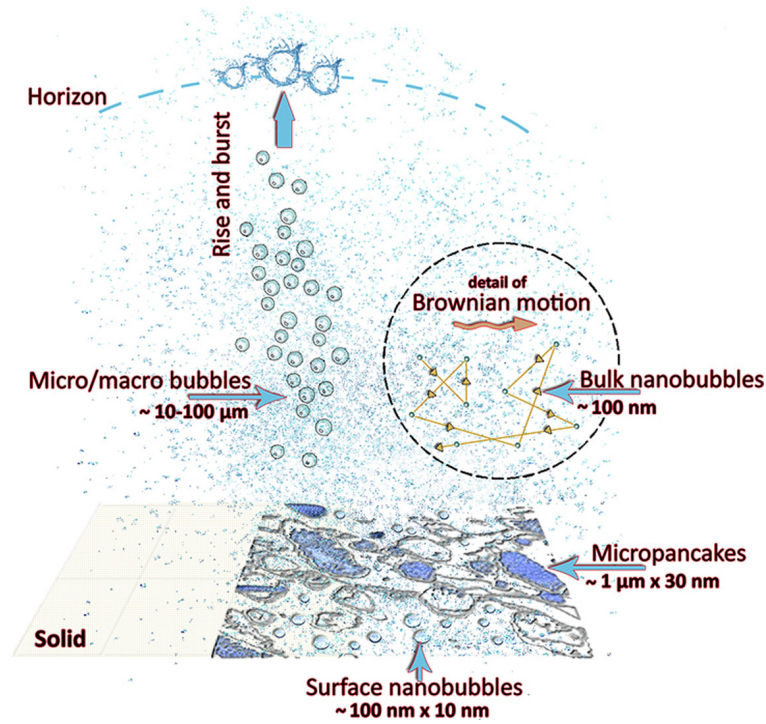


Figure 1.1: Schematic illustration of the formation of nanobubbles [1].

between two hydrophobic surfaces, and eventually resulted in the first atomic force microscopy (AFM) image [31, 32]. The pinning force was assumed to restrict the triple-phase contact line [33, 25], resulting in a difference in contact angles of surface bubbles at macro- and nanoscale [34]. Simultaneously, contact line pinning contributed to surface nanobubble stability by reducing inner pressure and preventing nanobubbles from dissolving into liquids [35]. The three-phase contact line is unpinned and modified when a surface nanobubble merges with another; as a result, the morphology and inner pressure of surface nanobubbles may vary, exposing some unique phenomena or significant information about the inherent features of nanobubbles. Although the majority of the research used AFM in tapping mode [36], nanobubbles were also analyzed using infrared spectroscopy [37, 38], neutron reflectometry [39, 40], quartz crystal microbalance [41, 42], and rapid shock-freeze cryofixation [43]. Among various methods for inducing surface nanobubbles summarized under investigations, the most commonly used protocol is the solvent exchange process [44]. In this method, alcohol that has been saturated (or even supersaturated) with air or a particular gas is replaced by water, a poor solvent. As a result, a local transient gas supersaturation is created. Supersaturation is caused by (a) the lower solubility of air in water than in the initial solvent, and (b) the drop in solubility caused by the temperature rise caused by the exothermic mixing of water and the first solvent [45, 37]. Surface nanobubbles could also be employed for fine particle separation via air bubble flotation [46], adsorption manipulation on hydrophobic surfaces [47], wall slip enhancement to achieve drag



reduction in microfluidic devices, and as soft nano templates for the production of hollow nanomaterials [48], among other proposed applications.

### 1.3 Introduction to bulk nanobubbles

Bulk nanobubbles are a unique nanoscale bubble system with unusual features that provide a challenge to our understanding of bubble behavior [49, 50]. The area of bulk nanobubbles is gaining more attention from a wide range of sectors. This is mirrored in the ISO standard (ISO/TC281) [51] for fine bubble technologies, which is working on standardization for bubbles with an average size of less than 100  $\mu\text{m}$ . This includes ultrafine bubbles of diameter less than 1  $\mu\text{m}$ . According to the Epstein-Plesset hypothesis, a bubble with a radius of 100 nm has an internal pressure that is 14.4 times that of the surrounding atmosphere and cannot persist for even less than 1  $\mu\text{s}$  [52, 53]. This tends to have dismissed the stable presence of nanoscale gas bubbles in liquids and allowed them to remain for hours, days, or even months, thus reducing their ability to agglomerate [17, 54, 55]. The expanding prominence of nanotechnology, as well as the unique characteristics of nanobubbles, has sparked intense interest in a diverse range of industries, including mining [56, 57], medicine [58, 59, 60], agriculture [61, 62], wastewater treatment [63, 64], and surface cleaning [5, 65].

#### 1.3.1 Milestones of bulk nanobubbles

Conceivably, the first direct evidence of bulk NBs (nanobubbles), with a mean diameter less than 1  $\mu\text{m}$  was reported by Johnson and Cooke in 1981 [66]. They stated that bubbles created by shear in seawater remained stable for a longer period ( $t > 22$  h) due to the formation of films on the bubble-water interface from naturally occurring surfactants. Merely just a few investigations on bulk NBs were reported until almost a decade later when Bunkin et al., discovered stable microbubbles in dilute electrolyte solutions [67]. Following the year 2000, a substantial number of papers focused on bubble creation and its features, as well as their extensive applications [68, 69, 70, 71, 72].

#### 1.3.2 Generation techniques

Acoustic cavitation, microfluidics, electrolysis, water solvent mixing, pressure-driven supersaturation, and the periodic pressure change approach have all been used to create bulk nanobubbles.

##### 1.3.2.1 Hydrodynamic cavitation

When supersaturated water with air is driven via a venturi, orifice, or needle valve, the flow velocity increases and the pressure drops below the liquid's vapor pressure.

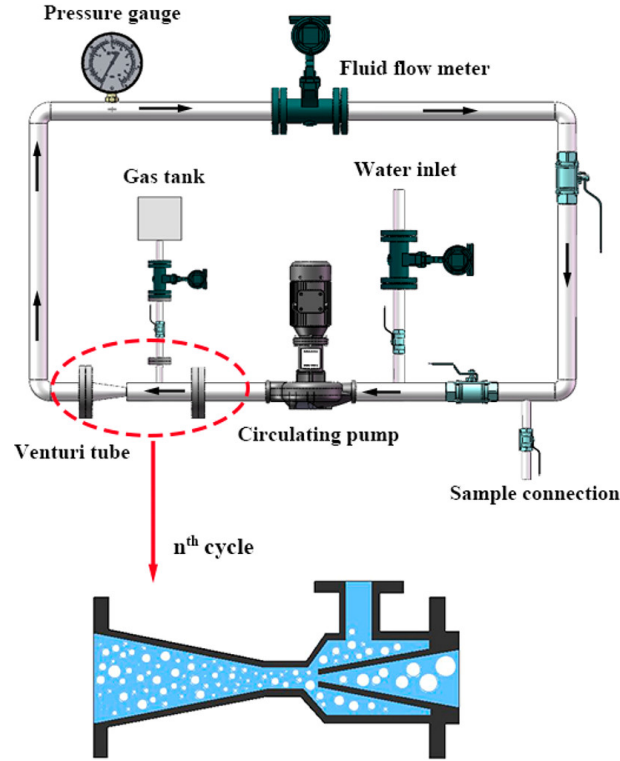


Figure 1.2: Generation of nanobubbles using hydrodynamic cavitation [2].

Besides, while gas mass transfers from the liquid to the gas phase, cavities (gas nuclei or nanobubbles) appear and evolve into microbubbles as shown in **Figure 1.2**. Thus according to Henry's Law, the amount of gas accessible for the formation mechanism of gas nuclei relies on the saturation pressure. Consequently, the formation of nanobubbles by hydrodynamic cavitation appears to be dependent on operating parameters including the minimum "energy"  $\Delta F$  required for bubble formation:

$$\Delta F = \frac{16\pi\gamma^3}{3(P_{sat} - P_0)^2} \quad (1.1)$$

where  $\gamma$  is the surface tension of the liquid,  $P_{sat}$  is the air-in-liquid saturation pressure, and  $P_0$  is the atmospheric pressure. As a result, a specific amount of energy must be transmitted to the liquid phase via a cavity phenomenon in order for bubbles to develop [73, 74, 75].

### 1.3.2.2 Acoustic cavitation

Acoustic cavitation [76, 77] may be induced by propagating ultrasonic radiation [71] through a liquid, causing pressure changes and the generation of bubbles. Ultrasonic waves can form gas bubbles via local compression-expansion cycles that aid to separate dissolved gases by substantially lowering the pressure below the value of saturated vapor pressure. Nirmalkar et al.[17] investigated the properties of

nanobubble suspension (i.e., ultrasound energy input, 20 kHz, and 750 W power of ultrasound probe). The bubble density rose dramatically as sonication time increased, indicating that the mean diameter of bulk nanobubbles produced by ultrasound varied from 10 to 600 nm.

### 1.3.2.3 Electrolysis

Chemical processes, such as electrolysis, can produce nanobubbles. During electrolysis, the breakdown of water into hydrogen and oxygen gases occurs as a result of the electric potential, and gas production happens at electrodes [78, 79, 80]. NBs can be formed if the concentration of the produced gas exceeds super-saturation in the anodic and cathodic streams of the bulk water. NBs having an average diameter of 100 nm, were stable for 24 hours, and successfully generated by the electrolysis method in the liquid supersaturated with O<sub>2</sub> and H<sub>2</sub> gases.

### 1.3.2.4 Porous membrane

The gas phase is forced through the pores of the applied membrane into a flowing aqueous phase by NBs as the medium for liquid and gas dispersion. The porous material might act as an array of orifices with varying diameters, releasing a cloud of nanobubbles of various sizes into the liquid phase [81, 82]. The forced flow of gas through a porous medium, such as a membrane, into a flowing aqueous/liquid, is an effective approach for the formation of bulk nanobubbles. Porous membranes, primarily ceramic, are already utilized in wastewater and sludge treatment operations as gaseous, bubble diffusers. surfactant. Monodispersed nanobubbles/microbubbles might be produced utilizing shirasu-porous-glass (SPG) membranes [83] with uniform pores in a system constituted of dispersed gaseous and continuous water phases containing a surfactant, according to Kukizaki and Goto.

## 1.3.3 Peculiar properties

Nanobubbles have unique characteristics owing to their size and structure, making them particularly efficient in improving water quality, enhancing water treatment operations, and increasing productivity in industrial and agricultural applications [84].

- Nanobubbles have a significant negative surface charge [85, 86] that keeps them stable in liquid and allows them to partake in and promote physical, biological, and chemical interactions continually.
- They are neutrally buoyant and can remain in liquid for weeks before rising to the liquid surface [87, 88].

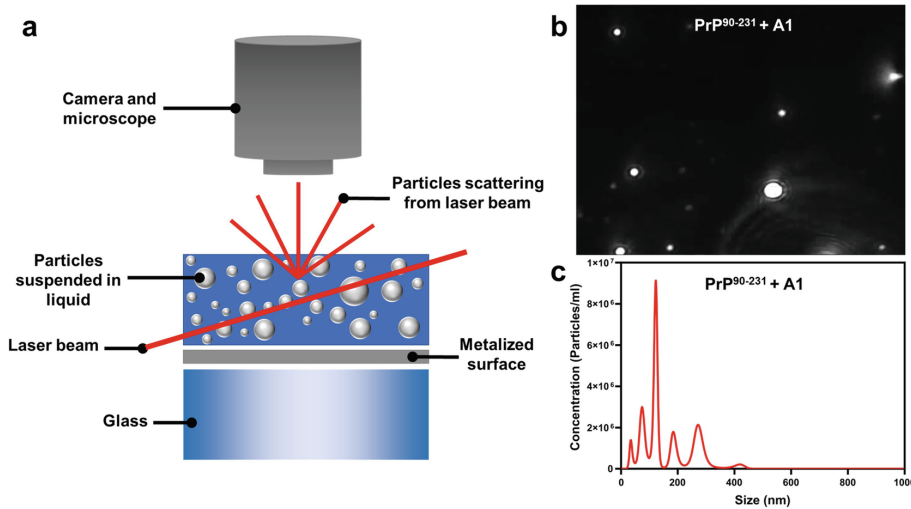


Figure 1.3: Working principle of nanoparticle tracking analysis (NTA) [3].

- Nanobubbles are unstable and disintegrate when agitated, producing the hydroxyl radical. The hydroxyl radical (HO) is one of the most powerful known oxidizers, and it is widely employed to eliminate difficult-to-treat and kill pollutants in water [89].
- Longer residence periods with superior stability against coalescence, greater specific surface areas, and better gas solubility in water are some of the notable features of NBs in bulk aqueous solution.

### 1.3.4 Characterization

Given the vast range of applications for NBs, it is critical to design a mechanism for demonstrating the presence of NBs as well as their size distribution in the applicable samples. At the moment, powerful tools such as nanoparticle tracking analysis (NTA), dynamic light scattering (DLS), atomic force microscope (AFM), transmission electron (TEM), and scanning electron microscopy (SEM) can be used to confirm the presence of gaseous nanoscale bubbles in bulk aqueous media as well as on boundaries between liquid and hydrophobic surfaces.

#### 1.3.4.1 Nanoparticle Tracking Analysis

It combines the use of both light scattering and Brownian motion to determine the nanoparticle size distribution of materials in liquid suspension as shown in **Figure 1.3**. The particle tracking equipment incorporates Brownian motion to characterize nano- and micron-size particles in liquid samples. The lighting of a laser beam reveals the particles in the sample [90, 91]. The scattered light of the particles is captured with a light-sensitive sCMOS camera, and the size of each individually monitored particle is determined, allowing the calculation of their size distribution and concentration to be done at the same time.

#### 1.3.4.2 Dynamic Light Scattering

When a laser is irradiated on the surface of a microscopic particle, it is not only absorbed and refracted but also dispersed, a phenomenon known as Rayleigh scattering. The intensity of Rayleigh scattering is related to the inverse of the fourth power of wavelength. To track the passage of the particles, the dispersed light is observed over a predetermined amount of time. Over time, the dispersed light intensity will change as smaller particles exhibit more oscillations than bigger particles. However, the amplitudes between the highest and minimum scattering intensities are increased for larger-sized particles. The second-order auto-correlation function of light intensity may be generated by making the adjustments. The radius of the observed particle may be calculated using the Einstein equation of Brownian motion in diffusion theory. Dynamic light scattering, on the other hand, necessitates that the particles in the system are spread evenly and at low concentrations, resulting in a test result [92, 93].

#### 1.3.4.3 Atomic Force Microscopy

Atomic force microscopy (AFM) is a promising surface examination method for micro/nanostructured coatings. This adaptable technology may be used to acquire high-resolution nanoscale pictures and investigate local areas in the presence of air (conventional AFM) or liquid (electrochemical AFM). It is done with a cantilever and a sharp tip of 10-20 nm in diameter. Si or Si<sub>3</sub>N<sub>4</sub> is used to microfabricate AFM tips and cantilevers.

The tip moves in response to tip-surface interactions, and this movement is monitored using a photodiode to concentrate a laser beam on the tip [94]. AFM may be used in two modes: contact and tapping. In the contact mode, the AFM tip is continually in touch with the surface, but in the tapping mode, the AFM cantilever is vibrated above the sample surface, allowing the tip to make intermittent contact with the surface. Imaging in the tapping mode helps to lessen shear pressures caused by tip movement. The tapping mode is the most frequent for imaging, whereas the contact mode is normally kept for specialist applications like force measurements [95, 96]. Furthermore, phase imaging can be performed in tapping mode with lower interaction forces and the AFM tip touches the end of the sample surface considering lateral friction forces to be negligible.

#### 1.3.4.4 Transmission Electron Microscopy

TEM is a very useful instrument for determining the form, size, and distribution pattern. Its examination employs a high-intensity electron beam passed through a very thin specimen layer on a copper grid, causing an interaction between the atoms of the specimen and the electron beam [97]. To be thin, a specimen must be

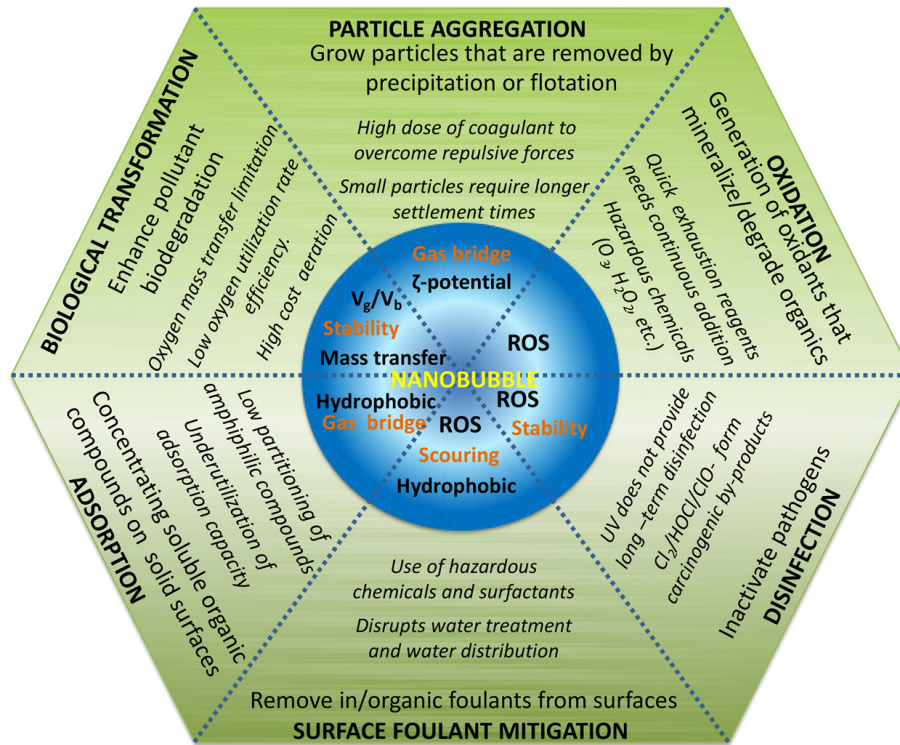


Figure 1.4: Water treatment processes enhanced by nanobubble technology [4].

electron transparent, which implies that enough electrons must be transferred such that the intensity falling on the screen of a cathode ray tube (CRT) or appropriate electron detector, such as a semiconductor detector, produces an interpretable image [98]. This however is determined by the electron energy as well as the specimen's average atomic number and thickness. For instance, biological specimens disappear within seconds in traditional TEM due to the high vacuum, whereas liquid cell TEM enables the study of processes that cannot be captured with conventional TEM or other methods. TEM provides a significantly better resolution ( $0.0001\ \mu\text{m}$ ), roughly one to two orders of magnitude higher than the SEM (Scanning electron microscope) [99].

## 1.4 Applications

NBs are used in a wide variety of applications across various sectors, and they may be used in the future. Nanobubbles serve as an essential component in wastewater treatment, surface cleaning, boosting animal and plant growth, and in biomedical as a nano medication loaded ultrasound contrast agent because of their extended residence duration and high specific surface area.

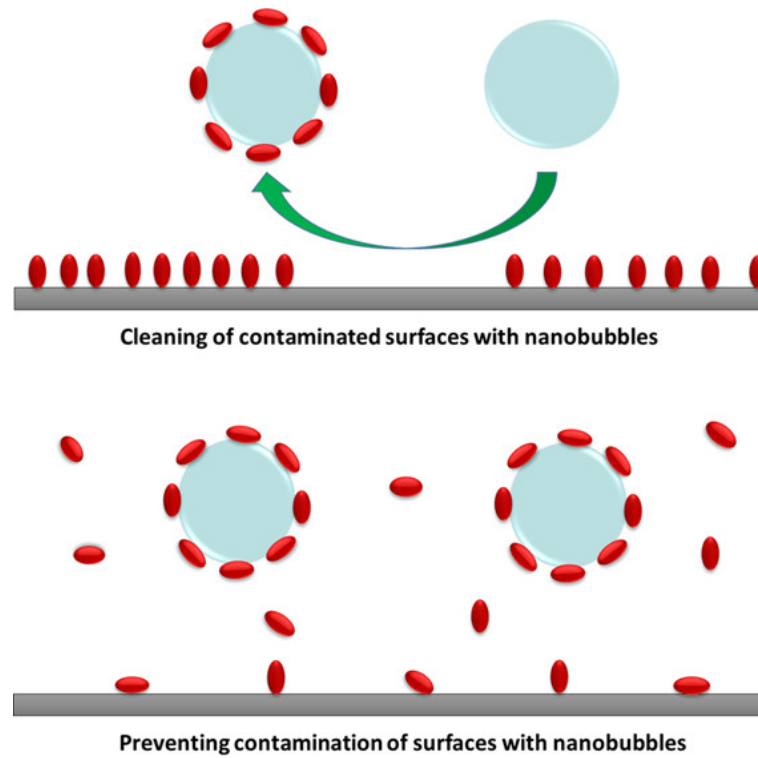


Figure 1.5: Nanobubbles capacity for fouling prevention [5].

#### 1.4.1 Water treatment technologies

NBs are crucial for improving the efficacy of drinking water and wastewater treatment (refer **Figure. 1.4**) because they act in the oxidation of persistent organic pollutants (POPs) (e.g. phenolic halogenated chemicals) and in the disinfection of pathogens. This technique provides a low-cost non-agent method that creates a variety of reactive oxygen species (ROSs), including hydroxyl radicals ( $\bullet\text{OH}$ ), superoxide anion radicals ( $\text{O}_2^-$ ), and singlet oxygen ( $^1\text{O}_2$ ), mostly during the NB collapse process [100, 101, 102, 103].

#### 1.4.2 Flotation technique

Flotation is a useful approach for separating minerals, phosphates, or coal from gangue. Flotation is also practiced in the recovery of recycled paper and the treatment of wastewater. The key mechanism that occurs in this technique is a decrease in the effective specific gravity of the oil droplets in Stokes' Law, which increases their rising velocity. This is accomplished by existing small gas bubbles attaching themselves to the oil droplets as they rise. The particle size and surface hydrophobicity of the treated materials are two major characteristics that influence three essential processes in the froth flotation process: particle-bubble collision, adhesion, and detachment [104, 105, 106].



### 1.4.3 Surface cleaning

Nanobubbles may clean formerly fouled hydrophilic surfaces as well as prevent fouling of both hydrophilic and hydrophobic surfaces as shown in **Figure. 1.5**. This ability for fouling avoidance is overcome when the contaminant concentration and the contamination's attraction to the surface rise [5, 107]. In situations where mechanical agitation is required for quick cleaning, detergents play the most essential function in increasing cleaning by preventing the redeposition of soil that has been mechanically removed from the surface [108].

### 1.4.4 Agriculture

Nanobubbles reduce the size of nutrient clusters while increasing ionic mobility, resulting in greater nutrient availability and absorption efficiency. Plants produced using nanobubble irrigation water are more resistant to stress conditions, which improves crop quality and reduces crop loss for farmers. Irrigation water treated with nanobubbles promotes soil flocculation, which causes individual clay particles to combine into bigger aggregates. This minimizes soil compaction, allowing for improved water penetration and root growth [109, 110, 111].

### 1.4.5 Aquaculture

In aquaculture, dissolved oxygen is one of the most important aspects limiting stocking density and production yields. Low oxygen levels harm the health and survival of agricultural animals while preventing nitrifying bacteria from decomposing organic waste [112, 113]. Nanobubble technology is rapidly growing in aquaculture, significantly improving water quality, lowering energy costs, and boosting fish biomass as compared to traditional techniques of oxygenation [114, 115, 116].

### 1.4.6 Biomedical

The growing usage of bulk nanobubbles in biomedicine is due to the variety of therapeutic and diagnostic tools provided by emerging bulk nanobubble technology. The possible applications range from cancer treatment administration and ultrasound contrast enhancement to malaria detection and the diagnosis of acute donor tissue rejection. Ultrasound image contrast enhancement is one of the most often described biological uses of bulk nanobubbles [47, 117, 118]. Due to the compressibility of the encapsulated gas, gas bubbles within tissues can behave as harmonic oscillators and oscillate/resonate in response to ultrasonic excitation. Because of their increased permeability and retention, nano-scale medicines can extravasate from the leaky tumor vasculature [119, 120, 121]. Functionalized nanobubbles can also be employed in molecular imaging in combination with



ultrasound or photoacoustic imaging modalities. Nanobubbles can be loaded with chemicals that bind to markers on tissues or cells of interest [122, 123, 124].

## 1.5 Research Objectives

The primary objective of this research is to focus on understanding the unusual characteristics of bulk nanobubbles generated in contaminated media (aqueous solutions, surfactants) and providing evidence for differentiating between nanobubbles and nanoparticles. The rationale for the research objectives and the tasks associated with them were approached as outlined below:

- *Rationale: Salt dissociation and subsequent ion solvation with water molecules occur during salt dissolution in water which decreases the affinity of gaseous molecules.*

Task 1: To investigate what happens to the excess gas released during the salting-out effect.

Task 2: Provide the evidence for nanobubbles by estimating the refractive index.

- *Rationale: Gas solubility varies linearly with pressure by Henry's law.*

Task 3: To unravel the origin, stability, and nanobubble dynamics under an oscillating pressure field followed by the salting-out effects.

Task 4: Mechanical stability model predicts the existence of stable nanobubbles.

- *Rationale: Jones-Ray effect is debated for the past  $\sim 80$  years on the existence of the minima in surface tension vs. salt concentration curve.*

Task 5: The Jones-Ray effect might be attributed to nanobubble nucleation during the salting-out action and the evidence of nanobubbles is supported in terms of refractive index measurement.

Task 6: Ultrasound waves affecting the stability of the nanoscale gaseous cavities.

- *Rationale: Impurities that actively adsorb at the gas-liquid interface of micro and nanobubbles impair the stability.*

Task 7: Study the dynamics of nanobubbles in surfactant solution.

Task 8: Differentiating nanobubbles and nanoparticles by observing the light scattering behavior.

## 1.6 Organization of the Dissertation

A brief introduction leading toward the objectives is given in Chapter 1. In Chapter 2, the nucleation of nanobubbles during the salting-out effect and its evidence are

discussed in detail. Chapter 3 describes the experimental and predictive modeling approaches for the bulk nanobubbles generated under the effect of an oscillating pressure field. Chapter 4 details the experiment for the Jones-Ray effect and the stability of nanobubbles influenced owing to ultrasound irradiations. In Chapter 5, the dynamics of nanobubbles in surfactant solution have been discussed. Lastly, the summary of all the chapters, the implication, and recommendations of this study are given in Chapter 6.

Chapter 2 is the extended version of the paper published previously by the author in Ultrasonics Sonochemistry (Kalyani et al., 2022), which is reprinted in part here. Chapter 3 and 4 is the submitted manuscript for publication. Chapter 5 needs to be submitted for publication.

## Chapter 2

### Does Salting-out Effect Nucleate Nanobubbles in Water: Spontaneous Nucleation?

---

The previous chapter summarised the current scenario in fundamental study and applications of nanobubbles. We anticipate that effectively incorporating nanobubble technology into environmental engineering will result in a technical revolution by considerably enhancing pollutant removal efficiency, reducing treatment facilities, and lowering operating times and costs. The solubility of gases in an aqueous salt solution decreases with the salt concentration, often termed the “salting-out effect.” Now it is interesting to know what happens to the excess gas released during salting-out. Since it is imperative to note that the transfer of the dissolved gas in the bulk liquid may often occur in the form of nanobubbles. In this work, we have answered this question by investigating the nano-entities nucleation during the salting-out effect. With this hypothesis, we have experimentally investigated whether the salting-out effect nucleates nanobubble or not. What is the strong scientific evidence to prove that they are nanobubbles? Does the salting-out parameter affect the number density? The answers to such questions are essential for the fundamental understanding of the origin and driving force of nanobubble generation.

#### 2.1 Introduction

Nanobubbles in bulk liquid has received significant attention over the past decades. They are gas-filled bubbles with a mean diameter ranging from 100 to 200 nm. Bulk nanobubbles possess distinct features such as extraordinary longevity, high surface-to-volume ratio ( $\approx \frac{6}{d}$ ), high mass transfer coefficient and Laplace pressure, and ability to generate reactive oxygen species. Owing to such peculiar properties, nanobubbles have a wide range of applications in the field of wastewater treatment [4, 8], medical application [125], food processing [20], environmental sectors [100], bio-engineering sectors [126], flotation [127], therapeutic delivery [128]. Despite such overwhelming applications, the fundamental understanding of nanobubble generation [16] and a unique characterization technique to distinguish nanobubbles from the particle and nanodroplets [129] are still in infancy. Broadly, nanobubble generation methods include acoustic cavitation [77], porous membrane [82], repeated compression and decompression [130, 131], electrolysis [5], external electric field [132], and alternating magnetic field [133]. Several characterization techniques have been employed to detect nanobubbles. For instance, optical methods such

as dynamic light scattering (DLS), nanoparticle tracking analysis (NTA), flow cytometry, etc., provide a measurement of the size and concentration of nanobubbles but do not distinguish nanoparticles and nanodroplets from the nanobubbles [5, 132, 134]. Freezing and thawing, vacuum, and centrifugation is the class of techniques based on physical perturbation [129], phase contrast microscopy techniques are based on the estimation of the refractive index of nanobubbles which may lie between air (RI = 1.00) and water (1.33). On the other hand, the refractive index of solid particles and droplets is supposed to be greater than 1.33 [135]. The off-axis digital holographic microscopy (DHM) enables the estimation of both the refractive index and the size of nanobubbles [136].

We are interested to understand what happens to the excess released gas during the salting-out effect. In general, the gas transfer in the liquid often occurs in the form of bubbles. Therefore, it can be speculated that excess dissolved gas may nucleate in the form of nanobubbles. Does the salting-out parameter play a role in nanobubble nucleation? The solubility of gas decreases in a salt solution with reference to pure water, the so-called salting-out effect. The quantitative study on the solubility of a gas in the electrolyte was reported by Setchenov where he proposed an empirical relation between electrolyte concentration and gas solubility as follows [137]:

$$\log\left(\frac{\alpha}{\alpha_0}\right) = KC_e \quad (2.1)$$

where  $\alpha_0$ ,  $\alpha$ , and  $C_e$  are the oxygen solubility in pure water, and oxygen solubility in salt solution of the concentration,  $C_e$ .  $K$  is the salting out parameter that depends on the gas type, temperature, and valency of the salt. For a low electrolyte concentration, **Eq. 2.1** can be modified using ionic strength as follows:

$$\log\left(\frac{\alpha}{\alpha_0}\right) = hI \quad (2.2)$$

where  $I$  is the ionic concentration as follows [138]:

$$I = \left(\frac{1}{2}\right) \sum c_i z_i^2 \quad (2.3)$$

For a mixed electrolyte system, **Eq. 2.2** can be modified as follows [139]:

$$\log\left(\frac{\alpha}{\alpha_0}\right) = \sum H_i I_i \quad (2.4)$$

where  $H_i$  is the specific salting-out constant for ions and the gas. Thus, the solubility of the gas in a mixed salt can be predicted by **Eq. 2.4**.

It is readily clear from **Eq. 2.4** that the higher the salting-out parameter value lowers the gas solubility in a given salt solution. It is also to be noted that the solubility of gas increases with the valency of the salt. In other words, the solubility

difference ( $\alpha_0 - \alpha$ ) decreases with salt valency. Several interesting questions can be posted here. For instance, does excess dissolved gas nucleate in the form of nanobubbles? What is the evidence that they are nanobubbles? What is bubble number density in mono-, di- and tri-valent salt solutions during the salting-out effect? How stable are these nanobubbles? What is the mean diameter of the nanobubbles in mono-, di- and tri-valent salt solutions? Does bubble number density increase with salt concentration as the solubility difference increases from **Eq. 2.1**? Are these bubbles stable in the acidic medium? Are these bubbles charged

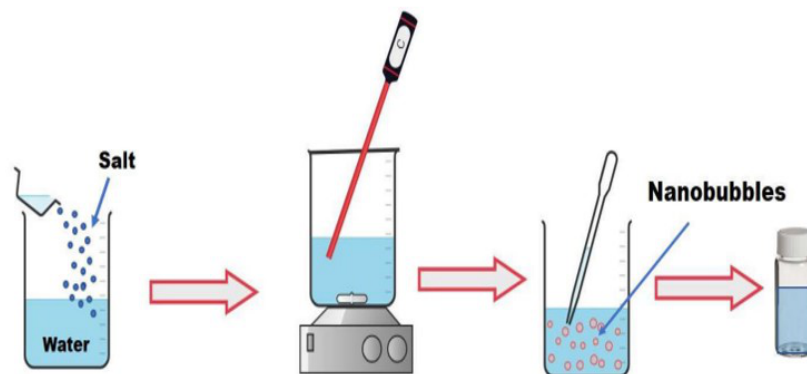


Figure 2.1: Schematic illustration of the generation of nanobubble suspension.

From a fundamental research viewpoint, Bunkin et al.[135] performed the experiments on an aqueous NaCl solution and characterized it by phase microscopy, DLS, and polarimetric scatterometry. The refractive index of micron-sized bubbles was estimated to be 1.26. The mechanism of charging the bubble essentially depends on the ion present in the solution. Bunkin et al.[67] reported that anions play a major role than the cations in the stabilization of bubbles. Due to the surface charge on the nanobubble, the colloidal stability has been investigated by DLVO theory, and the energy barrier was found to vary from  $20 \kappa_B T$  to  $60 \kappa_B T$  [134] depending upon the pH of the solution. Such a positive energy barrier warrants the colloidal system to be stable. More recently, the ion adsorption at the interface is explained by solving the modified Poisson–Boltzmann equation. The surface charge calculation by modified Langmuir adsorption expressions has been seen in good agreement with the experimental results over a wide range of pH [140]. The accumulation of surface charge density stabilizes the bubbles as the electrostatic pressure ( $P_e \approx \frac{1}{R^4}$ ) diverges must faster than the Laplace pressure ( $P_L \approx \frac{1}{R}$ ) [134, 87, 141, 127]. Interestingly, the nanobubbles are observed to be stable against temperature. The mean diameter of the nanobubble decreases with temperature but restores its original size upon cooling the nanobubble sample. Evidently, the temperature may enhance the self-ionization of water and the mobility of ions, and nanobubble stabilization may occur by charge redistribution [142].

The applicability of the Young–Laplace equation and Henry’s law for nanobubbles

are recently validated with experimental results [143]. The validity of the Young–Laplace equation facilitates the estimation of the internal gas pressure of nanobubbles. Shi et al. [144] compared the internal pressure by the two methods, namely, by contact mechanics approach and by using the Young–Laplace equation. The contact mechanics model utilizes the force between the bubble and the probing tip measured by atomic force microscopy. Both models reported consistent internal pressure in the range of (8–16 bar) for 200 to 400 nm nanobubbles. One of the distinctive properties of nanobubbles is the formation of  $\text{OH}^-$  radicals.

The recent measurement based on the electron paramagnetic resonance spectrum suggests the existence of  $\text{OH}^-$  radicals [49]. Perhaps this is one of the promising properties of nanobubbles, as free radicals are responsible for the degradation of many organic matters. More recently, nanobubbles in salt solution were generated by the hydrodynamic cavitation (external energy devices) method by Hewage et al. [145] and concluded that as the valency of the salt increases the surface charge on the bubble neutralizes and it further leads to the charge reversal. The co-ions and counter-ions have been shown to have a negligible effect on the surface potential or the surface charge ?

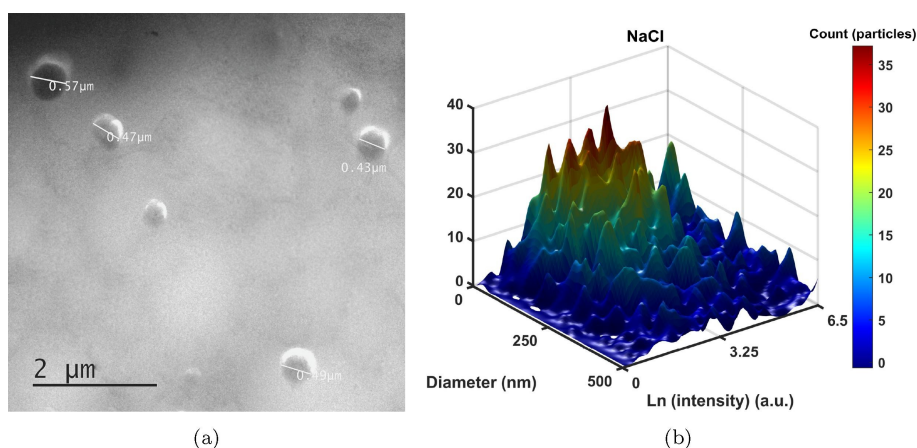


Figure 2.2: (a) Cryo-TEM micrograph of nanobubbles in 1 mM of NaCl solution (b) 3D histogram of bubble count, size, and light scattering intensity in nanobubble sample of 1 mM NaCl.

In a nutshell, it is reasonably clear that most of the literature is devoted to understanding the properties and colloidal stability of the nanobubbles. There are no prior studies investigating the origin and generation mechanism of the nanobubbles during the salting-out effect. We have presented a novel method to estimate the refractive index of nanobubbles based on the scattering power measurement. The effect of the valency of salt on nanobubble density, size, and charge at the surface of the nanobubbles has been studied extensively. The evidence for nanobubbles is provided by estimating the refractive index of nanobubbles using the Mie scattering theory based on the experimental data on scattering intensity. Cryo-TEM imaging of nanobubbles further supported the characterization

of nanobubbles. The different storage conditions also play an essential role in the long-term stability of nanobubbles.

## 2.2 Experimental methods

### 2.2.1 Materials

A double distilled water having an electrical conductivity of  $1.695 \mu\text{Scm}^{-1}$  and pH of 7.1 at a temperature of  $25^\circ\text{C}$  has been used in all the experiments. Aluminium chloride ( $\text{AlCl}_3$ , 99.9%), sodium sulphate ( $\text{Na}_2\text{SO}_4$ ), sodium chloride ( $\text{NaCl}$ , 99.5%) and calcium chloride ( $\text{CaCl}_2$ , 99%) were purchased from Merck Chemicals. Double distilled water is used to prepare all the stock solutions required for the experiments. A magnetic stirrer is used for 45 min to mix the powder chemicals into the water. The water used for the experiments and a stock solution was examined using NanoSight before the experiments. This is to make sure that there is no contamination at the nanoscale present a prior. Additional precautions during the cleaning and handling of the experimental rig have been taken care of. The disposable latex-free syringes, vials, and pipettes were used to avoid any form of contamination.

### 2.2.2 Preparation of nanobubble sample

Nanobubble samples were prepared by dissolving salts in pure water at room temperature as shown in **Figure. 2.1**. A magnetic stirrer is employed for dissolving salt at 1100 RPM for 45 min. The nanobubble formed during salt dissolution was stored at room temperature in 15 mL air-tight vials for further analysis. From a thermodynamic viewpoint, the change in free energy during the bubble generation is given as follows:

$$\Delta G = \frac{4}{3}\pi R^3 G_v + 4R^2 \gamma \quad (2.5)$$

where  $R$  is the radius of the bubble.  $G_v$  is the energy associated with the per unit volume of gas and it is a negative number. Therefore, increasing the value of  $G_v$  favors bubble generation. On the other hand, the surface tension,  $\gamma$  of the liquid is always positive, and increasing the value of surface tension hinders bubble generation. During salting-out effects, the Gibbs free energy of mixing tends to enhance the value  $G_v$  and therefore facilitates the nanobubble generation. The nanobubble generation by physical methods exploits the reduction in the pressure which reduces the solubility of the gas and therefore it tends to nucleate nanobubble. In the present technique, the reduction in the solubility of the gas is achieved by the dissolution of the salt which leads to the supersaturation of dissolved gas and forms nanobubble.

### 2.2.3 Refractive index estimation

Measuring the maximum scattering power,  $P_S$ (AU) using NanoSight NS300 we have determined the refractive index of the nanobubble sample. The measured scattering power of a standard polystyrene nanosphere of known size and refractive index is used to calculate the scattering cross-section  $\sigma_S$  ( $\text{nm}^2$ ) from the Mie theory [146]. MieConScat calculator v1.1.8 [147] has been used to calculate the scattering cross-section of the known size and refractive index of the particle. The MieConScat utilizes [147] the particle size, and refractive index of both particle and medium and the wavelength of the light source as the input parameter for the calculation of theoretical scattering cross-section. Mie theory is based on the analytical solution of Maxwell's equations describing the scattering of electromagnetic waves around spherical objects. The solutions of Maxwell's equations are expressed in terms of infinite series of vector spherical harmonics. MieConScat [147] is the software based on Mie scattering theory and the details of the calculation procedure are described elsewhere [146]. NanoSight NS300 is calibrated by standard polystyrene nanospheres of the known size (four sizes of polystyrene beads, namely 50 nm, 100 nm, 150 nm, and 200 nm, and concentration  $10^8$  particle. $\text{mL}^{-1}$ ). The refractive index of polystyrene nanosphere is 1.633 [148]. The measured  $P_S$  value has been correlated with the corresponding value of  $\sigma_{Mie}$  calculated from Mie theory using MieConScat [147]. A scaling factor  $\sigma_{Mie}/P_S = 0.0673$  is obtained by least-square fitting of the data points. This scaling factor is specific to the tracking instrument (i.e., NS300). All the measurements were performed at 22°C and 0.95 cP.

### 2.2.4 Sample preparation for Cryo-TEM imaging

Nanobubbles in salt solution were visualized using an FEI-Tecnai G2 12 Twin TEM 120 kV equipped with a low-temperature Gatan unit. The nanobubble samples were prepared for Cryo-TEM analysis by placing 1  $\mu\text{L}$  of nanobubble solution onto the holey carbon-coated gold grid, and it is further vitrified into liquid ethane by using Vitrobot (FEI Company). Subsequently, the grid containing the vitrified nanobubbles has been placed onto the Cryo holder, and images were taken at an acceleration voltage of 120 kV at a temperature -174°C. Nanobubbles generated during the dissolution of NaCl with 1 mM salt concentration have been characterized by Cryo-TEM as shown in **Figure. 2.2a**. Evidently, the spherical nanobubbles are visualized by Cryo-TEM; however, the size of nanobubbles is larger than that of the NTA measurement as shown in the 3-D histogram in **Figure. 2.2b**.



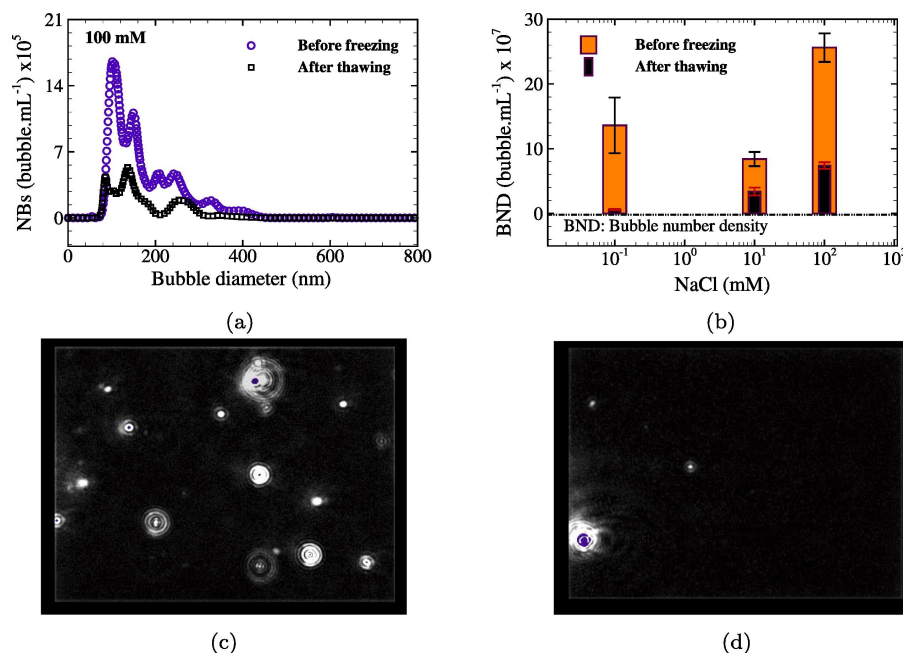


Figure 2.3: Freezing and thawing experiments on nanobubble sample generated by dissolution of NaCl (a) bubble size distribution before freezing and after thawing (b) bubble number density before freezing and after thawing (c) NTA micrograph before freezing (d) NTA micrograph after thawing.

## 2.3 Results and discussion

### 2.3.1 Physical perturbation of nanobubbles

The evidence of the gas-filled nano-objects has been a challenge. The sizing by optical techniques relies on the Brownian motion of the nano-entities; thus, it does not distinguish between bubbles and particles. In this work, we have provided multiple evidence of the nanobubble nucleated during the salting-out effect. The first approach is the so-called physical perturbations to the nanobubble suspension. The disappearance of nanobubbles during freezing and thawing provides an indication of a soft interface. However, this may also lead to the formation of aggregates during freezing and thawing. This has been verified by performing freezing and thawing of polystyrene nanospheres in water. Particle counts and mean diameter were observed to be more or less invariant of freezing and thawing. This observation strengthens the lower probability of particle aggregation during freezing and thawing. However, it does not rule out the possibility of coalescence of oil nanodroplets if a small fraction of oil entered the system. Three nanobubble samples, namely 0.1 mM, 10 mM, and 100 mM were prepared and characterized by NTA. A representative bubble size distribution for a 100 mM sample is shown in **Figure. 2.3a**. 10 mL of each nanobubble sample were frozen at a temperature of  $-18^{\circ}\text{C}$  for 12 h which is significantly lower than that of the freezing point of the 1 M salt solution ( $\approx -3.72^{\circ}\text{C}$ ). Nanobubble samples were further defrosted at room temperature for about 2h

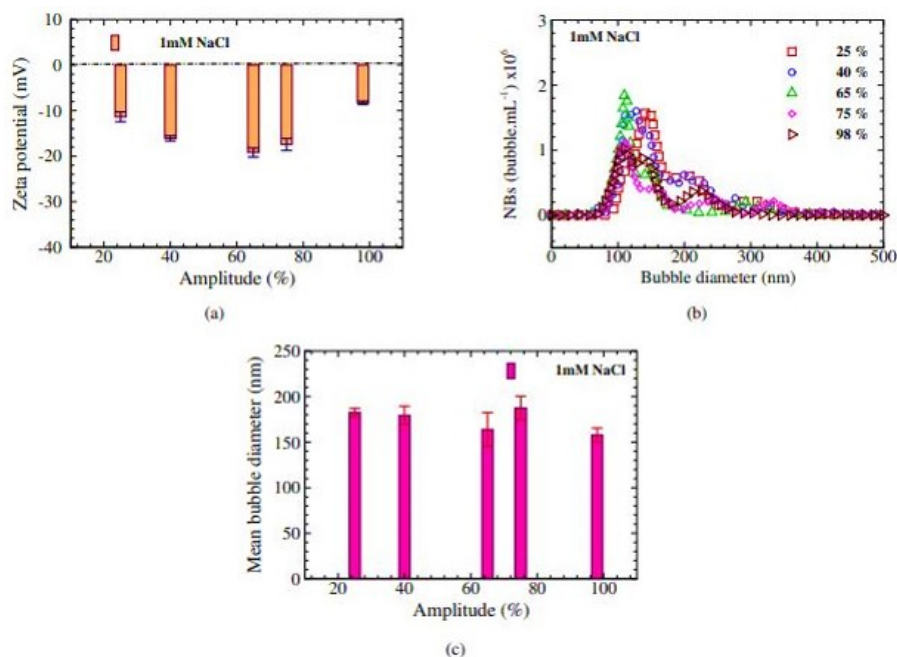


Figure 2.4: Effect of ultrasound amplitude on (a) zeta potential (b) bubble size distribution (c) mean bubble diameter of nanobubble sample generated by dissolution of NaCl.

before characterization by NTA. Typical results on the bubble number density are shown in **Figure. 2.3b**. At low salt concentrations, for instance, at 0.1 mM of salt, most of the nanobubble disappears; however, the remaining entities after thawing increase with the salt concentration. The corresponding NTA micrograph before freezing and after thawing are shown in **Figure. 2.3c** and **d**. The bubble count per frame was reduced from 17 to 3 bubbles per frame which is  $\approx 82\%$  decrease in the bubble count. Other physical perturbation techniques, such as pressurization, vacuum, and centrifugation, have also been employed in the nanobubble sample in the recent past. The size of the nanobubble increases and the bubble number density decreases by pressurization of the nanobubble sample. Such a compressible behavior of the suspension indicates the gas-filled nano-entities. In contrast, employing a vacuum to the nanobubble sample, mixing degassed water with the nanobubble sample exhibit disappearance of nanobubbles. The amplitude is varied from 25% to 98%. 60 ml of nanobubble sample is exposed to a titanium ultrasound probe with varying amplitude. From a theoretical standpoint, the pressure generated by ultrasound, the so-called acoustic pressure wave, gives rise to compression and the rarefaction cycle. During the rarefaction cycle, pressure in the liquid falls below the vapor pressure of the liquid and thus results in the nucleation of micro and nanobubbles. The bubble generation during the rarefaction cycle is only possible if there are gas sources present. If the system contains bubbles a priori, then the acoustic cycles tend to disintegrate the bubble, and therefore, we observe a significant reduction in the nanobubble population if the irradiated nanobubble solution is subjected to ultrasound. The surface charge in **Figure. 2.4a** on the

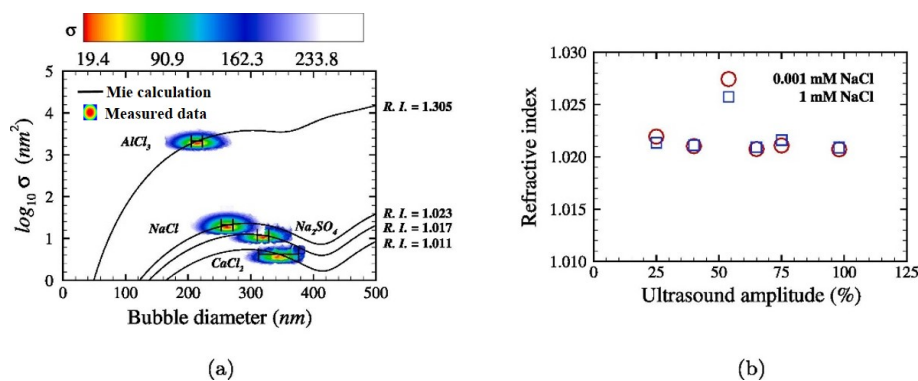


Figure 2.5: (a) Representative scattering cross-section for nanobubbles in NaCl, CaCl<sub>2</sub>, Na<sub>2</sub>SO<sub>4</sub>, and AlCl<sub>3</sub> solution versus mean bubble diameter (b) Refractive index of nanobubble sample of 0.001 mM and 1 mM of NaCl.

nanobubble significantly increases with ultrasound, but the mean diameter was found to be unaffected as shown in **Figure. 2.4c**. It is readily apparent that nano drops may also behave similarly to the nanobubbles by the physical perturbation mentioned above. Therefore, the evidence for nanobubbles is further strengthened by estimating the refractive index of the nano-entities in various salt solutions, as discussed in the next section.

### 2.3.2 Refractive index of nanobubbles

The refractive index is related to the chemical composition of the suspended material, and it is often used to differentiate different constituents in the medium. For instance, extracellular vesicles in biological samples (RI < 1.42) can be distinguished from lipoproteins (RI > 1.42) of similar size based on refractive index [149]. The refractive index of oil drops in water [150] and nanoparticles [151] was reported to be higher than 1.33. In this work, we have estimated the refractive index of nano-entities formed during the salting-out effect for mono-, di- and tri-valent salts as shown in **Figure. 2.5a** and **b**. As noted earlier, the scattering power of the known size and refractive index of polystyrene nanospheres have been used to calibrate the NTA. The instrument scaling factor is used to compare the measured scattering cross-section and theoretical from Mie theory calculations to estimate the refractive index of the nanobubble suspension. **Figure. 2.5a** demonstrates the overlap of the measured scattering cross-section and theoretical value from the Mie theory. For nanobubbles in mono and divalent salts, the refractive index value was estimated to be in the range of 1.011–1.023, whilst the refractive index of the nanobubbles in tri-valent salt was calculated to be  $\approx 1.305$ . Such a higher value of the refractive index of nanobubbles in trivalent salt is plausibly due to the absorption of Al<sup>3+</sup> around the nanobubble interface leading to a slight increase in the opacity. Interestingly, it is to be noted that the refractive index of nanobubbles in all the mono-, di, and tri-valent salt is less than that of 1.33. Evidently, this

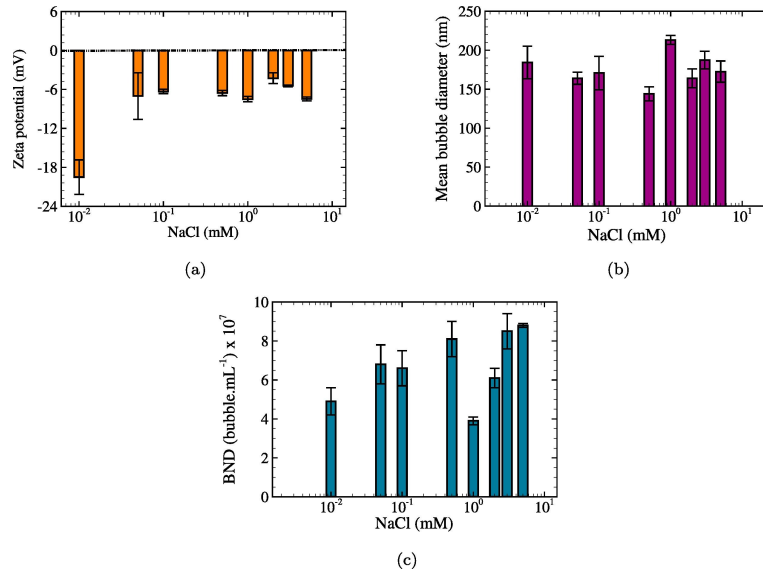


Figure 2.6: Nanobubbles in NaCl solution of varying concentration (a) zeta potential (b) mean bubble diameter (c) bubble number density. The pure water is analyzed using NTA before adding the salt, and no nano-entities were observed.

is within the range of gas bubbles. We have estimated the refractive index of the nanobubbles generated in 0.1 and 1 mM of NaCl salt by varying the ultrasound amplitude as shown in **Figure. 2.5b**. It is to be noted that the refractive index is estimated after the ultrasound as it requires reducing the temperature for NTA analysis. For ultrasound experiments, 50 mL of nanobubble sample were placed in a beaker. The ultrasound probe was dipped in the solution and irradiated for 5 mins in a continuous mode. The estimated values of the refractive index were shown to be invariant with the amplitude used. This effect probably suggests that ultrasound is not introducing any contamination even at a higher amplitude. In a nutshell, we have provided evidence for nanobubble generation during salting-out effects.

### 2.3.3 Influence of salt valency

Nanobubble generation during the salting-out effect is characterized by NTA in terms of bubble size distribution, bubble number density, and mean size. Surface charge is measured by zeta potential. The concentration of various salts has been varied up to 5 mM to understand the effect of salt concentration on nanobubble generation. Both Bubble number density and size of the nanobubbles increase with the concentration of the salt, and it is observed to be irrespective of the valency of the salt as shown in **Figure. 2.6** and **2.7**. However, the surface charge was observed to be more or less invariant with the salt concentration. Nanobubbles in NaCl, CaCl<sub>2</sub>, and Na<sub>2</sub>SO<sub>4</sub> were measured to be negatively charged while the nanobubbles in AlCl<sub>3</sub> possess a positive charge. The comparison of bubble number density for various salts is performed after concentrating the nanobubble sample using a Rotary evaporator. 250 mL of nanobubble suspension was reduced to 20 mL

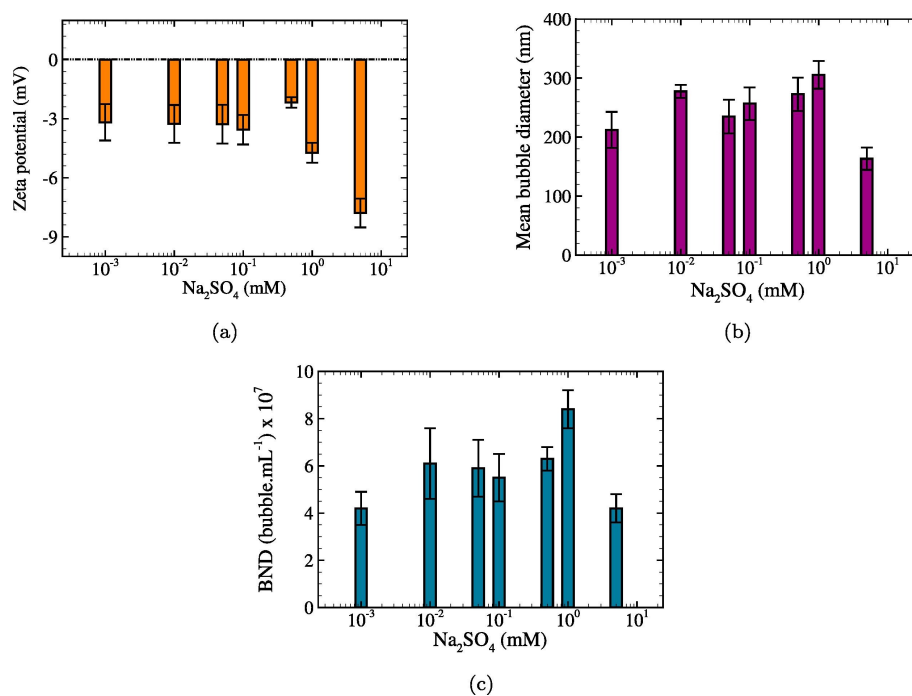


Figure 2.7: Nanobubbles in  $\text{Na}_2\text{SO}_4$  solution of varying concentration (a) zeta potential (b) mean bubble diameter (c) bubble number density.

by evaporating the solvent. A typical comparison of bubble number density, bubble size distribution, and zeta potential of different salts is shown in Fig. 6. Evidently, bubble number density in mono-valent salt is observed significantly higher than in the di- and tri-valent salt. The mean diameter of the nanobubble was observed to be slightly increased for di-valent salts ( $\text{CaCl}_2$  and  $\text{Na}_2\text{SO}_4$ ) in comparison with  $\text{NaCl}$ , as shown in **Figure. 2.8**. However, further, the mean diameter of nanobubble decreases in the tri-valent salt ( $\text{AlCl}_3$ ). Interestingly, the surface charge on the nanobubbles in the  $\text{AlCl}_3$  solution is measured to be positive. The zeta potential of nanobubbles in deionized water provides the speculation of the negatively charged air–water interface [134]. Such charged nano-entities form an electric double layer around the objects. The strong positive ions such as  $\text{Al}^{3+}$  may absorb in the interface, and therefore nanobubbles may exhibit a positive value of zeta potential.

The salting-out parameter denotes the slope of the solubility plot. A higher value of the salting-out parameter results in the low solubility of the gas. Table 1 shows the typical value of the salting-out parameters for the salts used in this work. Clearly, the value of the salting-out parameter is significantly higher in the case of  $\text{NaCl}$  than the other di- and trivalent salts. For a fixed value of the salting-out parameter ( $K$ ), the ratio of solubility expressed in terms of Bunsen coefficient varies proportionally with the concentration of the salt as shown in **Eq. 2.1**. For a fixed temperature and pressure, the solubility of the gas in pure water is constant; therefore, the solubility of the gas in the salt solution decreases with increased concentration. This correlates reasonably well with the increasing bubble number

Table 2.1: Salting out parameters of electrolytes for oxygen at 298.2 K

Salt	K (dm <sup>3</sup> /mol)	Molar concentration range (M)
NaCl	1.145	0-5
CaCl <sub>2</sub>	0.226	0-4.5
Na <sub>2</sub> SO <sub>4</sub>	0.376	0-1.2
AlCl <sub>3</sub>	0.274	0-1.7

density with the salt concentration, as shown in **Figure. 2.8**. In other words, the solubility difference ( $\alpha_0 - \alpha$ ) increases with salt concentration which is the available gas for nanobubble nucleation. The salting-out parameter also explains the higher bubble number density in mono-valent salt compared to di- and tri-valent salt. The salting-out parameter for monovalent salt is significantly higher than that of the di- and tri-valent as shown in **Table. 2.1**.

### 2.3.4 Temporal stability of nanobubbles in salt solution

Nanobubbles in pure water have been seen to be extraordinarily stable for days and months [144, 17, 152]. Bubble number density decreases monotonically while mean diameter increases 30–40% over the period of time. Since nanobubbles in pure water are negatively charged, bubble coalescence and dissolution can possibly be ruled out. Therefore, the disappearance of the nanobubbles is expected from the air–water interface at the top and by collision with the storage container wall. It is also to be noted that the mean square displacement of the smaller bubble is higher with respect to the larger bubble from the Einstein-Stokes equation. In other words, the probability of collision for smaller nanobubbles is more than the larger bubbles. Thus, the smaller bubble may disappear faster than the larger bubble. This might be the possible justification for the increasing mean bubble diameter over a period of time as a smaller bubble is expected to disappear earlier. In this work, we have examined the so-called long-term stability of nanobubbles in NaCl solution. The bubble number density was significantly higher in the NaCl solution, and therefore the sample is chosen for long-term stability. The nanobubbles in salt solution are seen to disappear much faster than in pure water, as shown in **Figure. 2.9**. Nanobubbles are observed to be stable for no more than three days. The mean diameter of the nanobubble increases by  $\approx 37\%$  in three days. This is in line with the nanobubbles in a pure water system [144, 152]. The faster decay of the bubble number distribution in salt solution may be attributed to the presence of salt that leads to an electric double layer screening around nanobubbles. A weak surface charge on the nanobubbles gives rise to lower colloidal stability of the system, and therefore, nanobubble disappears must faster in a salt solution.

Two 15 mL vials, namely, the glass and polypropylene material, have been used.



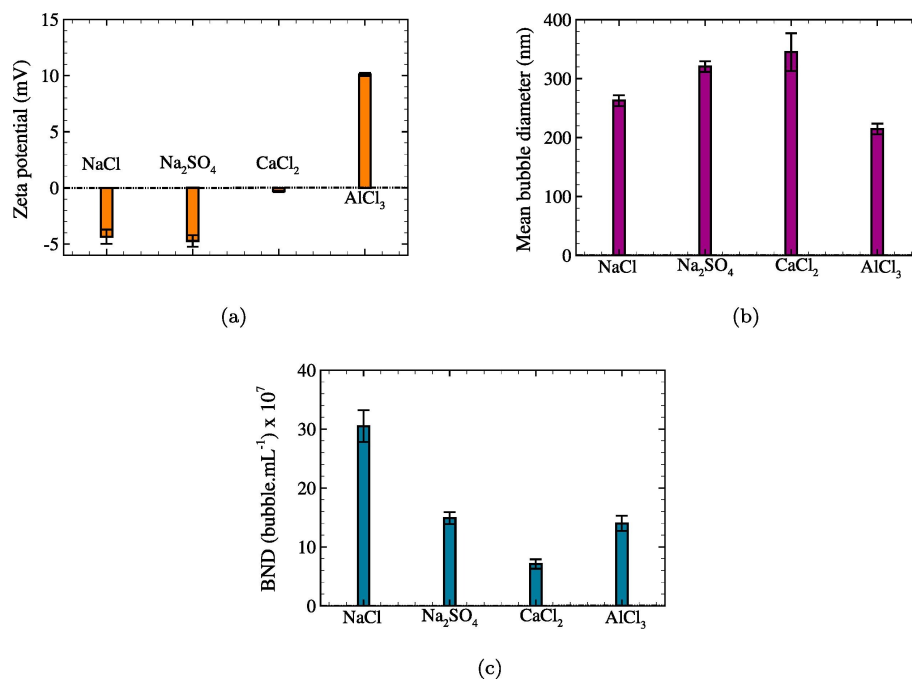


Figure 2.8: Nanobubbles in salt solution (1 mM) of different valency (a) zeta potential (b) mean bubble diameter (c) bubble number density.

The volume of stored nanobubble samples is kept to be equal. Evidently, the bubble number density decays faster in polypropylene vials than that in glass vials. The plausible reason could be the absorption of nanobubble inside the polypropylene vial. Indeed, it is difficult to claim the exact mechanism of nanobubble absorption in polypropylene containers, but the hypothesis on the nanobubble disappearance by striking the container wall seems possible. In addition, temperature and pressure conditions may also influence the stability of the nanobubbles. Brownian motion of nanobubbles is expected to be higher at high temperatures; therefore, the probability of collision with the container wall is expected to be enhanced. This, in turn, leads to a high rate of disappearance of nanobubbles at a higher temperature.

### 2.3.5 Nanobubbles in acidic and alkaline medium

Nanobubbles in pure water (at neutral pH) are extraordinarily stable. It is also known that nanobubbles are more stable in an alkaline medium [134, 5]. Bubble number density drops in the acidic medium, whereas the mean diameter increases. Surface charge approaches an isoelectric point in the acidic medium. It is also interesting to note that nanobubbles can be further charged negatively by adjusting the pH of the sample to the alkaline limit. This is plausibly due to the absorption of OH<sup>-</sup> at the air–water interface. This behavior is qualitatively similar to that of any charged nano-suspension. In this work, nanobubbles in NaCl solution are concentrated using a rotary evaporator for pH adjustment. Hydrochloric acid and sodium hydroxide are used to adjust the pH of the sample. Nanobubbles in the

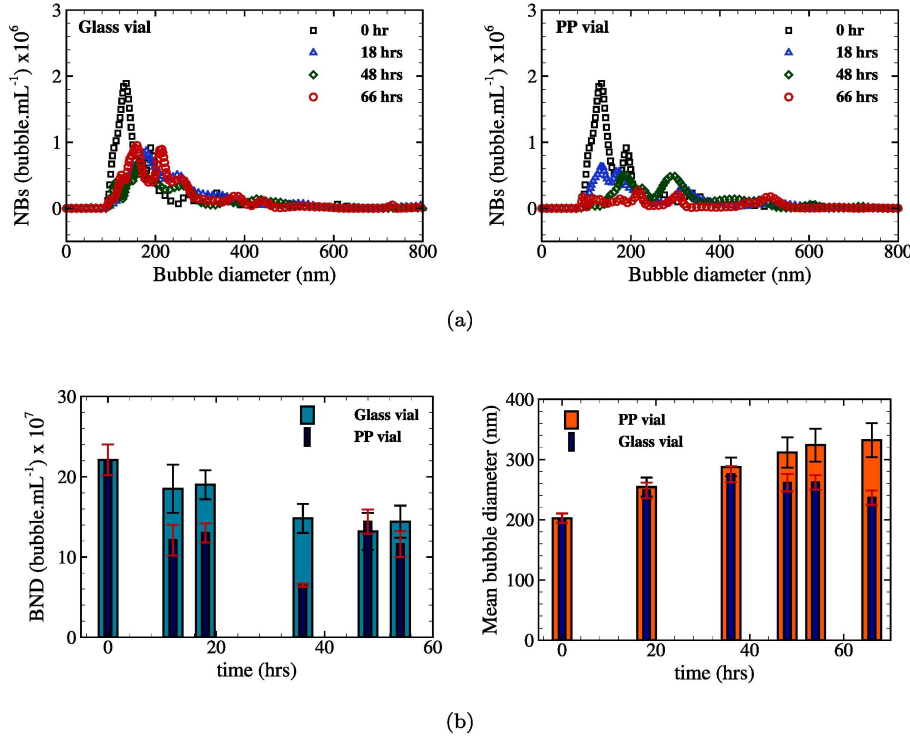


Figure 2.9: Effect of a storage container on the long-term stability of nanobubbles generated in NaCl (a) bubble size distribution (b) bubble number density and mean bubble diameter.

salt solution behave qualitatively similar to that in the pure water, as shown in **Figure. 2.10**. Bubble number density decreased by  $\approx 30 - 50\%$  from  $\text{pH} = 10$  to  $\text{pH} = 3.5$ . Similarly, the mean bubble diameter of the nanobubble increases by 30–40%. On the other hand, zeta potential approaches toward  $\approx -32$  mV at  $\text{pH} = 10$ . The higher mean bubble diameter at lower pH may be due to the screening of the electric double layer. The addition of  $\text{H}^+$  ion is expected to neutralize the air–water interface. The smaller size fraction of nanobubbles may be dissolved or shrink much faster than that of the larger bubble due to the screening of the electric double layer. Therefore, the measured diameter of nanobubbles at low pH exhibits a relatively larger mean. In summary, nanobubbles in salt solution behave similarly to that in pure water. Surface charge decreases in the acidic medium due to the screen of the electric double layer by  $\text{H}^+$  ion. On the other hand, nanobubbles are expected to be more stable in the alkaline medium due to the strong electrostatic interaction that gives rise to the higher total interaction potential.

## 2.4 Conclusion

Finally, we conclude that the excess dissolved gas indeed nucleates in the form of nanobubbles during the salting-out effect based on the refractive index calculation. Further evidence of nanobubbles was supported by the freezing and thawing



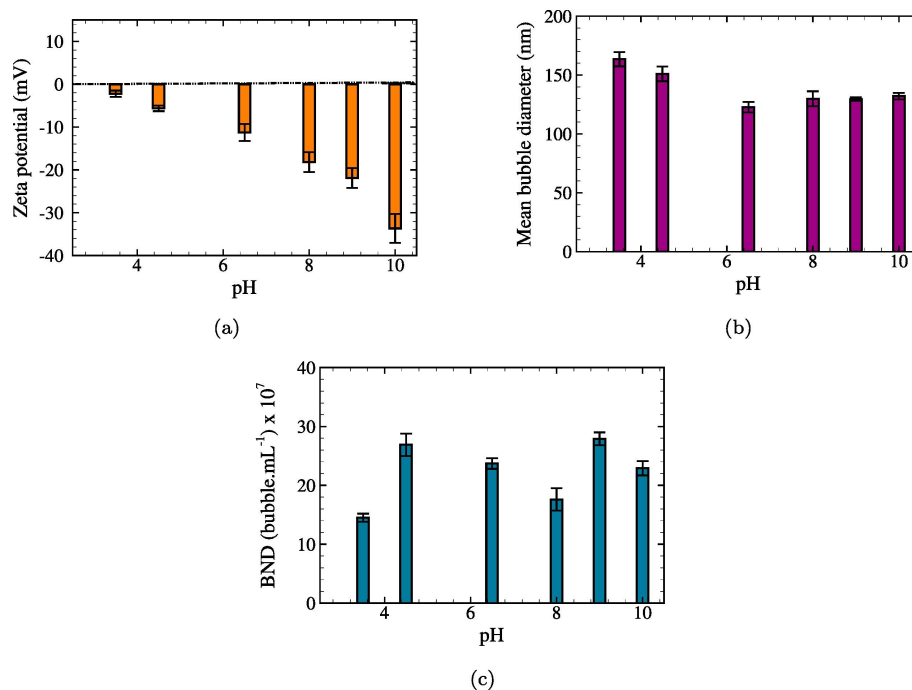


Figure 2.10: Effect of pH on nanobubbles in NaCl solution (a) zeta potential (b) mean bubble diameter (c) bubble number density.

process. A novel method for the estimation of the refractive index of nanobubble is proposed based on Mie theory calculations. The measured scattering power by NTA is utilized to calibrate the NTA using standard latex nanospheres and to estimate the refractive index of an unknown sample. The refractive index of nanobubble samples was calculated to be 1.012 for mono and di-valent salt and 1.302 for the tri-valent salt. The absorption of  $\text{Al}^{3+}$  ion in the electric double layer around the nanobubble is the expected reason for the increase in the refractive index of tri-valent salt. The bubble number density was observed to increase with the salt concentration, which is explained by the Setchenov solubility relation for electrolytes. The solubility difference increases with the salt concentration, and therefore, bubble number density exhibits a positive correlation with the salt concentration. We also conclude that bubble number density depletes with the salt valency. This is explained by using a salting-out parameter; the higher the value of the salting-out parameter lower the solubility of the gas in the solution. Therefore, the solubility difference yields a positive dependence on the salting-out parameter. The reported values of the salting-out parameter [138] corroborate the observed experimental trends.

We also conclude that nanobubbles during salting-out effects are only stable for up to three days, which is much shorter than nanobubbles in pure water.  $\text{NaCl}$ ,  $\text{CaCl}_2$ , and  $\text{Na}_2\text{SO}_4$  nucleate negatively charged nanobubbles whereas  $\text{AlCl}_3$  salt generates a positive charge nanobubble. We also hypothesize that the nanobubble disappears

by the collision of nanobubbles with the container wall. Polypropylene and glass containers were used to store the nanobubble sample in controlled conditions. Nanobubble decays relatively faster in polypropylene than that in glass vials. This confirms that nanobubble disappears by colliding with the storage container. Nanobubbles in salt solution respond similarly to pure water to the pH adjustment. Surface charge decreases in the acidic medium due to the screening of the electric double layer. On the other hand, nanobubbles are more stable in the alkaline medium due to the strong electrostatic interaction that gives rise to a higher total interaction potential.

## Chapter 3

### On Nanobubble Dynamics under an Oscillating Pressure Field during Salting-out Effects and its DLVO Potential

---

We have investigated the origin, stability, and nanobubble dynamics under an oscillating pressure field followed by the salting-out effects. The higher solubility ratio (salting-out parameter) of the dissolved gases and pure solvent nucleates nanobubbles during the salting-out effect and the oscillating pressure field enhances the nanobubble density further as solubility varies linearly with gas pressure by Henry's law. The novel method for refractive index estimation is employed to differentiate nanobubbles and nanoparticles based on the scattering intensity of light. The electromagnetic wave equations have been numerically solved and compared with the Mie scattering theory. The DLVO potentials of the nanobubbles predict the stable colloidal system. The zeta potential of nanobubbles varied by generating nanobubbles in different salt solutions, and it is characterized by particle tracking, dynamic light scattering, and Cryo-TEM. The novel mechanical stability model is proposed by considering both ionic cloud and electrostatic pressure at the charged interface. The ionic cloud pressure is derived by electric flux balance, and it is found to be twice the electrostatic pressure. The mechanical stability model for a single nanobubble predicts the existence of stable nanobubbles in the stability map.

#### 3.1 Introduction

Nanobubbles has gained significant attention from both applied and fundamental research viewpoints in recent times [49, 153, 154]. Nanobubble encompasses a wide range of applications, particularly towards the 21<sup>st</sup> century grand challenges such as water technology [4, 8, 126], food sector [20, 155], health technology [156, 157, 158, 159], energy sector, energy efficient aeration [160], surface cleaning [5], disinfection and sanitization [161], mineral flotation [162], ultrasound contrast agent [117], drag reduction [163], drug delivery and smart medicine [164, 165], tumor hypoxia [166] etc. Despite numerous applications, the fundamental of the nanobubbles is in their infancy. Broadly, the phase transition or formation of a new phase via nucleation or mixing is essentially a departure from the thermodynamic equilibrium. The out-of-equilibrium conditions give rise to steeper gradients, thereby leading to interesting colloidal and interfacial phenomena. Indeed, these non-equilibrium conditions are driven by either one or multiple influences of phase transfer, external volumetric forces/electric, magnetic forces, mixing, chemical

reaction-driven instabilities, non-uniform surface tension, etc. Nanobubbles are a two-phase system that can be created by manipulating such volumetric driving forces. In this work, we have investigated the nanobubble generation during the salting-out effect and the influence of the oscillating pressure field. The term “salting-out effect” is used interchangeably in salt precipitation by dissolving the higher soluble compound in the base solution. Similarly, the gas solubility decreases upon dissolving other more soluble components in the base solvent, also termed the salting-out effects [167, 168]. From a thermodynamic viewpoint, the dissolved gas in water at a fixed temperature and pressure can be considered in thermodynamic equilibrium. The Gibbs free energy of such a multi-component system is well defined by the Gibbs-Duhem equation (combined representation of the first and second law of thermodynamics). At constant temperature and pressure, Gibbs free energy solely depends on the chemical potential of the individual components. Furthermore, the salt dissolution is expected to increase the chemical potential of the system (for an ideal solution  $\mu_i = \mu_{io} + RT \ln(x_i)$ ). Now, the new thermodynamic equilibrium state can be achieved by minimizing the Gibbs free energy of the system, and, therefore, the new interfaces may be created in the form of nanobubbles due to the dissipation of additional free energy. In other words, salt mixing/dissolution is the volumetric driving force for the out-of-equilibrium of the system that gives rise to heterogeneity in the form of nanobubbles. Furthermore, the volumetric driving force can also be expected to have a proportional relationship with the new surface creation. The free energy of the system can also be enhanced by performing work on the system. For instance, oscillating pressure fields and ultrasound waves are expected to enhance the free energy of the system. Therefore, the nanobubble density should increase when the system undergoes energy minimization. In this work, we have experimentally verified this fact by employing the fluctuating pressure field, and our results show a higher concentration of nanobubbles under the oscillating pressure field.

Despite the overwhelming application of nanobubbles, the extraordinary stability of the nanobubbles is still puzzling. The early speculation was the probability of contamination, such as active surface molecules, dust or nanoparticles, etc. For the nanodroplet generation, diverse emulsification approaches have been utilized which are similar to bulk nanobubble formation including high-pressure homogenizer [13], ultrasonication [169], and light-driven mechanism enveloping porous membrane [170]. Therefore, it is customary to provide strong scientific evidence of the gas-filled nanobubbles which differentiate from nanoparticles or nanodroplets. Broadly, the evidence of the gas-filled nanobubbles is reported by various methods, for instance, optical methods [171], physical perturbation techniques [172, 173, 174], electron microscopy [175, 176], vibrational spectroscopy [177], surface charge measurement, etc. The advantages and disadvantages of the various techniques have been critically examined elsewhere [129]. The physical perturbation to the nanobubble suspension

results in the disappearance of nanobubbles during freezing and thawing which indicates the presence of a soft interface. This may lead to the generation of aggregates during freezing and thawing and is further confirmed by polystyrene nanospheres in water unaffected the particle count and mean diameter. This finding supports the theory that particle aggregation is less likely to occur during freezing and thawing. Furthermore, electron microscopy emerged as an important method for determining the structure of nanoscale entities at high resolution. The ultrahigh-resolution images of individual particles and their internal structure are used to investigate the sample properties and behavior. The electron beam as the imaging radiation source permits for higher spatial resolution (on the tens of picometers scale) than photons in optical microscopy (200 nanometers). Bunkin et al. [135] reported a phase contrast microscopy technique to estimate the refractive index of nano-sized entities. The refractive index of the gas bubble must lie around  $RI = 1.000$ , much lower than that of the water  $RI = 1.330$ . In addition, the refractive index of solid particles and droplets is expected to bear a refractive index value greater than 1.330. More recently, off-axis digital holographic microscopy (DHM) was also utilized to estimate both the refractive index and the size of nanobubbles [136]. In this work, we have developed a new method to estimate the refractive index of nanobubbles by measuring the scattering power during nanobubble tracking analysis. We have estimated the refractive index of nanobubbles generated during salting out and oscillating pressure fluctuation to be 1.001, which indicates that they are indeed gas-filled nanobubbles. Nanobubbles are reported to be stable for days and months in water; however, the existence of nanobubbles in liquids other than water is still an open question. Recently, several stability models for the nanobubbles have been proposed, namely, the skin model, dynamic equilibrium model, ion stabilization, etc. [87]. The most recent understanding of nanobubble stability is the ion stabilization [87, 127]. A mechanical stability model is proposed based on the force balance around the nanobubble. In general, the surface tension force is expected to compress the air-water interface whilst the electrostatic force between the ions at the interface acts opposite to the surface tension force. In addition, the ionic cloud pressure is expected to act opposite to the electrostatic force.

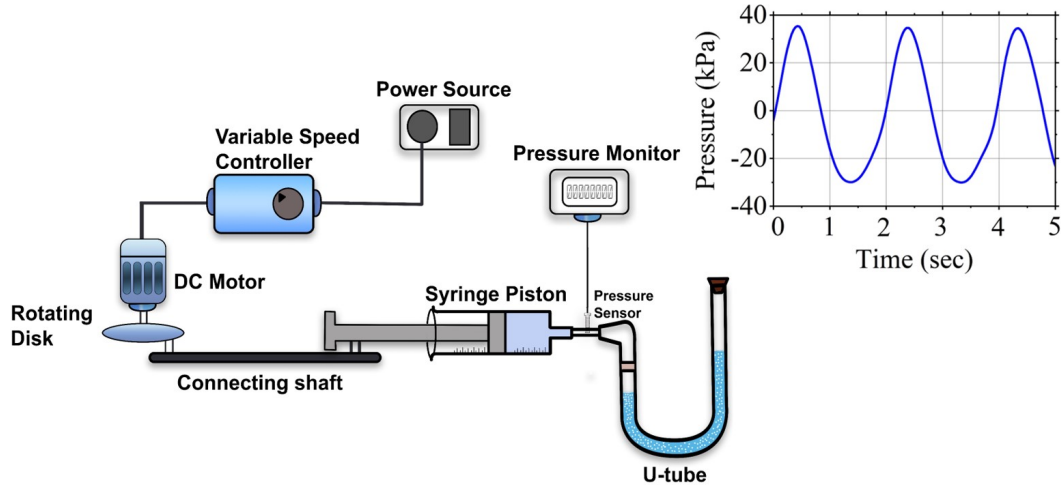


Figure 3.1: Schematic of the experimental setup and applied pressure wave.

## 3.2 Experimental methods

### 3.2.1 Oscillating pressure field setup

Pure water and salt solution of varying concentration (8 mL) respectively were poured into a glass U-tube manometer that was capped with one side and a 50 mL syringe connected onto the other side of the glass U-tube. The wet part in this setup was only the u-tube made of glass. Although the piston and syringe assembly is not in contact with water in order to make the experimental protocol uniform, the piston and cylinder system was also first cleaned with ethanol and water and dried by sparging with nitrogen gas. A similar cleaning protocol was followed in each step while transferring the sample from one to another. Silicon-free syringes were used for the particle tracking analysis.

An MPX5700 pressure sensor by NXP, a Freescale Semiconductors, Inc. subsidiary, is used for the pressure measurement. For better accuracy, the pressure sensor output is interfaced with the ADS1115-based ADC (Analog-to-Digital) converter module, and the built-in ADC converter of Arduino UNO is avoided. A DS3231 [3] based RTC (Real-Time-Clock) module calculates the sampling interval between consecutive measurements. The internal temperature sensor of DS3231 is used to obtain the temperature reading during the experiment.

Because of the presence of bus voltage in the sensor's pressure equation, the bus voltage is also interfaced with the ADS1115 through a precision resistor voltage divider. Nanobubble generation is carried out through an oscillating pressure field schematically illustrated in **Figure. 3.1**. The operating principle of the setup is the periodic change in internal pressure in the U-tube induced by the linear motion of the piston, which is transformed by the eccentric wheel rotating by an electric motor. Consequently, the pressure field generates the solubility difference leading to nanobubble generation. The motor frequency and operating time were set to 500

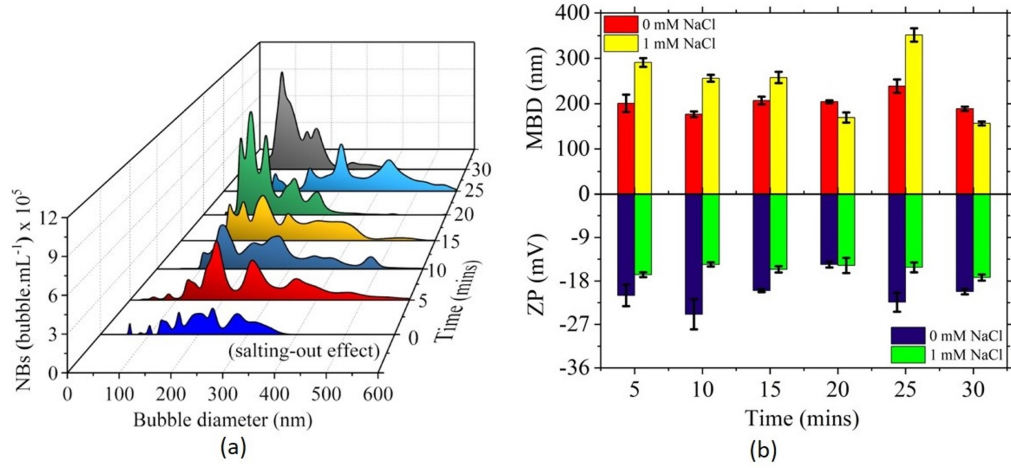


Figure 3.2: Effect of cycle time on nanobubble generation by oscillating pressure method (a) bubble size distribution (1 mM NaCl) (b) mean diameter and zeta potential.

rpm and 13 mins during the experiment.

### 3.2.2 Ultrasound irradiation

The horn-type ultrasound offers a frequency response of 20 kHz frequency with amplitude variation from 25% to 98% and delivers 750 W of constant power. The probe (1/2" dia  $\approx$  13 mm) is fabricated from high-grade titanium alloy Ti-6Al-4V due to its high tensile strength, good acoustical properties, high resistance to corrosion, low toxicity, and excellent resistance to cavitation erosion. The 60 mL sample was subjected to ultrasound irradiation for 5 minutes and further characterized using NTA and DLS.

## 3.3 Results and Discussion

### 3.3.1 Salting-out effects and oscillatory pressure fluctuation on nanobubble dynamics

As noted earlier, the salting-out effect is the decrease in the solubility of gases during salt dissolution. The dissolution of salt in water undergoes ion dissociation, which further forms the solvate of ions with water molecules. The solvation of the ions reduces the affinity of gaseous molecules with water molecules, and thus the solubility of the gas decreases. Recently, it was shown that the excess gas during the salting-out effect nucleates in the form of nanobubbles [178]. These nanobubbles were observed to have similar characteristics, such as extraordinary longevity, negative zeta potential, etc. The nanobubble density was reported to correlate positively with the salting-out parameter. The following expression relates the solubility of gas and the salting-out parameter:

$$\log \frac{S_0}{S} = \frac{h}{2} \sum z_i c_i \quad (3.1)$$

where  $S_0$ ,  $S$ ,  $h$ , and  $c_i$  are the gas solubility in pure water, gas solubility in the salt solution, salting-out parameter, and salt concentration, respectively. The salting-out parameter decreases with salt valency; therefore, the bubble number density in di- and tri-valent salts was less than that in mono-valent salt. From the salting-out experiments, it is reasonably clear that the solubility ratio gives rise to the nucleation of nanobubbles. The solubility ratio can be further increased by employing the oscillating pressure field as the partial pressure and solubility of the gas are linearly dependent on Henry's law ( $p_g = Hc_g$ ). The oscillating pressure field is applied in the pure water and salt solution filled in the u-tube geometry by cylinder and piston system. A pressure sensor records the pressure fluctuations and varies from +30 kPa to -30 kPa (see **Figure. 3.1**). The solubility difference created by oscillating pressure is approximately 30%. The time evolution of the nanobubble size distribution in 1 mM NaCl solution is shown in **Figure. 3.2a**. The bubble distribution area increases with the cycle time in pure water and NaCl solution, which translates into the bubble number density. In other words, the nanobubble density significantly enhances by oscillating pressure fluctuation due to a higher solubility ratio. On the other hand, the mean object diameter and zeta potential remain constant with the cycle time, as shown in **Figure. 3.2b**. Furthermore, the mean object diameter in pure water is always observed to be smaller than that in the salt solution. The mean object diameter of the nanobubbles exhibits an inverse dependence on the zeta potential (regardless of the sign). In other words, a higher zeta potential corresponds to a smaller object diameter. In addition, the mean object diameter during the salting-out effect was also observed to be larger than that generated under oscillating pressure fluctuation (see **Figure. 3.2b**). Interestingly, the zeta potential during the salting-out effect was significantly smaller than that generated by the oscillating pressure field.

From the preceding discussion, it is reasonably evident that the nanobubble density positively influences the solubility ratio. The oscillatory pressure field increases the solubility difference by 30% in comparison with the salting-out effect. The zeta potential of nanobubbles in pure water was higher than that in the salt solution (see **Figure. 3.2b**). The decrease in the zeta potential of nanobubbles in the salt solution is attributed to the screening of an electric double layer around nanobubbles. The mean object diameter directly relates to the zeta potential acquired by the bubble. The higher the zeta potential lower the size of the nanobubbles. Dynamic light scattering and the Cryo-TEM method have further verified this claim. The dynamic light scattering method measures the scattering light intensity in volume, and the average hydrodynamic diameter is the volumetric average of individual bubbles. The mean diameter measured by dynamic light scattering also confirms that the mean diameter of objects in the salt solution is higher than in pure water. However, the mean diameter measured by dynamical light scattering was slightly



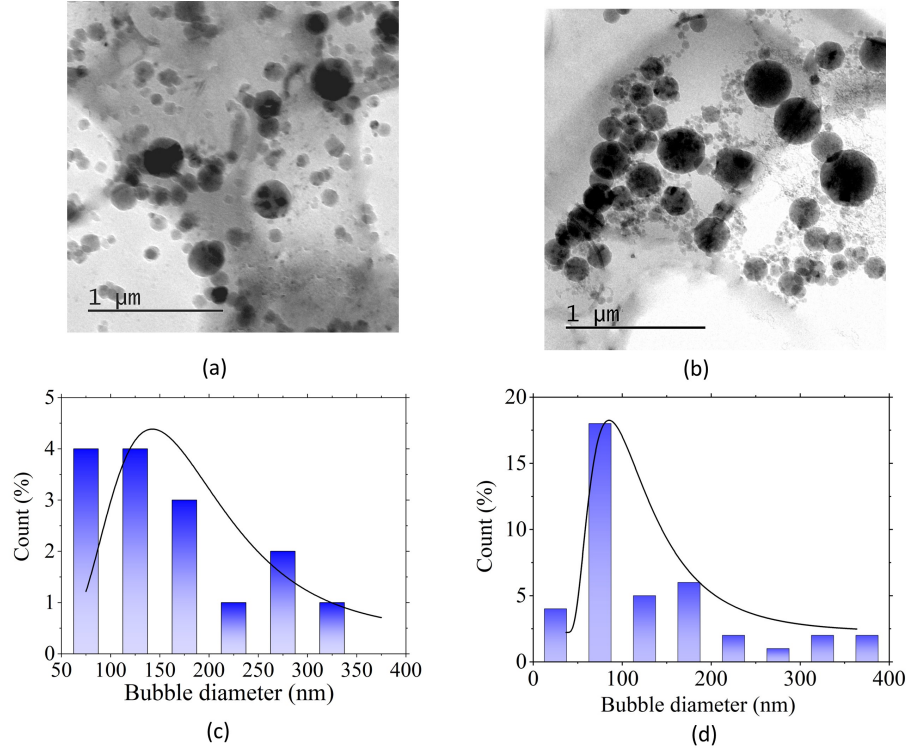


Figure 3.3: Cryo-TEM micrographs for nanobubble suspension generated in (a) 1 mM NaCl (b) 0 mM NaCl (c) nanobubble size distribution (1 mM NaCl) (d) nanobubble size distribution (0 mM NaCl).

higher than the particle tracking method. On the other hand, the Cryo-TEM method predicts a much smaller nanobubbles size range (50.113 nm is the lowest size) 1 mM NaCl (see **Figure. 3.3c**) and (12.185 nm is the lowest size) in 0 mM NaCl (see **Figure. 3.3d**). As expected, the Cryo-TEM method also predicts the mean diameter of objects in pure water to be higher than in salt solution (see **Figure. 3.3a** and **3.3b**). However, the Cryo-TEM method underestimates the bubble size (**Figure. 3.3b**) with respect to the dynamic light scattering and particle tracking method. Note that nanobubbles were frozen in liquid ethane, and the images were taken by TEM. So the state of water during the characterization of nanobubbles by Cryo-TEM and particle tracking method is different. Despite the different working principles of Cryo-TEM, dynamic light scattering, and particle tracking methods, the mean diameter of the objects in pure water is measured to be smaller than in the salt solution. The reasoning behind the behavior of nanobubbles in the presence of salt has been described by putting forward a new theoretical model for nanobubble stability, discussed in the later section. We attempted to measure the hydrodynamic size of nanobubbles in salt solution using DLS, DLS showed an error in the measurement that the suspension is very dilute. After preparing the stock solutions, the bubble number density is extremely low (observed in the NTA) which is further enhanced by employing generation techniques for nanobubble formation. The broad size distribution was scattered with a hydrodynamic diameter

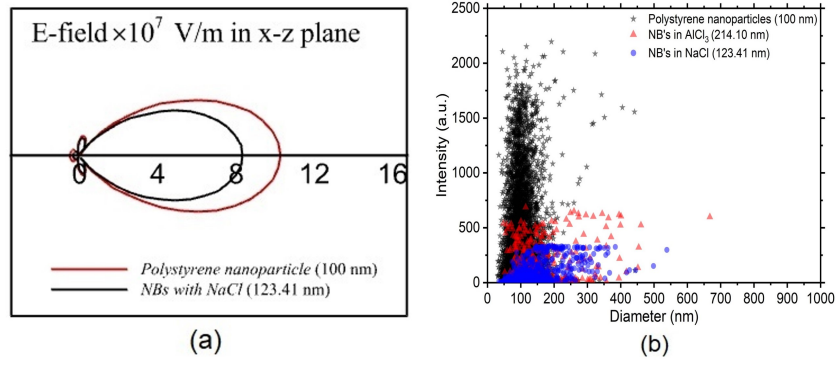


Figure 3.4: (a) Numerical comparison of the scattered electric field ( $E$ ) and (b) comparison of the Scattering intensities of 100 nm mono-dispersed Polystyrene Latex beads and the NBs generated by Salting-out effect using  $NaCl$  and  $AlCl_3$  measured by NTA

above approximately 700 nm in such polydisperse suspension of low concentration. Furthermore, it is important to compare the bubble number density by NTA and Cryo-TEM techniques. All else being equal, the bubble number density predicted by NTA and Cryo-TEM was  $\sim 10^8$  and  $\sim 10^{14}$  bubbles/mL, respectively. The Cryo-TEM not only predicts the significantly higher bubble number density but also captures the smaller size nanobubbles that are not detected by NTA owing to its inherent limitation.

### 3.3.2 Light scattering and electrical conductivity of nanobubbles

The experimental setup for oscillatory pressure fluctuation was designed to avoid the possible source of contamination (see **Figure. 3.1**). We have not only followed a strict experimental protocol but also estimated the refractive index of nanobubbles to provide experimental evidence of gas-filled bubbles. As noted earlier, bubbles, particles, and droplets behave significantly differently with light propagation. The scattered light through the nonentities contains information about the phase of the electromagnetic waves.

The light scattering from a nano-object strongly depends on its refractive index, the scattering cross-section increases with the refractive index [179, 149]. Based on the measured intensity of scattered light, the refractive index of the nano-suspension can be determined by Mie scattering theory. The scattering intensity of polystyrene nanoparticles ( $d = 100nm$ ) was used as a reference material. The scattering cross section by polystyrene nanoparticles has been compared with Mie scattering and electromagnetic wave simulation. A close match between theory and numerical simulation was observed. The corresponding simulation for nanobubbles in salt solution was performed and compared with Mie scattering theory. The far-field radiation of electromagnetic waves was gauged by the norm of the far electric field in the x-z plane. Clearly, the scattering of electromagnetic waves ( $\lambda = 405$  nm) is significantly higher for polystyrene nanoparticles in comparison with

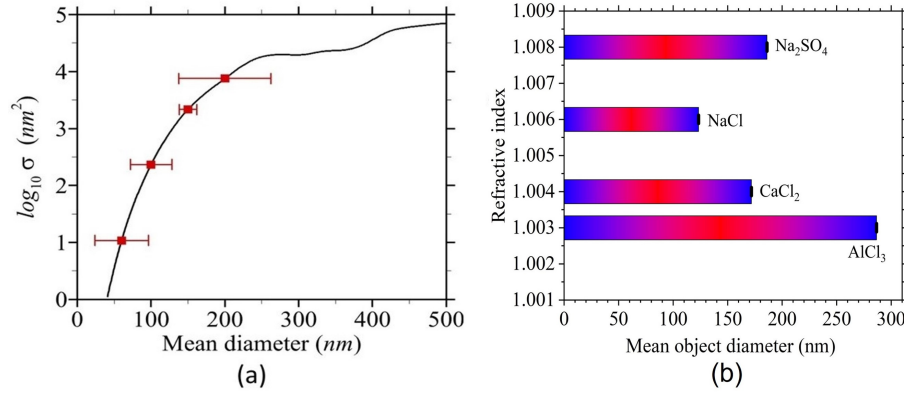


Figure 3.5: Refractive index estimation (a) The variation of scattering cross-section with the size of polystyrene nanoparticle (b) Refractive index of different salt valency.

Table 3.1: Refractive index variation with ultrasound amplitude.

Amplitude (%)	0mM NaCl	1mM NaCl
0	1.002	1.003
25	1.005	1.006
40	1.006	1.003
55	1.004	1.003
60	1.004	1.001
70	1.005	1.002
85	1.004	1.002
98	1.003	1.005

nanobubbles in NaCl solution (see **Figure. 3.4a**). The experimentally measured scattering intensity of laser light (405 nm) confirms the finding as shown in **Figure. 3.4b**. The particle tracking system is calibrated with the known refractive index of the particles, as shown in **Figure. 3.5a**. Which shows the refractive index of nanobubbles generated by oscillating pressure fluctuation in different salt solutions after salting out (see **Figure. 3.5b**). In both cases, the refractive index of nanobubbles was estimated to be close to 1. The ultrasound probe may generate nanoparticles depending on the tip quality and total operational time [180]. However, the ultrasound probe can be safely used at lower power and for a shorter operational time. We have estimated the refractive index of nanobubble treated by probe ultrasound as shown in **Table. 3.1**. The electric conductivity of the nanosuspension has also been measured. For instance, the conductivity of the Milli Q water and nanobubble water was measured to be 1.639  $\mu\text{S}.\text{cm}^{-1}$  and 1.214  $\mu\text{S}.\text{cm}^{-1}$ , respectively. The electrical conductivity of nanobubbles drops by  $\sim 25\%$ . The drastic decrease in electric conductivity can also be considered evidence of nanobubbles. Usually, the electrical conductivity of the nanoparticle suspension increases with the fraction of the nanoparticle. Since nanobubbles are gas-filled entities, the effective conductivity drops as gaseous molecules are poor conductors of electricity. In a nutshell, the electrical conductivity of the nanosuspension can

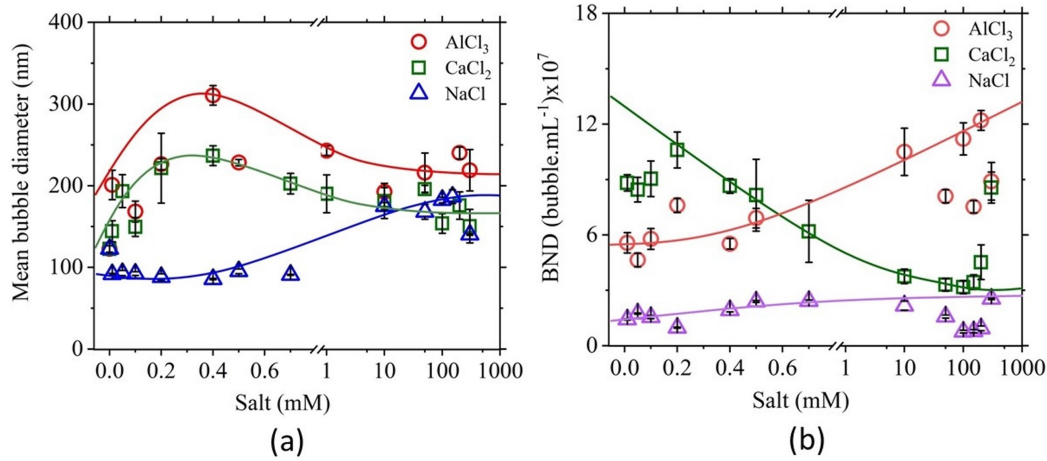


Figure 3.6: Nanobubbles dynamics in aqueous solutions of NaCl, CaCl<sub>2</sub>, and AlCl<sub>3</sub> of varying concentration (a) mean bubble diameter and (b) bubble number density.

be used to differentiate nanobubbles from nanoparticles. However, the refractive index method provides a piece of robust scientific evidence for the nanobubbles. The presence of dissolved gas shown to have a substantial influence on electrical conductivity at a lower salt as compared to higher concentrations. Though ionic effects dominate in changing the electrical conductivity, removing dissolved gases also contributes to this property. The high polarizability gas volume tends to destabilize the water structure and reduce electrical conductivity to much extent. Helium, for example, has the least effect on decreasing the electrical conductivity of water while having the lowest solubility and polarizability volume of all gases. Electrical conductivity was also shown to be temperature dependent, with conductivity increasing with increasing temperature with a slight tapering off at 60°C [181].

### 3.3.3 Nanobubble dynamics in the presence of charged ions

Indeed, nanobubbles (NBs) in bulk liquid offer enticing characteristics such as being buoyant, but their gravitational potential is small compared to  $k_B T$  and a steep rise in mass transfer efficiency. However, the puzzling stability of the nanobubbles is still in a paradoxical state. Despite the enormous Laplace pressure at the nano-sized bubble, the lifetime of the nanobubble has been measured to be days and weeks. A set of experiments were carried out in the presence of various salts in order to understand the nanobubble dynamics. It is widely known that salt exhibits screening of the electric double, and it is also expected that screening of the electric double layer strengthens with salt valency. Furthermore, charge reversal is also expected in the charged colloidal suspension, depending on the salt valency. Nanobubble in pure water was measured to have a negative zeta potential. The magnitude of the zeta potential on nanobubble decreases with the salt concentration (see **Figure. 3.7**) for NaCl and CaCl<sub>2</sub>. This is perhaps attributed to screening an electrical double layer

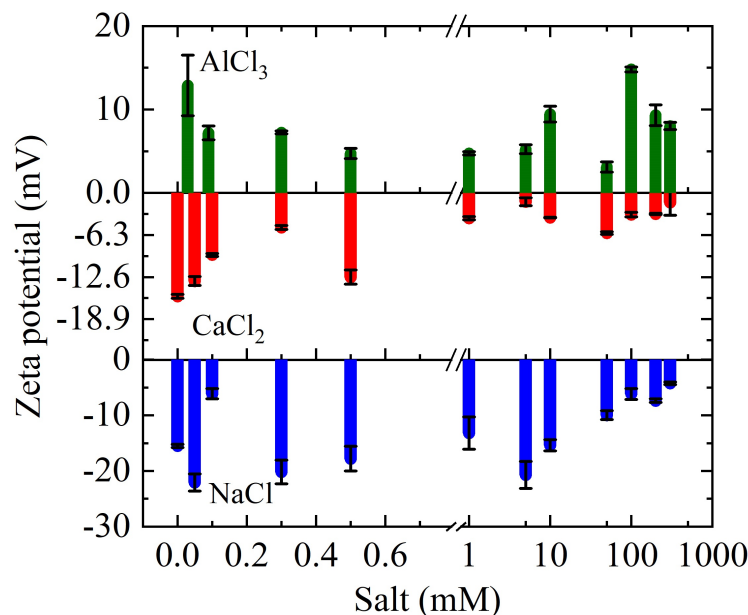


Figure 3.7: The DLS measurement of the Zeta Potentials of *NBs* aqueous solutions of *NaCl*, *CaCl*<sub>2</sub>, and *AlCl*<sub>3</sub> of varying salt concentration.

around the nanobubbles. On the other hand, the density of nanobubbles more or less decreases with salt concentration (see **Figure. 3.6b**) for *NaCl* and *CaCl*<sub>2</sub>, whereas *AlCl*<sub>3</sub> exhibits the opposite trend. The mean size of the nanobubbles was observed to be higher in the presence of salt (see **Figure. 3.6a**). The mean diameter is also measured with dynamic light scattering, confirming this trend. In other words, the equilibrium size of nanobubbles increases with a decrease in the magnitude of the zeta potential. A similar set of experiments were carried out for the divalent (*CaCl*<sub>2</sub>) and trivalent salts (*AlCl*<sub>3</sub>) (see **Figure. 3.6**). The nanobubble behavior in di-valent salt is typically similar to that of mono-valent. However, as expected, the drop in zeta potential is much steeper, as shown in **Figure. 3.7**. In other words, lower zeta potential nanobubbles are generated in the divalent salt. The higher mean diameter of the nanobubbles is generated for a given salt concentration. Some experiments were also conducted on symmetric divalent (*Na*<sub>2</sub>*SO*<sub>4</sub>) salt. However, all else being equal, the steepness of the zeta potential with salt concentration was somewhat similar to the mono-valent salt. On the other hand, a positive charge nanobubble was generated in the trivalent salt, even at a lower concentration. Trivalent salt exhibits the charge reversal at a very small salt concentration (see **Figure. 3.7**) with respect to the nanobubbles in pure water. It is also to be noted that *AlCl*<sub>3</sub> forms *HCl* by a hydrolysis reaction; therefore, the medium already becomes acidic for nanobubble generation. This is similar to the zeta potential variation with pH, where an acidic medium gives rise to the charge reversal. In addition, the proton released during the hydrolysis reaction also enhances the polarization of water molecules. Furthermore, the magnitude of the zeta potential is observed to decrease with *AlCl*<sub>3</sub>

concentration. Interestingly, the zeta potential again exhibits an inverse correlation with the equilibrium size of nanobubbles.

It is also seen that the maximum size of the nanobubbles monotonically increases with the salt valency. In a nutshell, the zeta potential seems to govern the nanobubble dynamics, and the size of nanobubbles grows in the presence of the salts. The theoretical understanding of the behavior of nanobubbles in the salt solution is explained in the later section. The zeta potential of the nanobubbles seems to play a vital role in determining their stability. It is interesting to examine the charge acquired by the nanobubbles. The property of the water at the gas-water interface and in bulk differ significantly; the libration frequency at the gas-water interface and in bulk was estimated by Sum-frequency vibrational spectroscopy (SFVS) to be  $834\text{ cm}^{-1}$  and  $670\text{ cm}^{-1}$ , respectively [182]. Although, time-averaged structure,  $\text{OH}^-$  stretch, and pico-second structural dynamics do not differ between the gas-water interface and the bulk water. Indeed, the libration frequency has a direct correlation with the stiffness of the rotational potential of water, the increase in the libration frequency may, as a result of the termination of the hydrogen bonding network at the gas-water interface retarding rotation of water around intact hydrogen bonds [182]. The electrical properties (dielectric permittivity, dipole moment) of the water at the interface differ from their bulk water values within more or less a nanometer. Similarly, the solvation and dissociation properties of the water also change at the interface, the gas molecules prone to dissolving rather than the ions and hydrophilic solutes. This phenomenon perhaps directly affects the surface tension, and the drop in the surface tension is the so-called Jones-Ray effect [183]. The ions inherently abundant in the water, such as hydrogen and hydroxide ions, also exhibit differently at the air-water interface than the bulk water. Both  $\text{OH}^-$  and  $\text{H}_3\text{O}^+$  can adsorb at the gas/water interfaces, but certainly, they can not absorb simultaneously because of their rapid association and dissociation to form water. From the experimental zeta potential, the gas-water interface prefers  $\text{OH}^-$  ions over the  $\text{H}_3\text{O}^+$  ions. In addition, other gases, such as carbon dioxide, may form the carbonate and bicarbonate ions, further enhancing the negative zeta potential [184]. On the other hand, strong acids like HCl may undergo re-association at the gas-water interface [185].

### 3.3.4 Nanobubble charging by ultrasound waves

From the preceding discussion, it is pretty clear that the zeta potential acquired by the nanobubbles is one contributor to the extraordinary stability of the nanobubbles. We also examined the presence of ions on nanobubble generation and concluded that the nanobubbles grow with the concentration of the ions. Now, it will be equally interesting if we revert the process and if we can start charging the nanobubbles. Hydrodynamic and ultrasound cavitating waves have been shown to form reactive oxygen species and free radicals together with enhanced dissociation of  $\text{OH}^-$  and



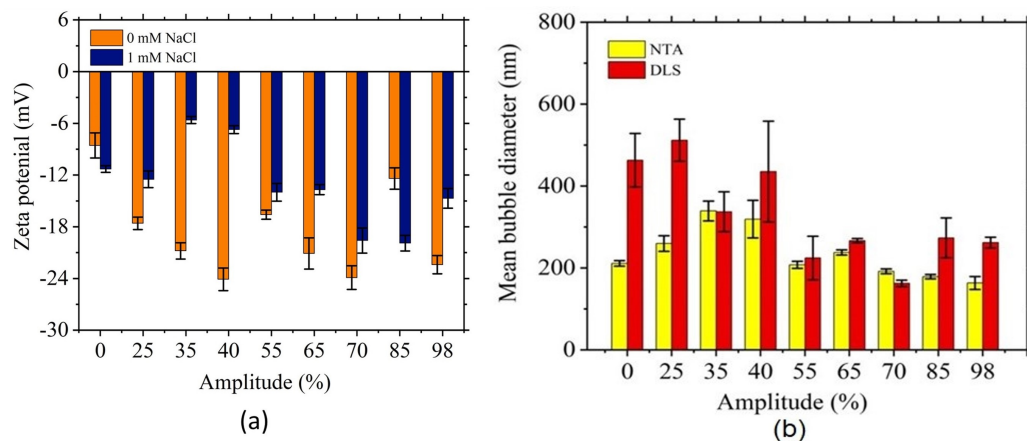


Figure 3.8: Nanobubble dynamics in terms of (a) zeta potential (b) mean bubble diameter under the effect of ultrasound amplitude.

$\text{H}_3\text{O}^+$  ions without the addition of foreign materials. Ultrasonic irradiation was performed in the bulk nanobubble suspension both in the presence and absence of the salt ions. The bubble number density, mean diameter, and zeta potential were measured with increasing amplitude percentage (increasing power) for a fixed period. The molar concentration of monovalent salt (NaCl) was chosen to be one mM, on which the nanobubble was generated by oscillating pressure fluctuation. The nanobubble sample of 60 mL volume was subjected to the 20 kHz ultrasound for 5 mins. The same procedure is adopted for pure water nanobubble samples. The bubble size distribution was observed to be shifted towards the left, leading to the narrow bubble size distribution. This narrow size distribution is reflected in the mean bubble diameter. This trend has been verified further by the dynamic light scattering (DLS) method in addition to the particle tracking technique. Furthermore, the zeta potential of the nanobubble was observed to be enhanced with the increase in the ultrasound amplitude (see **Figure. 3.8a**). However, this effect was observed to be more pronounced in pure water than in the presence of ions. Similar experiments were performed for pure water (see **Figure. 3.8b**). In summary, the mean bubble diameter of the nanobubbles decreases with the zeta potential during the charging of the nanobubbles by ultrasound waves.

The long-term stability of the nanobubbles was measured by monitoring the bubble size distribution over 2 to 3 weeks. The nanobubbles in the presence of salt ions are observed to die out much faster in comparison to the nanobubbles in pure water. Nanobubbles in pure water was observed to be survived for more than two weeks, while nanobubbles in the presence of salt ions decay in a week. The plausible reason is that perhaps the screening of the electric double layer may be responsible for the rapid decay of the nanobubbles in the presence of ions. In addition, the weak zeta potential on the nanobubbles also results in less colloidal stability of the system, and therefore, it can also be speculated that nanobubbles

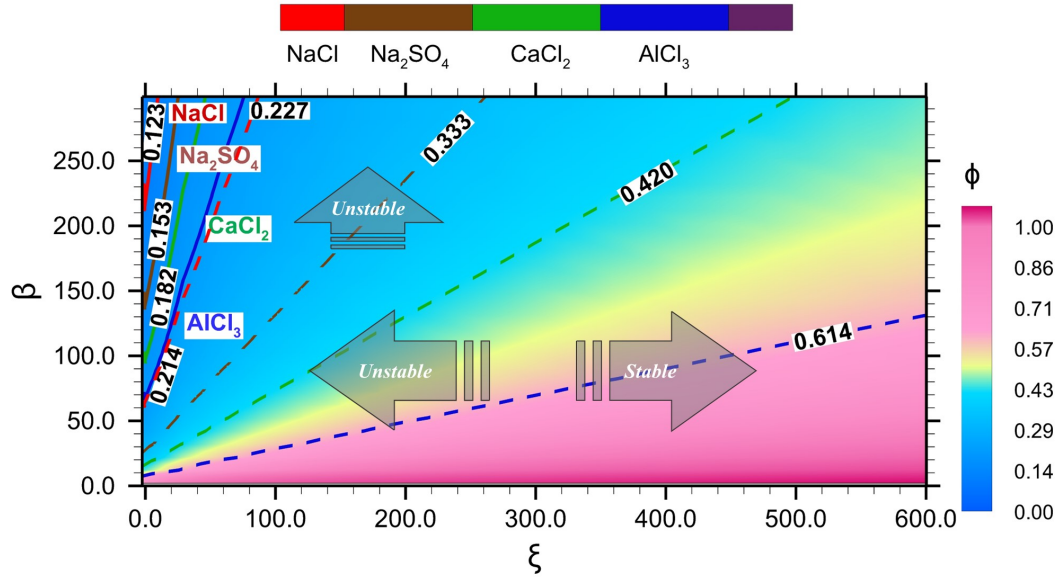


Figure 3.9: The nanobubble mechanical stability map comprising the contour value of  $\phi$  obtained from the **Eq. 3.12** for various values of  $\beta$  and  $\xi$  and for a fixed  $\alpha = 1$ . The values obtained using the experiment are shown with the solid lines, and the corresponding theoretical values of  $\beta$  and  $\xi$  are estimated from the relation **Eq. 3.13**.

should disappear relatively faster in the presence of salt ions rather than in pure water. On the other hand, nanobubbles treated with ultrasound waves were observed to have the highest stability due to the strong zeta potential. The refractive index of the nanobubbles was also estimated during the charging of the nanobubbles by ultrasound waves to avoid contamination. The refractive index of oil droplets in water and nanoparticles was reported to be more than 1.330. For nanobubbles in pure water and electrolyte solution, the refractive index value was evaluated to be in the range of 1.020 - 1.030, which affirmed the absence of contamination during the charging of nanobubbles. Long-term monitoring of the nanobubble suspensions over more than two weeks shows that the bubble size distribution retains its shape, but the peak gradually steps down over time. There is no such substantial difference in the mean diameter, suggesting the absence of significant bubble coalescence, bubble breakage, or Ostwald ripening effects due to the zeta potential. In a nutshell, the electrically charged liquid-gas interface provides a repulsive force to prevent bubble coalescence and the high dissolved gas content in the water. This highly contributes to nanobubble stability over a period of time.

### 3.3.5 Single nanobubble stability theory

Nanobubbles have various peculiar characteristics discussed in the preceding section, extraordinary longevity, negative zeta potential, strong DLVO potential, etc. However, the mechanical stability of the nanobubbles is still a puzzling question. Considering the electrostatic pressure provides stability to the nanobubbles, which



acts opposite to the surface tension force. On the other hand, the ionic forces are expected to act against the electrostatic and Laplace pressure. Recently, [87] considered these ionic forces derived from the solution of the spherical Poisson-Boltzmann equation. We have adopted this term in the force balance in the stability model. Consider a charged spherical nanobubble experiencing an electrostatic expanding pressure due to the zeta potential. The surface tension force acts tangential at the interface of the bubble. On the other hand, the liquid and the gas pressure are expected to exert opposite to each other. Let us consider the ionic pressure arising from the Coulombic force between opposite ions at the interface as shown in **Figure. 3.9**. The Poisson equation around the nanobubble for potential distribution can be written as follows:

$$\frac{\partial^2 \psi}{\partial x_i^2} = -\frac{\rho_e}{\epsilon_r \epsilon_0} \quad (3.2)$$

where  $\rho_e$  is the local electric charge density in C/m<sup>3</sup>,  $\epsilon_r$  is the relative dielectric constant, and  $\epsilon_0$  is the permittivity of the free space. Based on the assumption of axial symmetry, the Poisson equation can be written as follows:

$$\frac{1}{r^2} \frac{d}{dr} \left( r^2 \frac{d\psi}{dr} \right) = -\frac{\rho_e}{\epsilon_r \epsilon_0} \quad (3.3)$$

The boundary conditions can be written as follows:

$$\frac{d\psi}{dn} = -\frac{\sigma_i}{\epsilon_r \epsilon_0} \quad (3.4)$$

where  $\sigma$  is the surface charge density and  $n$  is normal to the surface at the sphere. For any conservative force field, the force field can be written as follows:

$$E = \frac{\partial \psi}{\partial n_i} \quad (3.5)$$

where  $F_{ionic} = qE$ .

The pressure can be written as follows:

$$p = \frac{F}{4\pi R_c^2} = \frac{q\sigma_i}{4\pi R_c^2 \epsilon_r \epsilon_0}$$

$$\text{or } P_{ionic} = \frac{\sigma_i^2}{\epsilon_r \epsilon_0}$$

On the other hand, the electrostatic pressure act opposite to the ionic pressure. The electrostatic pressure can be derived by assuming two hemispheres and the force is acting to expand these hemispheres. The following expression can be written for electrostatic pressure:

$$P_{electrostatic} = \frac{\sigma_e^2}{2\epsilon_r \epsilon_0}$$

The thickness of the first layer of the opposite ion can be assumed to be much smaller than the radius of the nanobubble. The ions can be considered to be the point charge. We can assume the validity of the local electro-neutrality condition near the surface of the nanobubble. With this reasoning, the surface charge density

can be approximated  $\sigma_e \approx \sigma_i = \sigma$ . Therefore, the force balance around nanobubbles can be given as follows:

$$P_g + P_{electrostatic} = P_L + \frac{2\gamma}{R_c} + P_{ionic} \quad (3.6)$$

$$P_g + \frac{\sigma_e^2}{2\epsilon_r\epsilon_0} = P_L + \frac{2\gamma}{R_c} + \frac{\sigma_i^2}{\epsilon_r\epsilon_0} \quad (3.7)$$

or

$$P_g = P_L + \frac{2\gamma}{R_c} + \frac{\sigma^2}{2\epsilon_r\epsilon_0} \quad (3.8)$$

The equation of the state for the real gas can be expressed as follows:

$$P_g = P_{BO} \left( \frac{R_0}{R_C} \right)^3 \quad (3.9)$$

where  $P_{BO}$  is the gas pressure at  $R_0$ . From the charge conservation, the surface charge density can be written as follows:

$$\sigma = \frac{\sigma_0 R_0^2}{R_c^2} \quad (3.10)$$

Upon substitution **Eq.3.7** can be re-written as follows:

$$P_{BO} \left( \frac{R_0}{R_C} \right)^3 = P_L + \frac{2\gamma R_0}{R_c R_0} + \frac{\sigma_0^2}{2\epsilon_r\epsilon_0} \left( \frac{R_0}{R_C} \right)^4 \quad (3.11)$$

or

$$\phi^3 - \zeta \phi^4 - \beta \phi - \alpha = 0 \quad (3.12)$$

where

$$\frac{R_0}{R_C} = \phi; \frac{P_L}{P_{BO}} = \alpha; \frac{2\gamma}{R_0 P_{BO}} = \beta; \frac{\sigma_0^2}{2\epsilon_r\epsilon_0 P_{BO}} = \zeta \quad (3.13)$$

The inverse of the roots of the cubic equation (**Eq. 3.12**) for a range of value of  $\alpha, \beta, \zeta$  have been plotted in **Figure. 3.9** for a fixed value of  $\alpha$  and range of values of  $\beta$  and  $\zeta$ . The surface charge density is calculated by the zeta potential and size of nanobubbles using the Debye-Huckel approximation ( $\sigma = \frac{\epsilon_0 \epsilon_r \psi}{\lambda_d}$ ). Sample calculations were also performed using the complete analytical solutions of the Possion-Boltzman equation reported by [186]. No significant differences were observed between these two methods. The theoretical value of  $\phi^{-1}$  was estimated and compared with the experimental results for a given value of zeta potential and surface tension. The difference between the two values indicates the experimental deviation from the proposed theory. The nanobubble stability map predicts the existence of stable nanobubbles. Our results fall in the stable regime of the nanobubbles. However, the theoretical and experimental results deviate significantly as we compared the stability of the single nanobubble with the nanobubble cloud from the experiments. The present model does not predict the actual behavior of nanobubble clouds. However, the theory is important to understand the effect of surface charge and surface tension on nanobubble dynamics. The parameter  $\zeta$  corresponds to the zeta potential on the nanobubbles, and the critical size of the nanobubbles increases with an increase in  $\zeta$ , and for a fixed value of  $\beta$  and

$\alpha$ , a decrease in charge of the nanobubble reaches towards the unstable regime of nanobubbles. On the other hand,  $\beta$  corresponds to the surface tension and leads to the collapse of the nanobubbles system in an unstable regime. In a nutshell, nanobubbles are not stable for all values of  $\zeta$  and  $\beta$ , but it is only stable when the zeta potential and surface tension of the nanobubbles are balanced with gas pressure inside the bubble.

### 3.3.6 DLVO interaction potential of nanobubbles

In the preceding discussion, it was noted that the long-term stability of the nanobubbles strongly depends on the zeta potential. For instance, the nanobubbles treated with ultrasound waves acquired the highest zeta potential, and the nanobubbles in the presence of salt ions were measured to be the lowest zeta potential. The long-term stability was observed to be highest for the nanobubbles with higher zeta potential. The zeta potential also contributes to the colloidal stability of the nanosuspension. The nanobubbles suspended in the water can be considered a nanosuspension, and the DLVO interaction potential may be used to gain insight into the long-term stability of the nanobubbles. Undoubtedly, any charge interface undergoes the formation of an electric double layer characterized by the Debye length. The salt valency and the concentration determine the Debye length. Debye length exponentially decreases with salt concentration. The classical DLVO theory has been used to evaluate the total interaction potential of the nanobubbles. The classical DLVO theory includes van der Waals and electrostatic potentials. The total interaction potential ( $w_T(D)$ ) between nanobubbles consists of the van der Waals and electrostatic potentials that can be written as follows:

$$w_T(D) = w_R(D) + w_A(D) \quad (3.14)$$

i.e.,

$$w_T(D) = \frac{1}{2}RZ\exp(-\kappa D) - \frac{AR}{12D} \quad (3.15)$$

where  $w_R(D)$ ,  $w_A(D)$ ,  $R$ ,  $D$ , and  $A$  are, respectively, the electrostatic potential, van der Waals potential, mean radius of the nanobubbles, the interspacing distance between nanobubbles and the Hamaker constant.  $\kappa$  is the inverse of the Debye–Hückel screening length. The interaction constant ( $Z$ ) is stated by the following expression [187, 186]:

$$Z = 64\pi\epsilon\epsilon_0\left(\frac{k_BT}{e}\right)\tanh^2\left(\frac{ze\Psi_0}{4k_BT}\right) \quad (3.16)$$

where  $\psi_0$  is the surface potential. According to Lifshitz theory, the Hamaker constant  $A_{132}$  between material 1 and material 2 interacting over material 3 can be calculated from the frequency dependence of the dielectric function  $\epsilon$  using the following equation [188]:

$$A_{132} = \frac{3}{4}k_B T \left( \frac{\epsilon_1 - \epsilon_3}{\epsilon_1 + \epsilon_3} \right) \left( \frac{\epsilon_2 - \epsilon_3}{\epsilon_2 + \epsilon_3} \right) + \frac{3h}{4\pi} \int_{v_1}^{\infty} \left( \frac{\epsilon_1(iv) - \epsilon_3(iv)}{\epsilon_1(iv) + \epsilon_3(iv)} \right) \left( \frac{\epsilon_2(iv) - \epsilon_3(iv)}{\epsilon_2(iv) + \epsilon_3(iv)} \right) dv \quad (3.17)$$

where  $k_B$  is the Boltzmann constant,  $T$  is the absolute temperature, and  $h$  is Planck's constant. Equation 3.16 is approximated formula for eq 3.15 that is often used for organic and inorganic materials.

$$A_{132} = \frac{3k_B T}{2} \sum_{n=0}^{\infty} \sum_{s=1}^{\infty} \frac{(\Delta_{13}\Delta_{23})^s}{s^3} \quad (3.18)$$

The prime symbol that refers to the first summation indicates that the value is multiplied by 0.5 when  $n = 0$  (the static contribution). Each parameter in eq 3.18 is calculated employing Eqs 3.19-3.21.

$$\Delta_{kj} = \frac{\epsilon_k(i\xi_n) - \epsilon_j(i\xi_n)}{\epsilon_k(i\xi_n) + \epsilon_j(i\xi_n)} \quad (3.19)$$

$$\xi_n = n \frac{4\pi^2 k_B T}{h} \quad (3.20)$$

$$\epsilon(i\xi_n) = 1 + \frac{C_{UV}}{1 + (\xi_n/\omega_{UV})^2} + \frac{C_{IR}}{1 + (\xi_n/\omega_{IR})^2} \quad (3.21)$$

By this approach, the Hamaker constant for an air-water system is estimated based on Lifshitz theory and is given by:

$$A = \frac{3}{4}k_B T \left( \frac{\epsilon_1 - \epsilon_2}{\epsilon_1 + \epsilon_2} \right) + \frac{3h\nu_e}{16} \frac{(n_1^2 - n_2^2)^2}{(n_1^2 + n_2^2)^{3/2}} \quad (3.22)$$

where  $\epsilon_1$ ,  $\epsilon_2$ ,  $h$ ,  $\nu_e$ ,  $n_1$  and  $n_2$  are permittivity of air and water, Planck constant, absorption frequency of water and refractive index of air and water. The values of these constants are as follows:  $\epsilon_0 = 8.854187 \times 10^{-12} m^{-3} kg^{-1} s^4 A^2$ ;  $k_B = 1.380 \times 10^{-23} m^{-2} kg s^{-2} K^{-1}$ ;  $\nu_e = 3 \times 10^{15} s^{-1}$ ;  $h = 6.626 \times 10^{-34} J$ . Based on the eq (10), the estimated value of the Hamaker constant for bulk nanobubbles in pure water is  $3.679 \times 10^{-20} J$ . The total interaction potential is normalized by the microscopic kinetic energy of the molecules ( $k_B T$ ) and it is plotted against the dimensionless inter-spacing distance ( $\kappa D$ ) as shown in **Figure. 3.10**.

The energy barrier in the potential curve denotes the strength of the colloidal stability. The energy barrier decreases from the monovalent ions to the trivalent (from  $785 k_B T$  to  $720 k_B T$ ). This suggests that the higher valency of the salt is more prone to destabilize than the monovalent salts. Furthermore, the energy barrier also decreases with ion concentration in the water (see **Figure. 3.10**). The lower zeta potential may be the reason behind the reduced energy barrier. Similarly, the total interaction potential has also been calculated for the charging of the nanobubbles by ultrasound waves. Evidently, the energy barrier enhances with the amplitude due to the fact that the charging of the nanobubbles gives rise to higher zeta potential on the nanobubble interface. The colloidal behavior of the nanobubbles is also seen to have in agreement with the long-term stability measurement. In summary, nanobubble

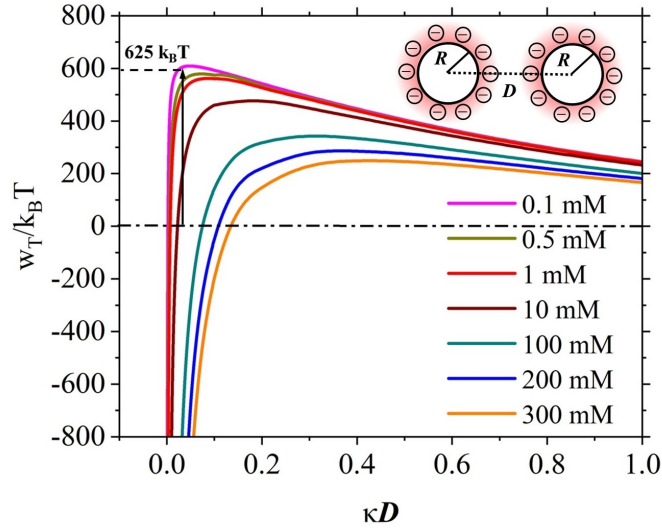


Figure 3.10: DLVO interaction potentials of bulk nanobubbles generated in aqueous salt solution of varying concentration.

in the presence of salt ions deteriorates the colloidal stability of the nanobubbles, while nanobubble charging promotes the colloidal stability of the nanobubbles.

### 3.4 Conclusion

In this work, we have examined the evidence of nanobubble generation during salting-out effects. The influence of an oscillating pressure field on nanobubble dynamics during salting-out effects has been extensively discussed. The refractive index calculation and the electrical conductivity of the nanobubbles confirmed the evidence for the gas-filled nanobubbles. A novel method for the refractive index of nanobubble is proposed based on the measured scattering power during particle tracking, where the Mie theory of light scattering is employed for scattering cross-section calculation. The screening of the electric double layer decreases the zeta potential of the nanobubbles depending on the valency of the salt. Therefore, the equilibrium size of nanobubbles was observed to be higher in the presence of salts. The mean diameter of nanobubbles exhibits the inverse dependence on the zeta potential. Our experimental findings agree well with the theoretical prediction based on the mechanical stability model. The presence of an oscillating pressure field enhances the concentration of nanobubbles compared to solely due to salting-out effects. The behavior of nanobubble under the ultrasound field has also been investigated, and it observed that the presence of the ultrasound field further enhances the nanobubble concentration and zeta potential. The colloidal stability of nanobubbles in the presence of an ultrasound field is investigated, and it is reported that the energy barrier for colloidal stability of nanobubbles under an ultrasound field is significantly higher than both nanobubbles by salting-out and

oscillating pressure field. A novel mechanical stability model for nanobubbles has been proposed by considering the ion cloud pressure, and it is shown to be twice the electrostatic pressure. The present nanobubble stability model not only predicts the existence of stable nanobubbles but is also in line with the experimental results obtained in this work.

## Chapter 4

### Does nanobubble contribute to Jones-Ray effects in aqueous salt solution?

---

The Jones-Ray effects have been debated extensively over several decades, and explanations have been put forward to understand the minima in surface tension versus salt concentration curve. However, there has yet to be a consensus about the unified theory to explain the reduction in surface tension. We have tested the hypothesis that Jones-Ray effects are due to the nucleation of nanobubbles during the salting-out effect rather than the active surface impurities. The nano-entities in the aqueous solutions of the mono-, di- and trivalent salts were characterized by particle tracking and dynamic light scattering. The measured scattering intensity is used to determine the refractive index. We find that nano-entities in the aqueous salt solutions are nanobubbles, and the refractive index was estimated to be 1.01 in all the experiments. The nanobubble contributes to the Jones-Ray effects as the minima in the surface tension curve correlate with the nanobubble number density. The minima in the surface tension curve have been seen to foster by the presence oscillatory pressure field, which also gives rise to the nucleation of nanobubbles. The charge nanobubble is expected to be adsorbed in the gas-liquid interface, resulting in a drop in the surface tension curve.

#### 4.1 Introduction

Recently, the existence of nanobubbles was discovered in dilute salt solution [189] by salting-out effects. Nanobubbles are gaseous charged nano-interface nucleates in salt solution due to gas supersaturation. From a thermodynamic viewpoint,

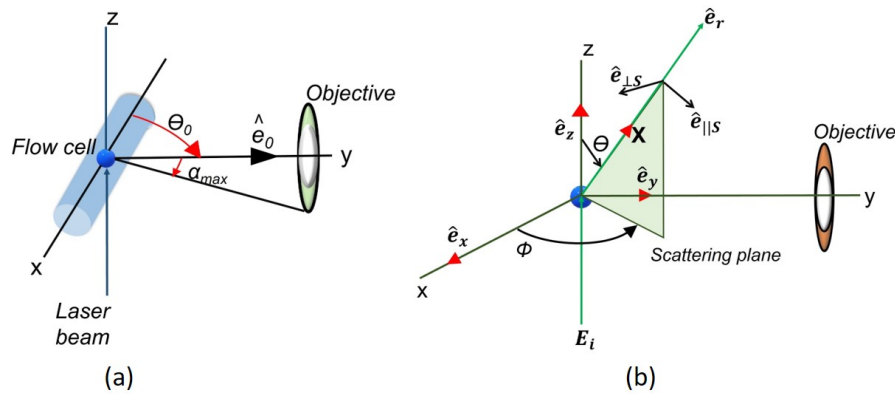


Figure 4.1: (a) Optical configuration of the NS-300. (b) The reference frame and variables used to determine the scattering intensity of a laser-illuminated spherical particle.

the formation of a new phase via nucleation is owing to the departure from the equilibrium condition. The out-of-equilibrium undergoes the formation of new interfaces and gives rise to new colloidal and interfacial phenomena. Such non-equilibrium conditions are often driven by either one or multiple volumetric forces. The salting-out effect is a decrease in the solubility of the gas by dissolving the salt in water [167, 168]. The amount of dissolved gas in water at a given temperature and pressure is expected to be decided by thermodynamic equilibrium. The equilibrium condition for such a multi-component system is often described by Gibbs free energy. At a given pressure and temperature, Gibbs free energy exhibits dependence on the chemical potential of the individual components. In the salting-out effect, the chemical potential of the system (for an ideal solution  $\mu_i = \mu_{io} + RT \ln(x_i)$ ) increases by salt addition. Furthermore, the system may be shifted to a new equilibrium state by minimizing the energy of the system. The energy dissipation may be utilized to create new interfaces in nanobubbles. Similarly, the system's energy can be enhanced by work done on the system. For instance, the presence of an oscillating pressure field and ultrasound wave is expected to increase the free energy of the system. Therefore, the nanobubble population is expected to foster during the energy minimization in such cases. In a nutshell, both chemical and physical energy forms are expected to generate nanobubbles. Nevertheless, nanobubbles have shown application in engineering and medical fields, for instance, wastewater treatment [190], pharmaceutical industries [47], aquaculture [191], medical applications [192], mining [193], agriculture [194], food processing [195], etc.

Nanobubbles in the bulk liquid may also influence the interfacial properties of the liquid, such as surface tension. Surface tension is often expressed by Gibbs free energy per unit area at constant temperature and pressure ( $\gamma = (\partial \Delta G / \partial S)_{T,P}$ ). Although the free energy at thermodynamic equilibrium will be constant, the interfacial area of the system boundary may increase by the migration of nanobubbles towards the interface. In addition, the nanobubble may also facilitate the slip condition at the interface. With this reasoning, the surface tension during the salting-out effect is expected to decrease with reference to pure water. Coincidentally, the surface tension in salt solution has been reported extensively, and it decreases with salt concentration and exhibits minima at a lower salt concentration regime, widely known as the Jones-Ray effect. This effect has been debated for the past  $\sim 80$  years and provided several explanations on the existence of the minima in surface tension vs. salt concentration curve, but there is no such a consensus about the unified theory even though the experimental measurement of surface tension has been reproduced by several researchers by the wide range of measurement techniques [196, 197, 198, 199, 200, 31, 201]. The surface tension of the aqueous solution is often quantified by Gibbs adsorption isotherm, which



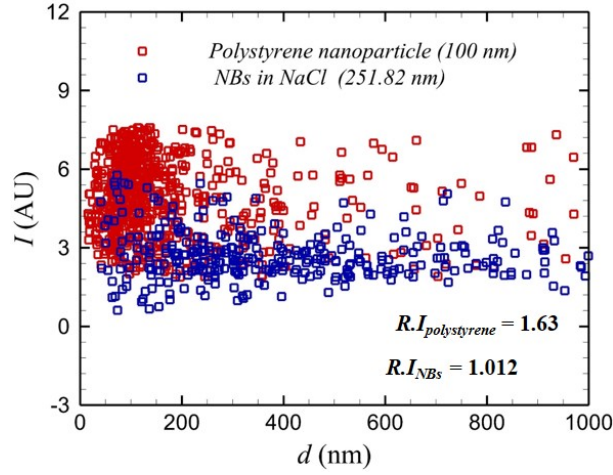


Figure 4.2: Light Scattering intensities of 100 nm mono-dispersed Polystyrene latex beads and NBs generated by the salting-out effect.

relates the surface tension with the excess surface concentration. All else being equal, ion repulsive forces are expected to exist within the limit of the higher salt concentration. Therefore, the surface tension must increase with ion concentration. Onsager and Samaras [202] considered the screened dielectric ion-surface repulsion in their model and obtained this trend quantitatively. The increase in the surface tension with salt concentration was shown to be ion-specific, and several models were proposed over the decades [203, 204, 205, 206, 207, 208, 209]. However, the minima in the surface tension curve in the limit of very low concentration have been explained by Onsager and Samaras [202] model. From a thermodynamic viewpoint, the increase in the surface tension is only justified when the ions are in excess, whilst the surface tension is expected to decrease when ions are in deficit. Jones and Ray have first reported the minima in the surface tension curve of aqueous KCl solution at very low ionic strength [210, 211, 212, 213]. The capillary rise method for surface tension measurement reported the minima in the surface tension curve at 1 mM. Subsequently, the experiments were conducted for 13 different electrolyte solutions [210, 211, 212, 213] and reported that minima in the surface tension curve occur near  $1 \pm 0.5$  mM. Later the Jones-Ray effects were reproduced by many researchers [214, 215, 216, 217]. Langmuir [200] blamed the surface charge at the water interface responsible for Jones-Ray effects. Cassel [183] reported an alternative view that perhaps the enhanced wettability or increase in wetting contact angle is responsible for a decrease in the surface tension.

The early speculations were the experimental artifacts and presence of surface active agents, and therefore, researchers attempted different measurement techniques. For instance, Dole and Swartout [218] used a surface tension apparatus having twin-ring made of 90% Platinum and 10% Iridium. They [218] successfully reproduced the Jones-Ray results. Similarly, Long and Nutting [31] utilized the bubble pressure method; however, the measurement was suspected

of the presence of organic and atmospheric CO<sub>2</sub> impurities. More recently [219] theoretically investigated the presence of minute surfactant impurities by solving the Poisson-Boltzmann equation for electrostatic potential with the Gibbs adsorption isotherm. The author claimed that the low concentrations of surfactant impurity might be sufficient for the Jones-Ray effect, and perhaps that may not fall under the detection limit of the spectroscopic techniques. However, the recent work by Okur et al. [220] and Bu et al. [221] ruled out the possibility of the surfactant. Okur et al. [220] repeated the surface tension measurements with the addition of a small amount of surfactants. The surface tension measured by the Wilhelmy plate exhibits minima, but the values are significantly different. Petersen et al. [214] investigated the effect of surface concentration of anions in the salt solutions to verify the Jones-Ray effects. Petersen et al. [214] used a surface-selective second-order non-linear optical response to measure the iodide concentration at the surface. No such physical binding sites for anions were revealed in their experiments. To date, the Jones-Ray effect is considered a surface phenomenon, and most researchers assume that rare or unknown ion or ion pair binding sites are a plausible mechanism for the Jones-Ray effect. The mechanism of the non-ion-specific binding site is difficult to believe at very low concentrations of salts.

In this work, we have investigated the role of nanobubbles while measuring the surface tension of water during the salting-out effect. We have tested the hypothesis that Jones-Ray effects may be due to the nucleation of nanobubbles during the salting-out effect. The evidence of the nanobubbles is provided in terms of refractive index measurement of nano-object based on Mie scattering and electromagnetic wave simulation. The nano-entities in the aqueous solutions of the mono-, di- and trivalent salts were characterized by particle tracking and dynamic light scattering. The measured scattering intensity is used to determine the refractive index. The surface charge of the nanobubbles was measured by dynamic light scattering. The nanobubbles during salting-out effects were also observed to be extraordinarily stable in the aqueous solution.

## 4.2 Experimental methods

### 4.2.1 Materials

Milli-Q water (Merck Millipore water purification system) is characterized by a pH of 6.9 and an electrical conductivity of 1.357  $\mu\text{S}\cdot\text{cm}^{-1}$  at 20°C. Both salting-out experiments and oscillating pressure fields were carried out using Milli-Q water. The AR grades of salts were purchased from Merck chemicals (aluminum chloride (AlCl<sub>3</sub>, 99.9%), calcium chloride (CaCl<sub>2</sub>, 99.5%), sodium sulphate (Na<sub>2</sub>SO<sub>4</sub>, 99.5%) and sodium chloride (NaCl, 99.5%). Stringent experimental methods were followed to avoid contamination; disposable silicon-free syringes (HSW NORM-JECT®), glass

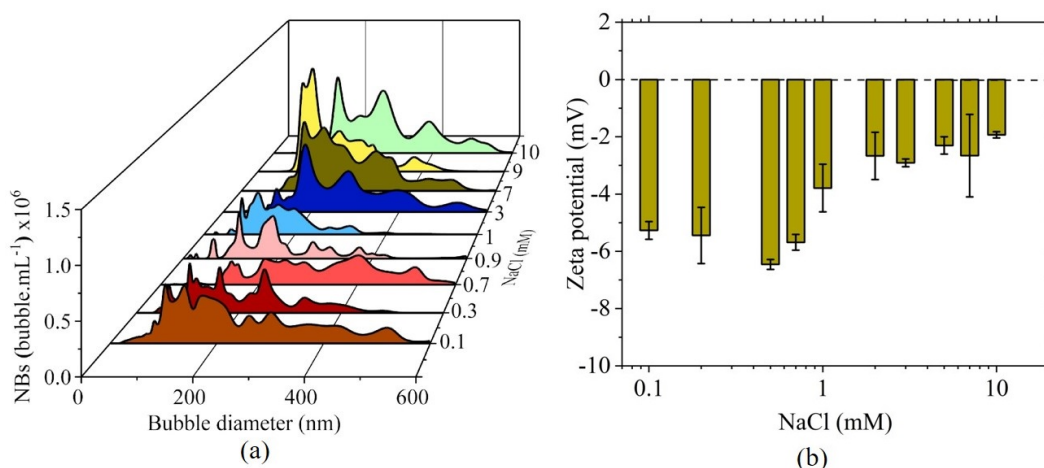


Figure 4.3: Nanobubbles during salting-out effects in NaCl solution (a) bubble size distribution (b) zeta potential.

vials, and glass pipettes were used throughout the experiments. A 20 mL vial is used to store the sample for further analysis. Similarly, a careful characterization of the nanobubble size distribution and the surface charge was performed and ensured reliability by triplicating the measurements.

#### 4.2.2 Nanobubble characterization by particle tracking and dynamic light scattering method

The nanobubble concentration and size distribution were measured by the nanoparticle tracking analysis. A 405 nm Violet laser is used to illuminate the nanobubble sample. The scattered light and the Brownian motion of the nanobubbles were captured by an sCMOS camera. Furthermore, the size and concentration of the nanobubbles were determined by nanoparticle tracking analysis (NTA) software (NanoSight NS300 & NTA 3.3 Analytical Software, Malvern Instrument, United Kingdom). The mean square displacement facilitates the calculation of the diffusion coefficient and further the mean size and concentration of the nanobubbles via the Einstein-Stoke equation. The surface potential is estimated by measuring the electrophoretic mobility of the nanobubbles by the dynamic light scattering (DLS) technique (Zetasizer Nano ZSP, Malvern Instruments, UK)

#### 4.2.3 Surface tension measurement

The Wilhelmy plate method is used to measure the surface tension of nanobubble water by the Attension Sigma Force Tensiometer 700. All the experimental protocols are followed to avoid errors in the measurement. After every measurement, flaming is used to clean the surface to avoid organic impurities. The surface tension measurement was obtained at precisely 25°C using the software provided by the manufacturer.

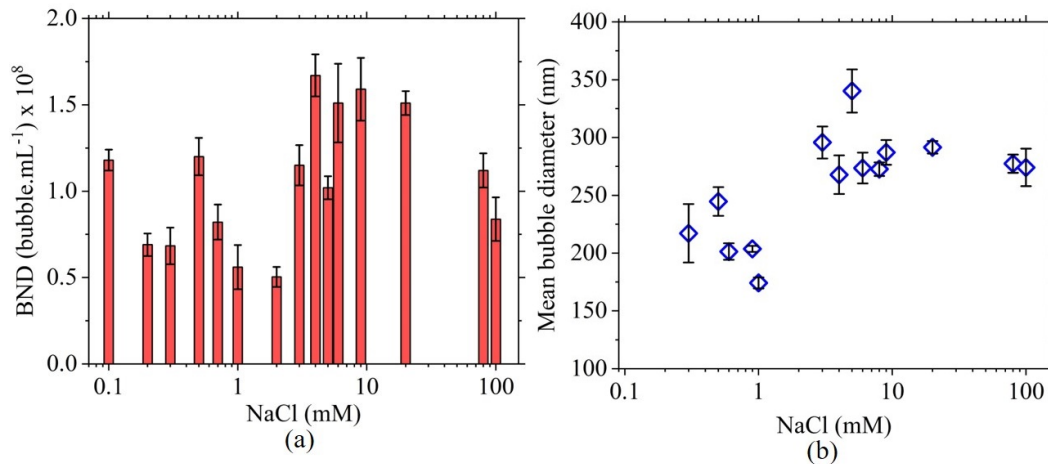


Figure 4.4: Nanobubbles during salting-out effects in NaCl solution (a) bubble number density (b) mean bubble diameter.

## 4.3 Results and discussion

### 4.3.1 Evidence of nanobubbles

From a thermodynamic viewpoint, it is pretty clear that the system undergoes energy minimization and attains a new equilibrium state. The salt ions now replace the dissolved gas molecules, and one can deduce from the drop in the gas solubility. Now the critical question is how the gaseous molecules spontaneously form the nanobubbles. Part of the free energy may be invested in creating the nanobubbles during the energy minimization. Thus, from thermodynamics, the formation of the new surfaces is justified. Here we have examined if they are gas-filled nanobubbles; they must exhibit the properties of the bubble. Before discussing the detailed results, it is necessary to mention that additional precautions were taken to avoid contamination in the experimental rig. The wetted part of the experimental setup for the oscillatory pressure field is made of all glass. Although the piston and syringe assembly is not a wetted part, the piston and cylinder system was cleaned with ethanol and dried with nitrogen. In this work, scattered light from the nanobubbles and nanoparticles is measured and compared. Evidently, the intensity of the scattering from a given object depends on the refractive index of the medium and the dispersed objects. The scattering cross-section of the dispersed object increases with the refractive index [179, 149]. The light propagation around a dispersed object can be modeled by solving the electromagnetic wave equations. The analytical solutions of the electromagnetic waves around a spherical object are available in terms of Mie scattering theory. The measured values of the scattering intensity can be used to calculate the refractive index of the nano-suspension by Mie scattering theory (see **Figure. 4.1**). Standard nanoparticles have been used to calibrate the NS300. Polystyrene nanoparticles ( $d = 100\text{nm}$ ) of refractive index 1.63 were

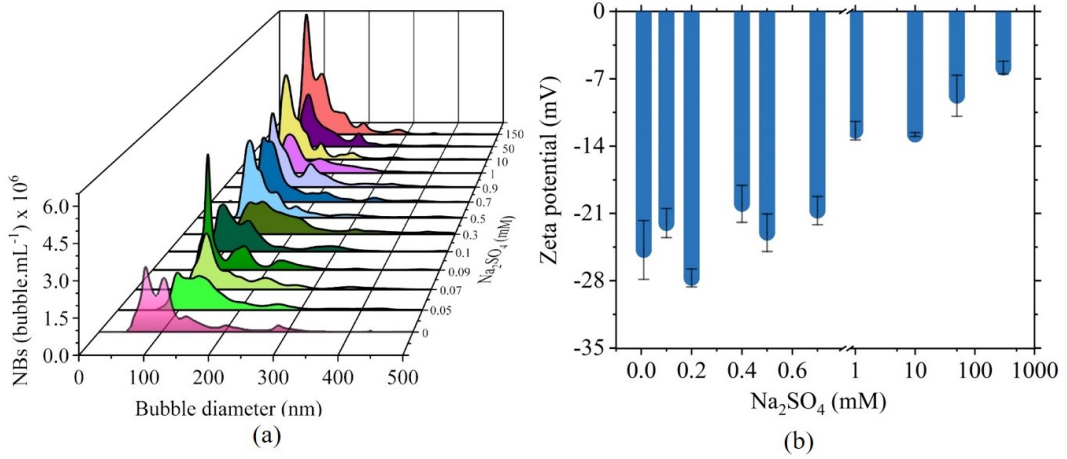


Figure 4.5: Effect of oscillating pressure on nanobubble generation in Na<sub>2</sub>SO<sub>4</sub> (a) bubble size distribution (b) zeta potential.

used to calculate the machine constant. The distribution of scattering power of the nanobubble sample was recorded. The maximum scattering power  $P_S$  (AU) is chosen as a representative scattering intensity. The scattering power of the polystyrene nanoparticles of four different sizes (50, 100, 150, and 200 nm) is correlated with the scattering cross-section  $\sigma_S$  (nm<sup>2</sup>) using the Mie theory. Open-source MieConScat software calculates the scattering cross-section for a given particle size, the refractive index of a given material and medium, and the light source wavelength. The measured  $P_S$  value is matched with the scattering cross-section  $\sigma_{Mie}$  calculated from Mie theory. The instrument constant  $\sigma_{Mie}/P_S = 0.0673$  is obtained by linear regression of the data point. The light scattering intensity of the nanobubbles and nanoparticles are shown in **Figure. 4.2**. The corresponding refractive index is calculated, and the refractive index of nanobubbles is close to 1.002. This confirms that the nano-objects during the salting-out effect is gas filled nanobubbles.

#### 4.3.2 Nanobubbles by salting-out effects

Salting-out effects are the displacement of the dissolved gas in the liquid by adding salt. The salting-out effects give rise to gas supersaturation, which is expected to release the additional dissolved gas in the liquid. In this work, we have observed that the excess dissolved gas nucleates in nanobubbles. NTA measured a wide range of nanobubbles (50-600 nm) in the different salt solutions. The bubble size distribution is observed to be shifted towards the left, suggesting that the mean nanobubble diameter is expected to be higher in the limit of higher salt concentration (see **Figure. 4.3a**). The nanobubbles during salting-out effects were measured to bear a slightly negative zeta potential ranging from -3 mV to -8 mV (see **Figure. 4.3b**). However, the magnitude of the zeta potential decreases with the salt concentration. The bubble size distribution The concentration of nanobubbles was observed to vary  $\sim 0.5 \times 10^8$  bubbles/mL to  $\sim 1.55 \times 10^8$  bubbles/mL in the low salt concentration

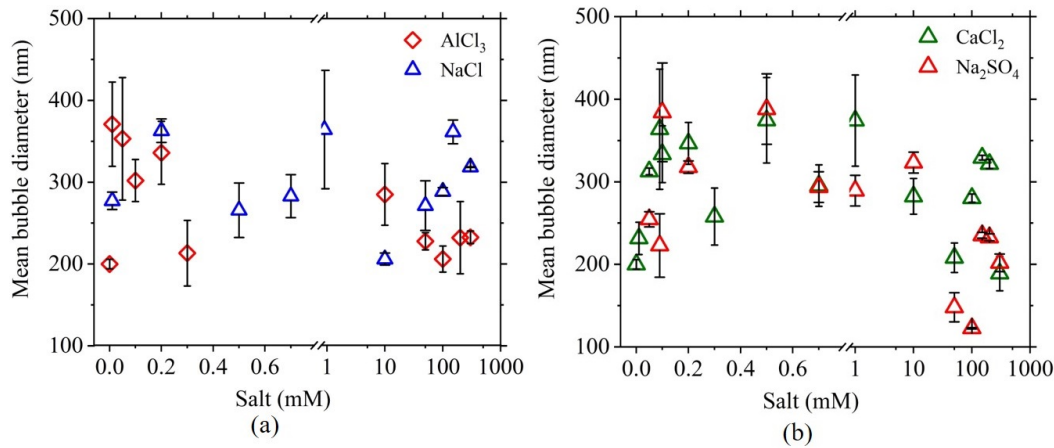


Figure 4.6: Mean bubble diameter of nanobubble suspension measured by DLS (a) mono- and trivalent salts (b) divalent salts.

regime (up to 1mM) to the higher salt concentration (from 1 mM to 100 mM, see **Figure. 4.4a**). The mean diameter of the nanobubbles in the low salt concentration regime (see **Figure. 4.4b**) was measured to be smaller than that in the higher salt concentration regime.

From the experimental measurement, it is clear that the salting-out effect generates nanobubbles of mean size ranging from  $\sim 175 - 350$  nm depending on the salt concentration. These nanobubbles also carry a negative surface charge, and the magnitude of the surface potential decreases with increasing salt concentration. The surface charge has an inverse correlation with the size of the nanobubbles. This experimental behavior can be explained by considering the force balance at the nanobubble interface [153]. The nanobubble interface carries an inherent surface charge depending on the preferential adsorption of the  $\text{OH}^-$  or  $\text{H}_3\text{O}^+$  [222]. The majority of the literature supports the adsorption of  $\text{OH}^-$ ; therefore, a negatively charged air-water interface may be a reasonably good assumption. Furthermore, the adsorbed ions  $\text{OH}^-$  are also expected to be a point charge and participate in the Coulombic interactions. The interface may not exert any normal force as long as they are flat. The curved interfaces will exert a force normal to the interface due to Coulombic interaction between similar ions. Clearly, this electrostatic force is acting to expand the interface. In addition, the charged interface also tends to form an electric double layer, and the counter ions present in the salt solution are expected to exert a net compressive force opposite to the normal of the interface. The magnitude of the so-called ion pressure force directly depends on the electrostatic force acting on the interface. When the salting-out effect occurs in the high concentration regime, the electric double layer screens, and therefore the ion pressure force weakens in the presence of the higher amount of salt ions in the solution. Therefore, the equilibrium size of the nanobubble increases with the salt concentration.

The oscillating pressure field is employed during the salting-out effect. The



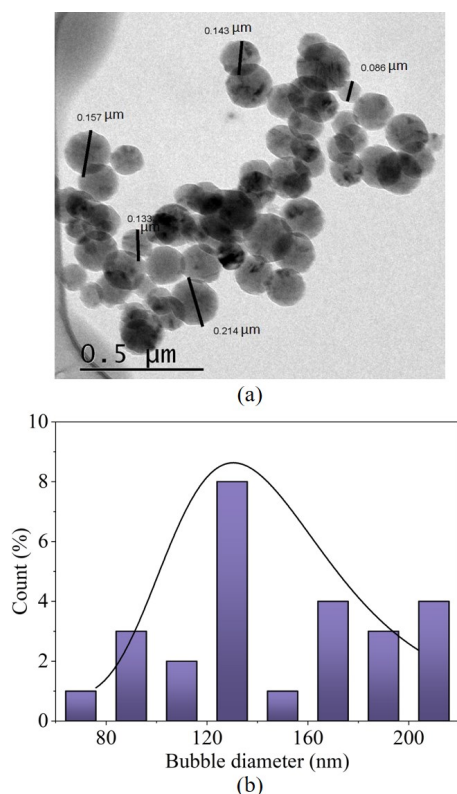


Figure 4.7: Cryo-TEM micrograph for nanobubble suspension generated in (a) 0 mM NaCl (b) nanobubble size distribution (0 mM NaCl).

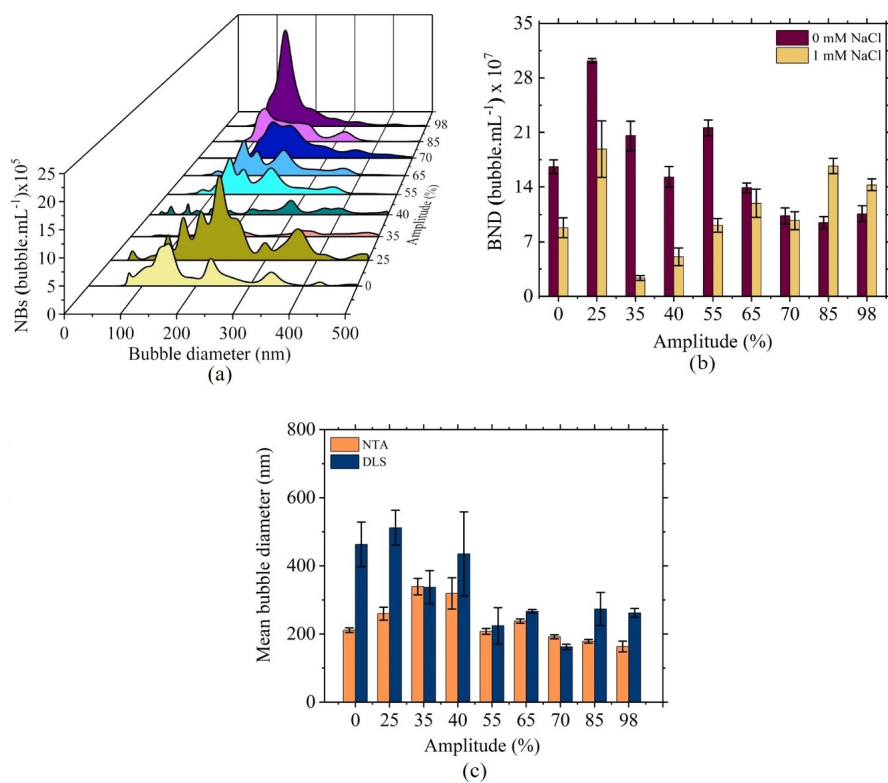


Figure 4.8: Effect of ultrasound amplitude on nanobubble solution in NaCl (a) bubble size distribution (b) bubble number density (c) mean bubble diameter.

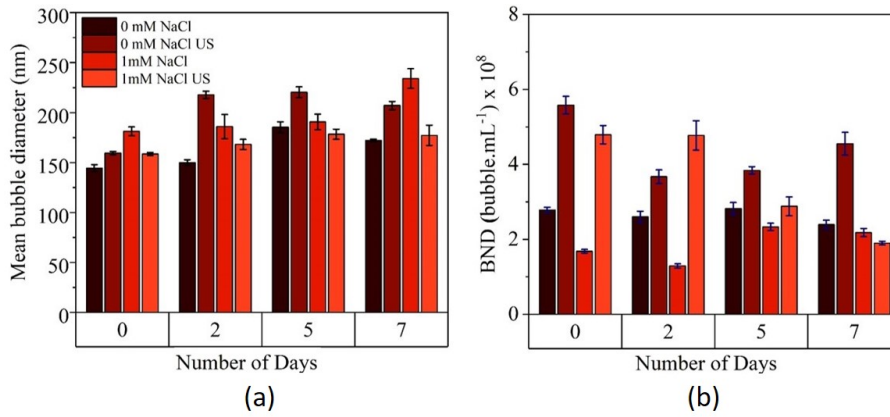


Figure 4.9: Effect of ultrasound amplitude on nanobubble stability (a) mean bubble diameter (b) bubble number density.

oscillating pressure field is generated in the U-tube by a piston pump and recorded the pressure fluctuation (it oscillates between  $-40$  to  $+40$  kPa). For instance, the bubble size distribution and zeta potential are measured in **Figure. 4.5** in  $\text{Na}_2\text{SO}_4$  solution. The bubble size distribution was observed to show qualitatively similar behavior to that of the salting-out effect alone. The distribution is observed to be shifted towards the right. The zeta potential of the nanobubbles was also measured, and the trends are qualitatively similar to the salting-out effect. However, the magnitude of the concentration of the nanobubbles and zeta potential were observed to be twice that in the salting out-effect. Some dynamic light scattering measurements on the size of the nanobubbles were also performed, as shown in **Figure. 4.6**. However, the size of the nanobubble by DLS is slightly overestimated. Cryo-TEM imaging was also performed in the case of oscillating pressure experiments, as shown in **Figure. 4.7**. The mean diameter of the nanobubbles was estimated to be  $\sim 140$  nm.

### 4.3.3 Nanobubble temporal stability

Nanobubbles during the salting-out effect carry a surface charge and therefore, the curved interface undergoes electric double-layer formation. We have observed that the nanobubbles generated by hydrodynamic cavitation or electrochemical methods [153] exhibit extraordinary longevity. We also have seen that the surface charge plays an important role in determining the equilibrium size of the nanobubble. Here we have examined the influence of ultrasound waves on the nanobubbles during the salting-out effect. Indeed, the shock waves during the ultrasound field produced by ultrasonic horn have been shown to form reactive oxygen species and free radicals. It also enhances the dissociation of  $\text{OH}^-$  and  $\text{H}_3\text{O}^+$  ions. The bubble number density (see **Figure. 4.8b**), mean diameter and surface charge were measured by varying the ultrasound amplitude. 60 mL nanobubble sample was subjected to the 20 kHz



ultrasound for 5 mins. The ultrasound field was observed to narrow the bubble size distribution in comparison with the reference sample. This narrow size distribution (see **Figure. 4.8a**) is reflected in the mean bubble diameter shown in **Figure. 4.8c**. In summary, the mean bubble diameter of the nanobubbles decreases with the charging of the nanobubbles by ultrasound waves.

The temporal stability of the nanobubbles during salting-out and treated with ultrasound was measured by monitoring the bubble size distribution over a week time. The nanobubbles during salting-out effects are observed to disappear much faster with respect to the nanobubbles in pure water. The plausible reason is that perhaps the weak surface potential may be held responsible for the faster decay of the nanobubble population during the salting-out effect. Indeed, the weak surface potential may also result in a weak colloidal system, and therefore, it can also be speculated that nanobubbles should disappear relatively faster in the presence of salt ions rather than in pure water. On the other hand, nanobubbles treated with ultrasound waves were observed to have the highest stability due to the strong surface potential. Long-term monitoring of the nanobubble suspensions over more than two weeks shows that the bubble size distribution retains its shape, but the peak gradually steps down over time. There is no such substantial difference in the mean diameter as shown in **Figure. 4.9a**, suggesting the absence of significant bubble coalescence, bubble breakage, or Ostwald ripening effects due to the surface potential. In a nutshell, the electrically charged liquid-gas interface provides a repulsive force to prevent bubble coalescence and the high dissolved gas content in the water. This highly contributes to nanobubble stability over a period of time.

Additionally, the dynamic equilibrium model states the stability of bulk nanobubbles owing to the partial hydrophobized covering that might be formed during ultrasound irradiation. The gas diffusion occurs at the peripheral edge of the hydrophobic material which counterbalances the outward gas diffusion from the uncovered bubble surface. The gradient of chemical potential is the contributing factor of the dynamic equilibrium condition assuming the no-liquid flow condition. This results in zero change in both energy and entropy. Henceforth, the first and second principles of thermodynamics are acceptable by this model. On the contrary, the bubble enveloped with hydrophilic material could not be stable unless the surface coverage fraction is 1, and for hydrophobic material ranges from approximately 0.5 to 1, as observed numerically [53].

#### 4.3.4 Role of nanobubbles in Jones-Ray effects

Nanobubbles are expected to reduce the apparent surface tension measured by the Wilhelmy plate [223] or the du Noüy ring method [224] due to the interfacial slip on the bubble surface, while the solid nanoparticles may result in the enhanced surface tension of the water. The first measurement of the surface tension was

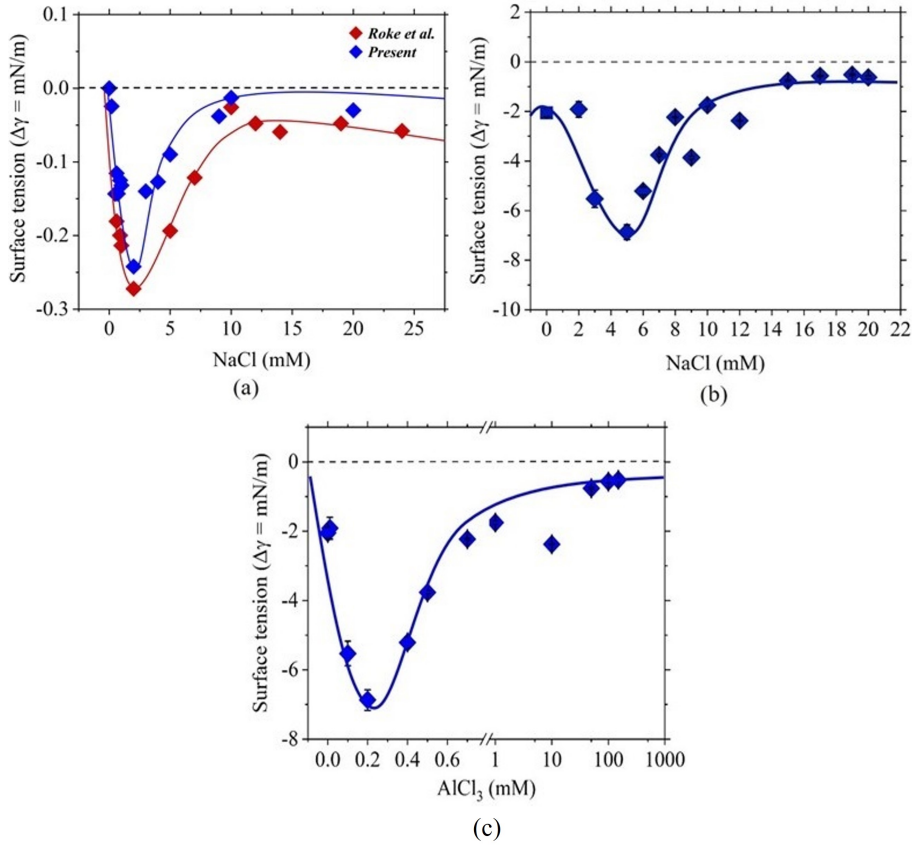


Figure 4.10: Surface tension difference ( $\Delta\gamma$ ) measured with salt concentration for nanobubble suspension (a) salting-out effect in aqueous NaCl and nanobubbles generated by pressure fluctuation in aqueous (b) NaCl (c)  $\text{AlCl}_3$ .

carried out for the salting-out effects, as shown in **Figure. 4.10a**. The surface tension drops between 1-2 mM for the NaCl, which is observed to be shifted to 1-10 mM for the  $\text{AlCl}_3$ . This drop in surface tension in the salt solution is the so-called Jones-Ray effect. As noted earlier, there is no unified theory for the Ray-Jones effect to explain the minima in the surface tension curve. We believe that the drop in the surface tension is perhaps due to the nucleation of nanobubbles [225] upon dissolution of the salt. The salting-out of the gas in the solvent occurs due to the dissolution and solvation of the ion with the water molecules. Furthermore, after the salting-out effect, the sample was treated with the oscillating pressure fluctuation device, and the surface tension was measured as shown in **Figure. 4.10b** and **Figure. 4.10c**. The minima in the surface tension curve are observed to shift towards the lower concentration of the salt. This is the expected trend as the bubble number density was highest in this limit. The nanobubble density decreases with the salt concentration, and therefore, the surface tension recovers further with increased salt concentration. This clearly suggests that surface tension and bubble number density go hand in hand. Additional experiments were performed for  $\text{CaCl}_2$  and  $\text{Na}_2\text{SO}_4$  yields similar trends (see **Figure 4.11**). The nanobubble generation during salting-out effects is due to the difference in the solubility of the gas upon the

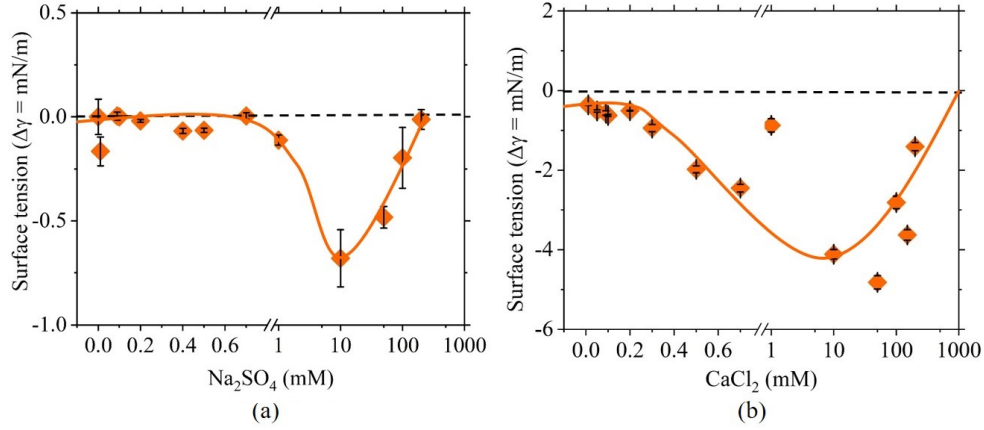


Figure 4.11: Surface tension difference ( $\Delta\gamma$ ) measured with salt concentration for nanobubbles generated by pressure fluctuation in aqueous (a) Na<sub>2</sub>SO<sub>4</sub> (b) CaCl<sub>2</sub>.

addition of salts. The refractive index measurement confirms that they are gas-filled entities. From a thermodynamic viewpoint, salt dissolution is expected to increase the free energy. Furthermore, the system may attain the next equilibrium state by minimizing the free energy. The nanobubbles may form at the expense of the additional energy to create new surfaces that undergo the out-of-equilibrium.

The decrease in the surface tension can not be explained by the Gibbs adsorption isotherm. A decrease in the surface energy requires solute adsorption near the interface. The Jones-Ray effect is a long-standing debate, and there is no consensus about the proposed mechanism discussed earlier. Most investigators assume several binding sites for ions adsorption at the air-water surface. On the other hand, the recent arguments were complex and considered a long-range ordering of the water structure having nuclear quantum effects [199, 226]. Since the Jones-Ray effect strongly violates the fundamental theory, the speculation was chance of impurities was hypothesized by theorists. However, the experimentalists were skeptical about the possibilities of impurities [199, 226]. Here, we demonstrate that the  $1.0 \times 10^8$  nanobubbles per mL exist in the bulk liquid by dissolving a very small salt concentration. These nanobubbles lead to the reduction of surface tension of the air-water interface. Refractive index measurement has proved the existence of nanobubbles in the salt solution. Now the nucleation of nanobubbles can also be explained by Gibbs adsorption isotherm. Experimental surface tension measurements have verified the claim by deliberately adding nanobubbles in the system using a pressure oscillating field.

## 4.4 Conclusions

In this work, the nanobubbles during salting-out effects and their influence on the surface tension of the water have been systematically investigated. The refractive index of the nanobubbles is estimated by Mie scattering theory based

on the measured scattering power from the nanobubbles. The nanobubbles during salting-out effects also bear a negative surface potential; however, the magnitude is much smaller than the nanobubbles generated by the oscillating pressure method. The nanobubbles, during salting-out effects, are also observed to have extraordinary longevity. The size of the nanobubbles during salting-out effects was observed to be higher than that generated by the oscillating pressure method. The surface tension of the salt solution exhibits minima in the low salt concentration regime, which is widely known Jones-Ray effect. The nanobubble may be one of the contributing factors to the Jones-Ray effects. The size of the nanobubbles in the low salt regime is smaller than that in the high salt concentration regime, and therefore, the activity of the nanobubbles is expected more in the low salt concentration regime. The magnitude of the surface tension drop significantly increases upon applying the oscillating pressure field. This perhaps indicates that nanobubbles are playing a role in decreasing the surface tension of the salt solution.

## Chapter 5

### Nanobubble Dynamics in the Presence of Surfactant Molecules and its Interaction with Nanoparticles

---

In this chapter, we have investigated how adsorbed surfactant molecules with amphiphilic behavior influence the formation of bulk nanobubbles in a gas supersaturation environment. The refractive index is computed by incorporating the data of measured scattering intensity from NTA (nanoparticle tracking analysis) using Mie theory. The surface tension of the surfactant solution was measured in the presence of nanobubbles. With an increase in the magnitude of the surface potential, the equilibrium size of the nanobubble decreases. This observation is found to be consistent with the ion-stabilized model.

#### 5.1 Introduction

Surfactants are the major pollutants in domestic and industrial wastewater [227]. Broadly, surfactants are amphiphilic molecules consisting of a hydrophobic head and hydrophilic tail group. The source of surfactants in the wastewater stream is often the application of surfactants as detergents and emulsifying agents. The processing industries such as textile, gas & oil, pulp & paper, mining & mineral processing utilize surfactants for various applications. Several methods are employed for the removal of surfactants from the wastewater, for instance, biological treatment [228, 229], chemical treatment [230, 231] and combined chemical & biological treatment [232, 233], nanotechnology-based treatment [234, 235, 236], etc. There are two approaches to treating the surfactant: degrading chemically or biologically and adsorption of surfactant on a dispersal medium. Aerobic digestion in an activated sludge process [229] and advanced oxidation process [237] are used to degrade the surfactant. On the other hand, adsorbents (zeolite, kaolin) can be utilized to remove surfactant molecules. More recently, carbon nanotubes have been shown to adsorb surfactants [238]. Surfactant molecules stabilize the nanomaterial by adsorbing at the interface. Nanobubbles are expected to offer adsorption of surfactants akin to carbon nanotubes to stabilize the interface. In addition, the collapse of microbubble during nanobubble generation also generates reactive oxygen species (ROS) [4, 239, 240], for instance,  $\cdot OH$ ,  $\dot{O}_2$ , etc. Thus, bulk nanobubbles can degrade the surfactants by ROS generation, and they also adsorb at the interface of nanobubble.

Despite such overwhelming applications, the extraordinary stability of nanobubbles [241] is still a paradox; nanobubbles encompass multitudinous properties that

macro-scale bubbles do not have, such as a large specific surface area, higher magnitude of zeta potential at the bubble surface, enhanced gas transfer coefficient [1], and the formation of hydroxyl radicals that encompass a strong affinity for gas-liquid interface at bubble surface [242, 4, 243]. Bulk nanobubbles are also termed ultrafine bubbles in the ISO standardization (ISO 20480-1:2017 [51]. Macro-micro bubbles rise quickly to the liquid surface and collapse. Nanobubbles are approximately 100-200 nm in diameter and undergo random drift due to Brownian motion. Nanobubbles are reported to be stable for several days and even months [244, 245]. These tiny bubbles has magnetised efficacy in medicine [246, 247] chemistry, agriculture [248, 1], decontamination [249, 250, 251], materials science [252], food technology [253], and other fields. It has been speculated that the life span of bulk nanobubbles is influenced by counterions confined to the gas-water interface, where the electrostatic interactions counteract the Laplace pressure [17, 16]. Furthermore, surface charge restricts the coalescence, which retains the small bubble size and hinders it from being destroyed due to buoyancy [254, 49]. Literature suggests that the surface charge on nanobubbles is owing to hydroxide ion adsorption, thus stabilizing the nanobubbles in alkaline medium [134, 131, 178]. The collapse of micro and nanobubbles results in reactive oxygen species (ROS) such as hydroxyl radicals, singlet oxygen, and superoxide [255, 256]. The free-radical generation occurs owing to the high density of ions at the gas-liquid interface before it collapses to form reactive oxygen species (ROSs). These characteristics prompted researchers to consider micro and nanobubbles as potential water treatment [257, 258] and disinfection technology.

Surfactants are classified as anionic, cationic, nonionic, or amphoteric. To achieve short-term stabilization, amphiphilic molecules (insoluble surfactants) adsorb at the interface of microbubbles [259]. Individual bubbles are perhaps survived for a few months if the molecules crystallize at the gas-liquid interface (condensed state). The formation of these nanobubbles is assessed by both dissolved gas molecules and the type of gas [260]. Few research findings have stated that the presence of nanobubbles influences the surface tension of various surfactant solutions. Ushida et al. [225] employed the Du Noüy approach to measuring the surface tension of nanobubble suspension in pure water (64.1 mN/m) and compared it to the surface tension of water (about 70 mN/m). Furthermore, using classical DLVO theory, the kinetic stability of bulk nanobubbles in surfactant is assessed. SDS-stabilized nanobubbles have a positive energy barrier against collapse or coalescence, whereas, in CTAB-stabilized nanobubbles, the energy barrier returns to positive only at a high concentration of surfactant solutions [261]. The charge-stabilization model unwraps the effect of surface charge density on the bulk surfactant concentration.

In this work, we have systemically investigated the nanobubble generation in surfactant solutions. The adsorption of surfactant at the nanobubble interface

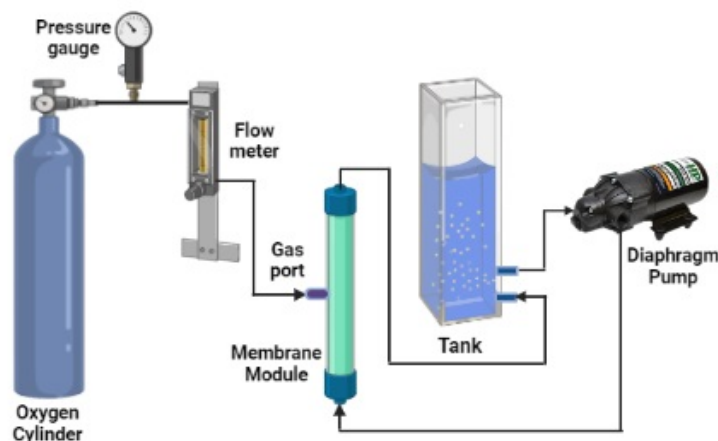


Figure 5.1: Schematic diagram of the nanobubble generation in surfactant solution.

is gauged by measuring the zeta potential. The nanobubble dynamics were investigated in terms of mean diameter with the surfactant concentration. The effect of the nature of the surfactant (SDS, CTAB, Triton-X 100, and Tween 20) on nanobubble generation and dynamics have been studied in terms of nanobubble concentration, mean bubble diameter, and the magnitude of surface charge. The nanobubble and nanoparticles have been distinguished by estimating the refractive index method. The surface tension of the nanobubble solution has been measured and compared without nanobubbles. The experimental trends have been explained by applying the single nanobubble stability model.

## 5.2 Experimental methods

### 5.2.1 Materials

Water used in this study was obtained from a Milli-Q unit (Merck Millipore water purification system, 19.5 M $\Omega$  resistivity). All the glassware was rinsed with 10% NaOH solution and subjected to oven drying. The tubing used in the experimental setup was made of Teflon. Sodium dodecyl sulfate (SDS, >99%, CMC: 8.2 mM), cetyltrimethylammonium bromide (CTAB, 99% CMC = 0.92 mM), Tween® 20 (CMC = 0.06 mM) and Triton-X 100 (CMC = 0.22mM) were procured from Sigma Aldrich. The solution was prepared by dissolving SDS in pure water using a magnetic stirrer at 25°C for 6 hrs to achieve complete dissolution. Furthermore, solutions of CTAB, Triton-x 100, and Tween 20 were prepared by gentle stirring for 12 hours at room temperature. All these surfactants were investigated at different concentrations: from lower to higher concentration regimes (0 to 10) times their critical micellar concentration (CMC). Before the experiment, ultrapure water and all stock solutions were screened for nanoscale impurities using NanoSight equipment (used to characterize the nanobubble size distributions, as explained in the later

section), and no substantial number of nanoscale entities were traced. Cleaning and handling of the experimental setup were done with extreme caution. To minimize further contamination in the sample, glass vials (15 mL) and silicone oil-free syringes were deployed.

### 5.2.2 Generation of bulk nanobubbles

This study employed a porous membrane diffusion method for nanobubble suspension in surfactant solutions. The generation of nanoscale bubbles was carried out using an in-house experimental setup. The apparatus includes a gas regulator encompassing the flow meter, enabling precise control of the gas flow rate. The illustration of the schematic diagram (**Figure. 5.1**), O<sub>2</sub> gas (purity > 99.5%), and surfactant solutions prepared by using ultrapure water (water purification system equipped with a reverse osmosis cartridge and modules of ion-exchange resins) were employed as the gas and liquid phases throughout the experiments. Compressed gas (oxygen) diffused between the tube walls at a pressure of 2 bar from the external tube through the nanopores in the internal tubes into the liquid flow. The nanoscale bubbles were chopped off from the surface of the tube due to shear stress and flow with the liquid, resulting in the formation of nanobubbles. The control set was O<sub>2</sub> NBs produced in ultrapure water, termed NB water. Nanobubble generated in the different surfactant solutions along with O<sub>2</sub> injection. This assured the findings obtained owing to the formation of NBs by injecting O<sub>2</sub> gas via the membrane module of the setup.

### 5.2.3 Characterization of bulk nanobubble suspensions

The size distribution of the nanobubble samples was investigated using NS300 based on NTA (Nanoparticle Tracking Analysis) and the surface charge by Zetasizer NanoZSP by Malvern, UK. As electrokinetic analyzers, it accounts for the classic streaming potential and current method for computing the surface charge density. The zeta potential is a significant variable for interpreting surface property and aids in developing a specialized material because of the correlation to the surface charge at a gas-liquid interface. Despite the fact that certain limitations with concentration measurement, DLS and NTA techniques majorly opt to provide the electrokinetic behavior of nanobubbles and the bubble size distribution.

The surface tension is examined by conducting the Wilhelmy plate measurement (immersion and withdrawal). The dynamic wettability approach relies on a multi-cycle Wilhelmy plate method for measuring interfacial tension at an air-liquid or liquid-liquid interface. The Wilhelmy plate is thin, with a few centimeters of surface area. The plate is either made of platinum that has been roughened to ensure complete wetting. The experimental outcomes are unaffected by the material used as long as the liquid wets it. The plate is thoroughly cleaned before being attached



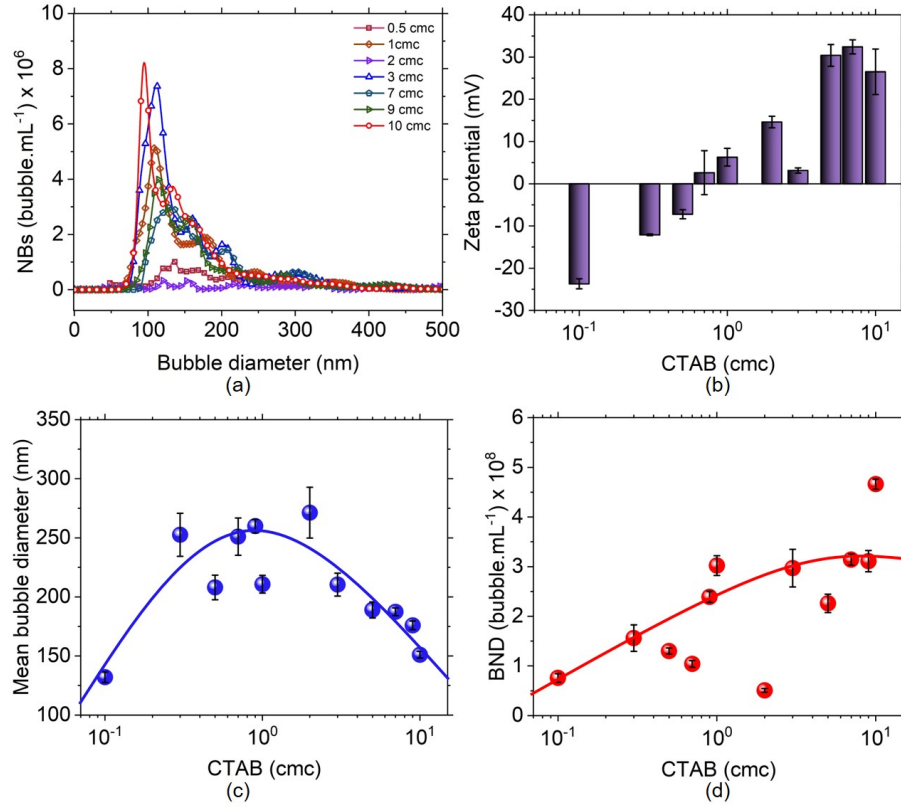


Figure 5.2: Effect of cationic surfactant (CTAB) on nanobubble generation (a) bubble size distribution (b) zeta potential (c) mean bubble diameter (d) bubble number density.

to a balance with a thin metal wire. Before the analysis, pure water ( $\gamma = 72.1$  mN/m) is used for calibration and to ensure the reliability of the equipment.

#### 5.2.4 Refractive index determination

The light scattering is measured during nanoparticle tracking analysis by NanoSight NS300 and the scattering power distribution of the nanobubble sample was measured. The average scattering power  $P_S$  (AU) is employed to estimate the refractive index. The instrument calibration is performed using standard polystyrene nanoparticles. The scattering intensity of polystyrene nanoparticles of four different sizes (50, 100, 150, and 200 nm) with a refractive index of 1.63, the scattering cross-section  $\sigma_S$  (nm<sup>2</sup>) is calculated and compared with the Mie theory. The open-source MieConScat software was incorporated to calculate the scattering cross-section required particle size, the refractive index of a given material and medium, and the light source wavelength needed for the theoretical scattering cross-section (See the details of Mie theory in SI). Mie scattering solves the Maxwell equations for scattering an electromagnetic wave with a dielectric spherical object analytically. An infinite series of vector spherical harmonics offers the solution. The measurable value  $P_S$  is compared to the scattering cross-section  $\sigma_{Mie}$ , computed using Mie theory. The instrument constant  $\sigma_{Mie}/P_S = 0.0673$  is obtained by linear

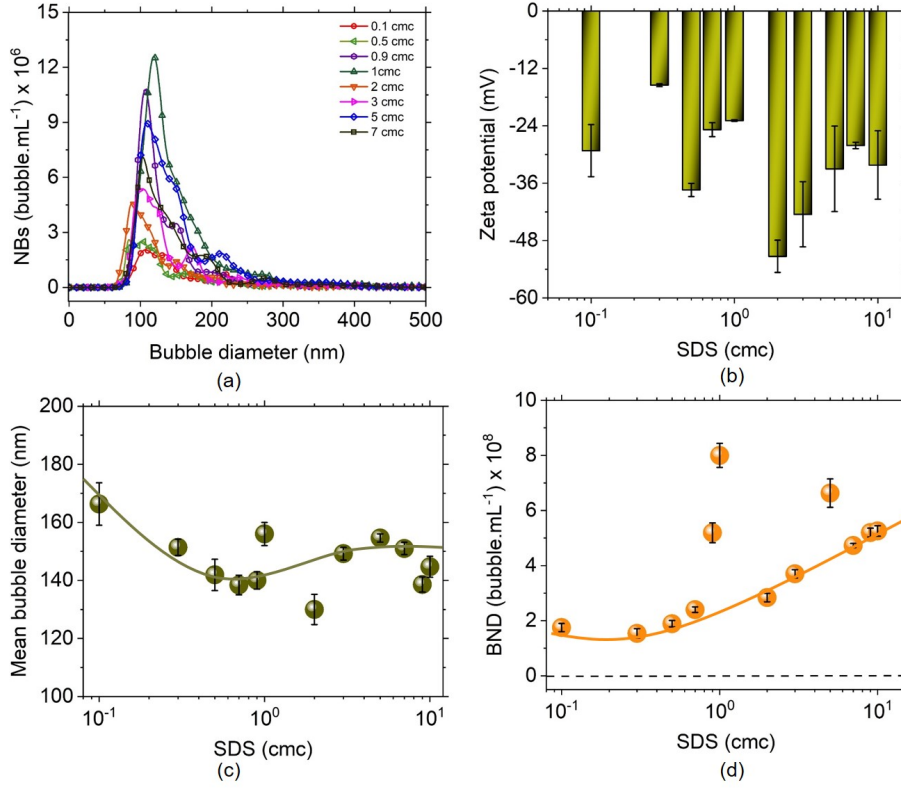


Figure 5.3: Bulk Nanobubbles evolution in anionic surfactant (SDS) (a) bubble size distribution (b) zeta potential (c) mean bubble diameter (d) bubble number density.

regression of the data point.

## 5.3 Results and discussion

### 5.3.1 Nanobubble dynamics in surfactant solutions

From a fundamental viewpoint, nanobubbles are speculated to be ion-stabilized in the absence of the surfactant molecule [262, 263]. The gas-liquid interface acquires a negative charge due to the absorption of hydroxyl ions [264]. The surface charge on the nanobubbles gives rise to an electrostatic pressure ( $P_{electrostatic} = \sigma_e^2 / 2\epsilon_r\epsilon_0$ ), which acts towards the outward normal of the surface of the nanobubble. Furthermore, the charged interface also tends to form the electric double layer around the nanobubble that exerts an ionic pressure force ( $P_{ionic} = \sigma_i^2 / \epsilon_r\epsilon_0$ ) towards the center of the nanobubble [153]. The surface tension force at the nanobubble interface acts towards the center of the nanobubble. All in all, an electrostatic force is expanding force, whilst the ionic and surface tension force is the collapsing force. The equilibrium size of the nanobubbles is determined by the interplay of these forces on the nanobubble interface. In this work, we have tested the hypothesis that the adsorption of the surfactant molecule at the nanobubble interface is expected to alter this equilibrium. Therefore, to get an insight into different surfactant behavior which

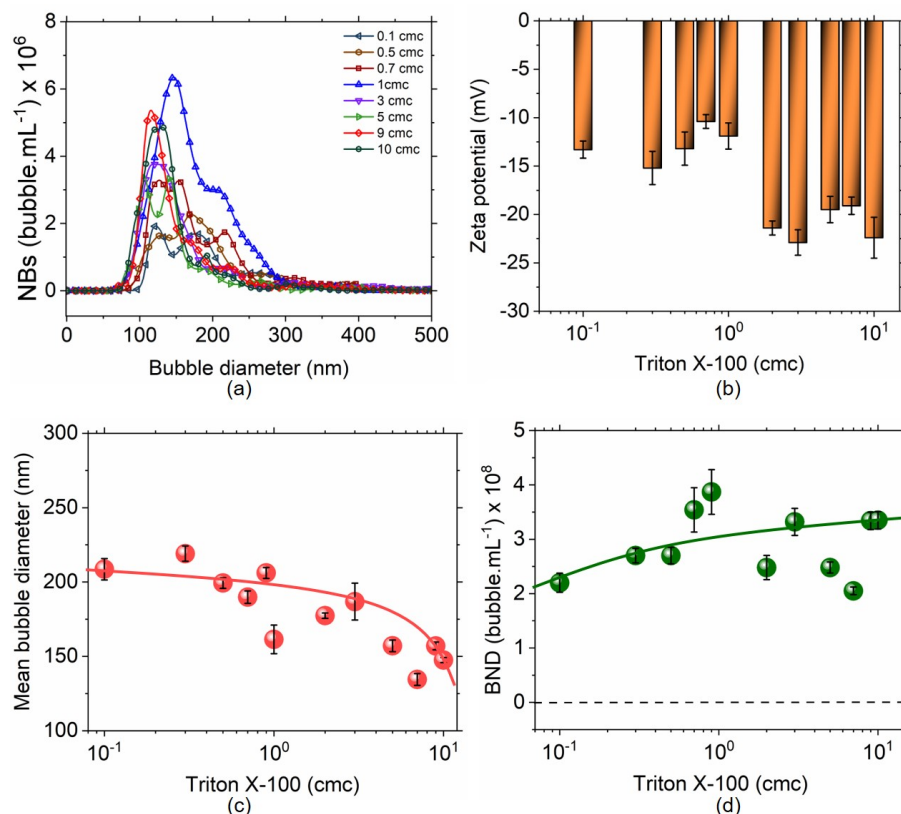


Figure 5.4: Bulk Nanobubbles evolution in non-ionic surfactant (Triton X-100) (a) bubble size distribution (b) zeta potential (c) mean bubble diameter (d) bubble number density.

tends to affect nanobubble dynamics, we examined the effects of altering the nature of surfactant (anionic, cationic, non-ionic) during the generation of nanobubbles. **Figure. 5.2** depicts the nanobubble size distribution, zeta potential, and mean bubble diameter in the presence of cationic surfactant (CTAB). It is evident that CTAB at higher concentration results in the charge reversal (see **Figure. 5.2b**). The zeta potential varies steadily from approximately -30mV to +30mV by varying the CTAB concentration from 0 to 10 cmc. The sign reversal occurs at the isoelectric point close to 0.9 cmc, where the mean bubble diameter is observed to be maximum (see **Figure. 5.2c**). It can be anticipated that the presence of cationic surfactant would result in the adsorption of  $\text{CTA}^+$  at the nanobubble interface. This, sequentially, neutralizes the negative charge, resulting in a charge reversal at the isoelectric point. The force balance can explain the nanobubble dynamics at the nanobubble interface. The ionic pressure force reduces upon increasing the CTAB concentration up to the iso-electric point ( $\sim 0.9$  cmc). The size of the nanobubbles is expected to increase as the ionic pressure is collapsing force at the nanobubble interface. Furthermore, the surface charge density on the nanobubble will increase beyond the iso-electric point, reducing the nanobubble's size.

When an anionic surfactant (SDS) was added at a varying dosage from 0 to 10 cmc, while generation of nanobubbles, as shown in **Figure. 5.3**, results in increase in

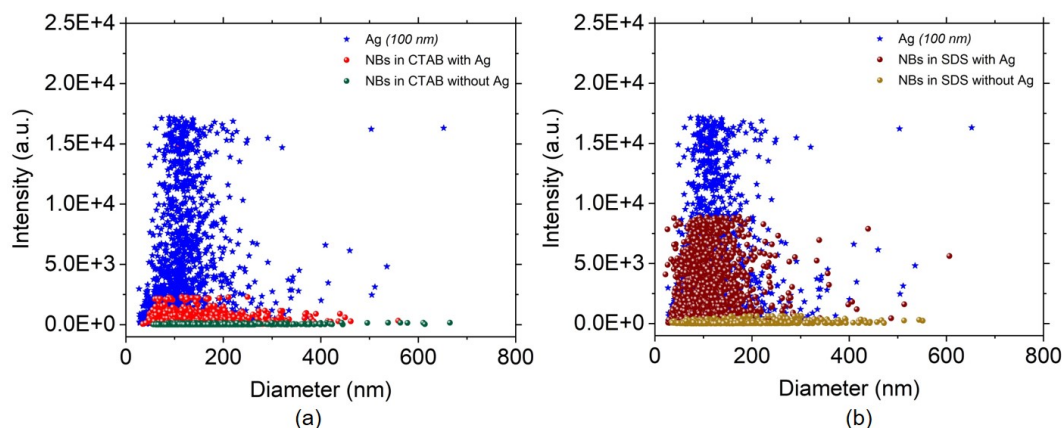


Figure 5.5: Comparison of light scattering intensities of 100 nm aqueous silver nanoparticle dispersion and NBs suspension in (a) CTAB (b) SDS.

the zeta potential from  $-15\text{mV}$  to  $-55\text{mV}$ . The increase in zeta potential is owing to the hydrophilic ionic head group  $\text{SO}_4$ , the SDS molecules oriented towards the liquid phase whilst the hydrophobic tail is expected to orient towards the gas phase. Furthermore, an increase in SDS concentration gradually enhances the nanobubble concentration  $\sim 2 \times 10^8$  bubbles/mL to  $\sim 4.12 \times 10^8$  bubbles/mL. As long as there was enough energy input, we deduced that bulk nanobubbles could nucleate in pure water as well as various aqueous solutions containing surfactants and electrolytes. Intuitively, there were more nanobubbles present in the solution with anionic surfactant (SDS) than in pure water. The surface tension reduced With an increasing concentration of SDS solution, while the surface electrostatic and ionic forces increased due to the enhanced surface charge density. As noted earlier, the stable equilibrium size of individual nanobubbles can be determined by the interplay of these forces. The adsorption of surfactant ions may break the initial equilibrium state, which may lead to an unpredictable bubble evolution (swell or shrinkage). The bubble number concentration (see **Figure. 5.3c**) rose with the increasing SDS concentration, indicating that the surfactant could facilitate the nucleation of nanobubbles. The colloidal stability or instability of bulk nanobubbles suspension resulting from the presence of surfactants was confirmed by the experimental results of the zeta potential.

Non-ionic surfactants are preferred over ionic surfactants as they can be altered to have a wide range of hydrophile-lipophile balance (HLB) by changing molecular structures, especially the hydrophilic fraction. The mean diameter of nanobubbles in non-ionic surfactant Triton X-100 was observed to be 120-200 nm (see **Figure. 5.4c**). The size of nanobubbles in non-ionic surfactants decreases with surfactant concentration. This is due to the increase in the zeta potential of the nanobubble. This also indicates that the surface potential governs the nanobubble dynamics rather than the surface tension despite the fact that surface tension drops

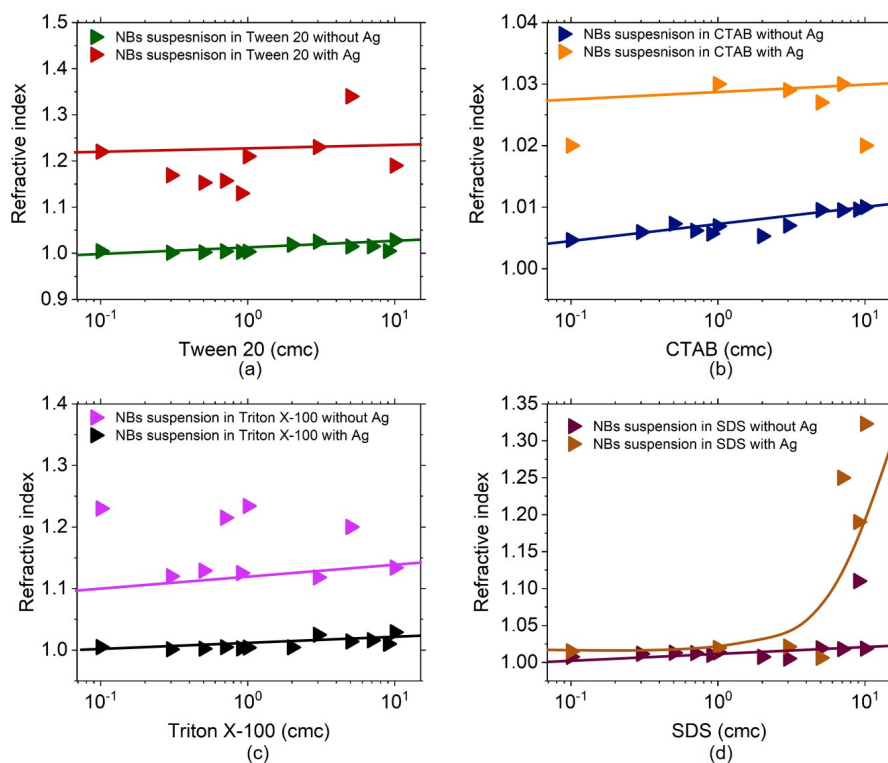


Figure 5.6: Differentiating bulk nanobubbles and nanoparticles based on refractive index (a) Tween 20 (b) CTAB (c) Triton X-100 (d) SDS.

significantly with increasing concentration of surfactant. However, the drop in surface tension facilitates the concentration of nanobubbles irrespective of the nature of the surfactants. From a thermodynamic viewpoint, surface tension lowers the surface energy of the fluid, and thus more surface area nucleates in the form of nanobubbles. In a nutshell, the nanobubble dynamics governs by the surface potential of the nanobubbles, irrespective of the nature of the surfactant. The equilibrium size of the nanobubbles decreases with an increase in the magnitude of the surface potential. This was seen to be in line with the ion-stabilized model.

### 5.3.2 Differentiating nanobubbles and nanoparticles in the presence of surfactant molecule

From a practical viewpoint, the process water is expected to contain solid nanoparticles. Therefore, it is customary to differentiate nanobubbles from nanoparticles. Understanding the interaction of nanobubbles and nanoparticles is vital for the practical applications of nanobubbles. The Light scattering methods are essential for studying nano-scale entities as well as identifying and characterizing colloidal particles in routine. Although light scattering methods cannot distinguish between bubbles, particles, and droplets, they can be used in conjunction with other optical properties to identify bubble behavior. This is accomplished by comparing light scattering intensity data for both particle and bubble (see **Figure**.

**5.5.** The scattering intensity of the nanobubbles is much smaller than that of the silver nanoparticles. It is also to be noted that the measured value of scattering intensity ultimately results in the scattering cross-section. Surprisingly, the scattering intensity/scattering cross-section of the nanobubble is significantly much smaller than the silver nanoparticles. This has been verified by numerical simulation and Mie theory calculations, which results in the same conclusion. This trend can be explained by using approximated relations on scattering cross-section. When the particle is smaller than the wavelength of light, the scattering cross section varies  $Q_{sca} \propto 1/\lambda^4$  and refractive index  $n \propto 1/\lambda$ . This implies that the scattering cross section should vary as  $Q_{sca} \propto n^4$  [146]. This could be the reason for predicting smaller scattering cross sections for nanobubbles compared to silver nanoparticles. Here we also demonstrate the ability of bulk nanobubbles to interact with silver nanoparticles. This inevitably results in the colloidal stability of particle-bubble agglomerations, proving that bulk nanobubbles can alter colloidal suspensions. The dispersed object's scattering cross-section is directly correlated with the refractive index. Before mixing the nanoparticle solutions with the nanobubble solution, the nanoparticle solution was subjected to ultrasonication for 5 minutes. The nanoparticle-nanobubble suspension was initiated by gently pouring the two solutions at a specific particle-to-bubble number ratio. Given that the optical techniques used here partially attribute data based on light scattering intensity, the difference in the scattering intensity of Au nanoparticles and gaseous nanobubbles may result in one population being lost in the noise of the other.

NTA employs a light scattering method based on real-time measurement for the analysis of nanoparticles, and it estimates individual particle size independent of refractive index. This study focuses on analyzing light scattering data from NTA and Mie scattering theory to estimate the refractive index of nanobubble and nanoparticle environment (see **Figure. 5.6**). We establish the probability of nanobubble suspension interrelating with the Au nanoparticles by computing the refractive index for the same. The inference can be drawn by characterizing the pure nanobubble solution and Au nanoparticles in the nanobubble solution. The instrument scaling factor is employed to quantify the measured scattering cross-section and theoretical from Mie theory calculations to determine the refractive index. As discussed, extracting the refractive index corresponds close to 1.01 in nanobubble solution of different surfactants, and distinctly, this is within the range of gaseous bubbles. In addition, we estimated the RI by measuring the diameter and light scattering power of individual particles with NTA independently and the refractive index value, which corresponds to be greater than 1.1 when coupled with bubble and particle interaction. This method differentiates between populations in a sample of nanoparticles in suspension with nanobubbles. The bubble and particle size probability distribution function from NTA is plotted in



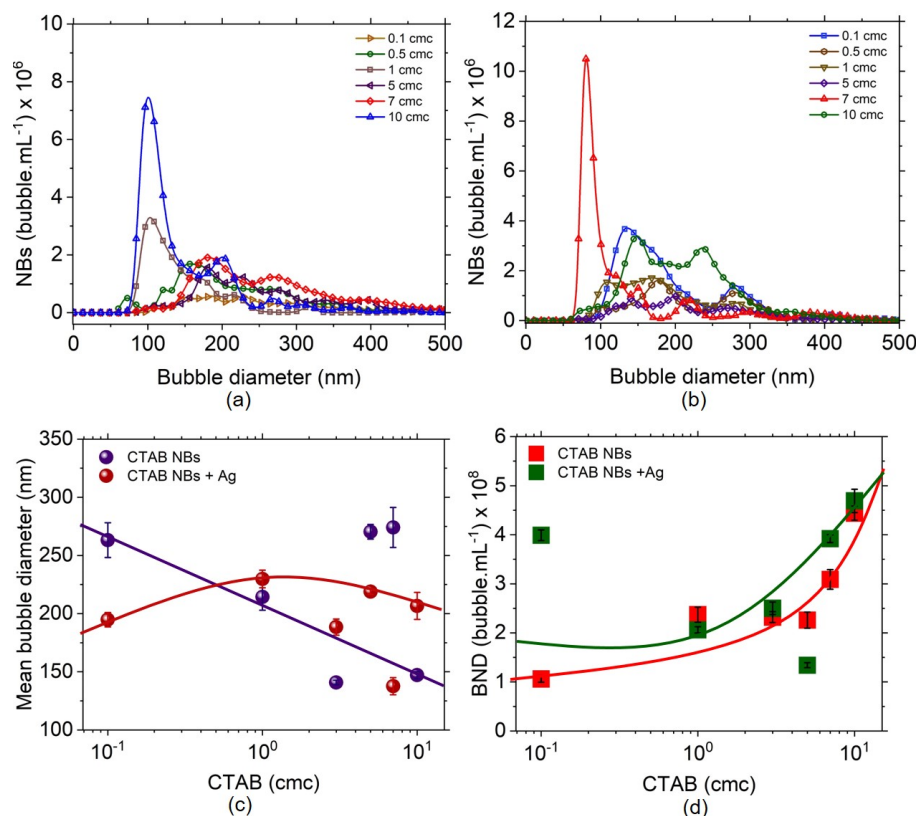


Figure 5.7: Dynamics of bulk nanobubbles in 100 nm aqueous silver nanoparticle dispersion (a) bubble size distribution in CTAB (b) bubble size distribution in CTAB and nanoparticle (c) mean bubble diameter (d) bubble number density.

**Figure. 5.7.** Aggregation cannot easily alter the size of the Au nanoparticles (they are colloidal stability with a very high energy barrier). We envision nanobubble with nanoparticles on its gas-liquid interface rather than large agglomerations of nanoparticles linked by bridging gas layers. The correlation between nanoparticles and nanobubbles is intriguing because it is pertinent to the potential applications of both nanoparticles and nanobubbles. Aside from the hypothesis that bulk nanobubbles are present as concentrated contaminated particles, or that they are coated with contaminated skin, or a combination of the two, another particularly intriguing aspect that is attempted to be answered here is how bulk nanobubbles interact with nanoparticles with a variety of different properties once they are stably generated.

### 5.3.3 Effect of ultrasound field on nanobubbles in surfactant solution

The ultrasound field is also used for nanobubble generation. The bubble dynamics in the ultrasound field can be classified into three groups: oscillation, growth, and collapse. When the magnitude of an ultrasonic wave exceeds the cavitation threshold, tiny nuclei form internally and exhibit a variety of behavior in the opposite/negative pressure zone. When the nuclei contract or dilate to a certain

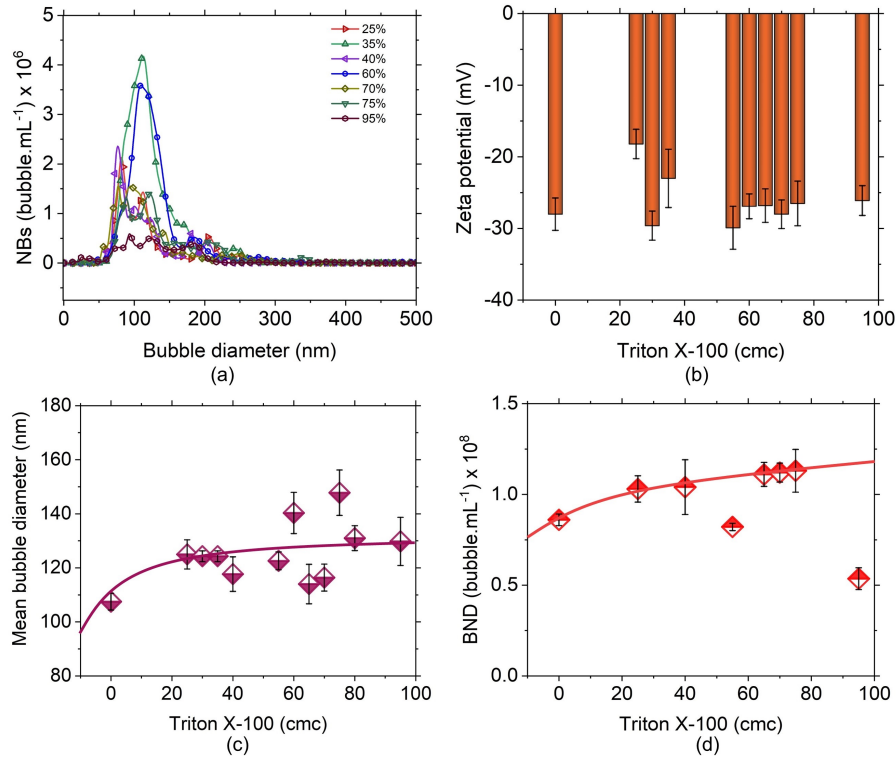


Figure 5.8: Effect of ultrasound amplitude on nanobubble suspension of Triton X-100 (2 cmc) (a) bubble size distribution (b) zeta potential (c) mean bubble diameter (d) bubble number density.

extent, the gas molecules dissolve in the solution, transfer into a nucleus, and grow to the size of a nanobubble. In this work, we have tested the hypothesis that ultrasonic irradiation on nanobubble suspension should destroy the already present nanobubble. This hypothesis was confirmed in the case of nanobubbles in pure water [265]. In this work, we performed ultrasonic irradiation in the bulk nanobubble suspension formed in a surfactant solution. The bubble number density, mean diameter, and zeta potential were measured with increasing amplitude percentages for a fixed period. The critical micellar concentration of surfactant was 2 cmc, as shown in **Figure. 5.8**, on which the nanobubble was generated by the nanopore diffusion method. The nanobubble sample of 60 mL volume was subjected to the 20 kHz ultrasound for 5 mins. The same procedure is adopted for other surfactant nanobubble samples. The bubble size distribution was observed to be invariant with the ultrasound amplitude. Furthermore, the zeta potential of the nanobubble was observed to remain unchanged with the ultrasound amplitude as shown for Triton-X 100 as shown in **Figure. 5.8b**. In summary, the mean bubble diameter does not change with the ultrasound amplitude during the charging of the nanobubble sample by ultrasound waves.

The electrically charged liquid-gas interface tends to create repulsion forces that inhibit bubble coalescence, similar to high dissolved gas concentration in water,



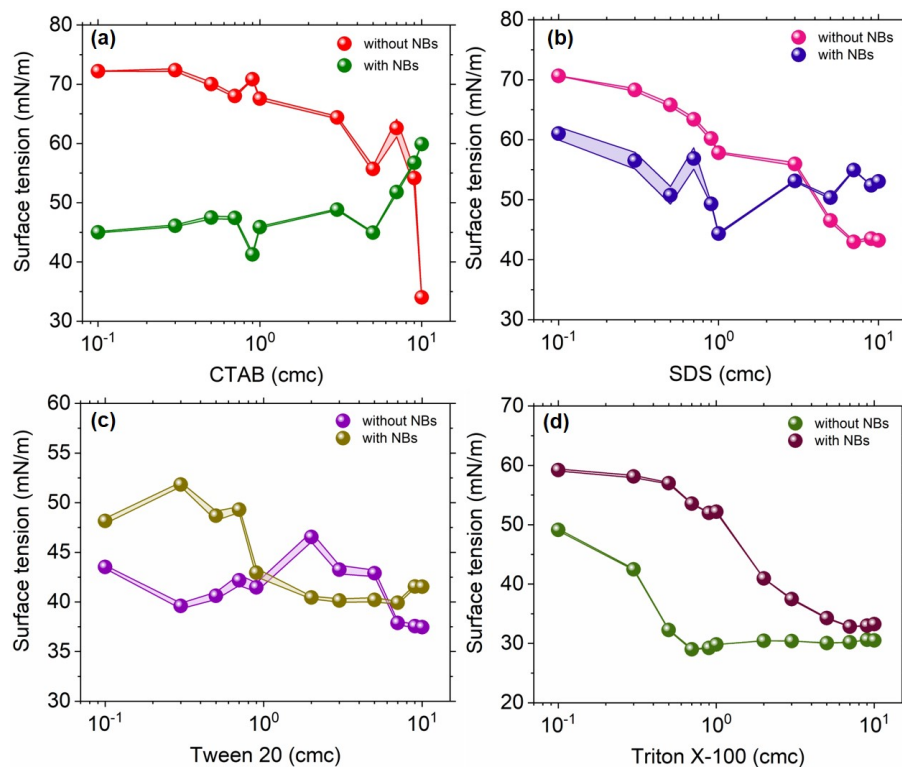


Figure 5.9: Surface tension measurements using the Wilhelmy plate method (a) CTAB (b) SDS (c) Tween 20 (d) Triton X-100.

which maintains a slight change in concentration gradient between the interface and the bulk liquid. When ultrasound is performed on nanobubble suspension, fine bubbles originate from bubble nuclei, grow to about resonance size under acoustic pressure fluctuations, and collapse. The shift in bubble number concentration and mean diameter was investigated with a constant irradiation time at different ultrasonic amplitude and fixed frequency and power; the bubble concentration increased and appeared to approach an equilibrium value. It was reported that ultrasound generates and destroys nanobubbles in water simultaneously in absence of surfactant; however, we did not observe significant destruction of the nanobubbles in the surfactant solution. As the ultrasonic amplitude percentage increased, the production rate coefficient of bubble concentration remained unchanged.

### 5.3.4 Surface tension in the presence of nanobubbles

Water has a high surface tension because of its molecules' strong, cohesive interactions. Surfactant molecule weakens these interactions as they dissolve in the water. Surface tension decreases upon the addition of surfactant owing to a decrease in the intermolecular forces between the water molecules. Nanobubble in the water may also reduce the surface tension of the water. Surface tension is often expressed by Gibbs free energy per unit area at constant temperature and pressure ( $\gamma = (\partial\Delta G/\partial S)_{T,P}$ ). The nanobubble may decrease the surface tension

by decreasing free energy. Similar to the surfactant molecule, nanobubble may also weaken the intermolecular force between water molecules. For instance, [225] reported the experimental results of the surface tension of nanobubbles generated in pure water was around 63 mN/m, which is about 14% lesser than that of pure water (about 72 mN/m). In this work, we have measured the surface tension of surfactant solution with and without the presence of nanobubbles. Anionic and non-ionic surfactant solution shows a  $\sim 10\%$  (at 0.1 cmc) reduction in surface tension estimated by the du Noüy ring method owing to the presence of nanobubbles. On the other hand, the presence of bulk nanobubbles reduces the surface tension by  $\sim 37.5\%$  (at 0.1 cmc) in a cationic surfactant solution, as shown in **Figure. 5.9**. The plausible explanation for the reduction in surface tension could be the reduced collision frequency of a surfactant-coated nanobubble with the liquid surface. The nanobubbles are presumed to be concentrated at a liquid surface due to their hydrophobic nature. This may attribute to the reduction in surface tension owing to the easy rupture of the liquid film by the presence of nanobubbles. The interaction between dynamical gas saturation and surface tension controlled the ultimate stable size of bulk nanobubbles throughout the shrinking process, which may be adjusted by the concentration of the surfactant adsorbed at its surface. Nanobubbles partly covered with hydrophobic material are concentrated at the surface of liquid water. The presence of these bubbles on the surface of a liquid film easily ruptured. When a nanobubble breaks and disappears at the liquid surface, the liquid film may be broken by guiding the exposed portion of the nanobubble into the gas phase above the liquid surface. The surface-tension-area isotherm of the nanobubbles coated with surfactants is vital to understanding the underlying phenomena of stabilizing these nanoscale bubbles. The inclusion of the surfactant aids in nanobubble stabilization by bringing down surface tension and, thus, the Laplace pressure. The impact of the surfactant limited the gas-liquid surface tension of nanobubbles, which could further lessen the Laplace pressure inside these bubbles and, thus, enhance their stability.

## 5.4 Conclusions

In this work, we have investigated the nanobubbles dynamics in surfactant solution. The effect of the nature of the surfactant (SDS, CTAB, Triton-X 100, and Tween 20) on nanobubble generation have been studied in terms of nanobubble concentration, mean bubble diameter, and the magnitude of surface charge. By changing the CTAB concentration from 0 to 10 cmc, the zeta potential steadily shifts from about -30mV to +30mV. The mean bubble diameter is observed to be at its highest at the isoelectric point near 0.9 cmc, where the sign reversal occurs. It is reasonable to assume that the presence of cationic surfactant will cause CTA<sup>+</sup> to adsorb at the nanobubble interface. As a result, the negative charge is

successively neutralized, which causes a charge reversal at the isoelectric point. The nanobubble and nanoparticles have been distinguished by estimating the refractive index method. The surface tension of the nanobubble solution has been measured and compared without nanobubbles. The surface tension of the surfactant solution further decreases in presence of nanobubbles. The easy rupture of the liquid film by the presence of nanobubbles at its surface may be the reason for the reduction in the surface tension. The nanobubble dynamics observe to govern by the surface potential of the nanobubbles, irrespective of the nature of the surfactant. The equilibrium size of the nanobubbles decreases with an increase in the magnitude of the surface potential. This was seen to be in line with the ion-stabilized model.

## Chapter 6

### Conclusions, Implications, and Recommendations

---

This dissertation investigated the fundamental properties of bulk nanobubbles in aqueous solutions and surfactants. The primary objectives of this work were

1. To understand the role of the salting-out parameter during nanobubble nucleation.
2. To investigate nanobubble dynamics under an oscillating pressure field and elucidate the mechanical stability of the nanobubbles.
3. How the longevity of nanobubbles is affected when subjected to ultrasound waves.
4. The Jones-Ray effects have been debated for the past 80 years to understand the minima in surface tension versus salt concentration curve. Does nucleation of nanobubble impart this effect?
5. To investigate the presence of surface-active agents like surfactants and nanoparticles affecting the dynamics of nanobubbles.

These objectives were addressed with a combination of experiments performed in contaminated media (aqueous salt solutions of variable valency), surfactants (anionic, cationic, and non-ionic), and numerical simulation on electromagnetic waves to confirm the scattering behavior of nanobubbles and nanoparticles. Moreover, the dissertation assessed the novel method for estimating the refractive index of nanobubble which aids in differentiating from nanoparticles using the Mie Scattering theory. Here, we made one of the first attempts to investigate the mechanical stability model by considering both ionic cloud and electrostatic pressure at the charged interface.

#### 6.1 Conclusions

##### Nucleation of nanobubbles during Salting-out effect

- A novel method for estimating the refractive index of nanobubble is proposed based on Mie theory calculations.
- Excess dissolved gas nucleates in the form of nanobubbles during the salting-out effect based on the refractive index calculation.

- The bubble number density was observed to increase with the salt concentration, which is explained by the Setchenov solubility relation for electrolytes.

### **Nanobubble dynamics under oscillating pressure field**

- The energy barrier for colloidal stability of nanobubbles under an ultrasound field is significantly higher than both nanobubbles by salting-out and oscillating pressure field.
- The refractive index calculation and the electrical conductivity confirmed the evidence for the gas-filled nanobubbles.
- The screening of the electric double layer decreases the surface potential of the nanobubbles depending on the valency of the salt.

### **Nanobubbles contributing to Jones-Ray effect**

- The magnitude of the surface tension drop significantly increases upon applying the oscillating pressure field. This perhaps indicates that nanobubbles are playing a role in decreasing the surface tension of the salt solution.
- A novel mechanical stability model for nanobubbles has been proposed by considering the ion cloud pressure, and it is shown to be twice the electrostatic pressure.
- Numerical simulation of electromagnetic waves around nanobubbles and nanoparticles confirms the scattering behavior of the nanobubble and nanoparticles.

### **Role of surfactant in bulk nanobubble suspension**

- The presence of nanobubbles in surfactant solution allows the rupture of the liquid film, lowering the surface tension value in the Wilhelmy plate method.
- The surface potential of the nanobubble was observed to be enhanced with the increase in the ultrasound amplitude, as shown for non-ionic surfactant.
- The inclusion of the surfactant aids bubble stabilization by bringing down surface tension and, thus, the Laplace pressure.

## 6.2 Implications and Recommendations

The scope of this technology can be implied in real-life applications which are stated as follows:

- During the salting-out effect, the bubble number density increases with the salting-out parameter. In other words, the solubility difference is the driving force for nanobubble generation. This information can be utilized to maximize the bubble number density in the commercial nanobubble generator to enhance performance.
- Bulk nanobubbles are stable in saltwater and thus the nanobubble generator can be used for water treatment in coastal regions.
- A novel technique to estimate the refractive index of nanobubbles based on the scattering power measurement provides strong scientific evidence for the existence of nanobubbles. This technique can be used for the validation and testing of a commercial nanobubble generator.
- The fundamental theory supports the nucleation of nanobubbles if surface tension drops in the salt solution and can be deeply investigated on the long-standing debate about the Jones-Ray effect.

## References

---

- [1] Evangelos P Favvas, George Z Kyzas, Eleni K Efthimiadou, and Athanasios Ch Mitropoulos. Bulk nanobubbles, generation methods and potential applications. *Current Opinion in Colloid & Interface Science*, 54:101455, 2021.
- [2] Ting Li, Zhao Cui, Jing Sun, Chang Jiang, and Guangyue Li. Generation of bulk nanobubbles by self-developed venturi-type circulation hydrodynamic cavitation device. *Langmuir*, 37(44):12952–12960, 2021.
- [3] Mariana J do Amaral, Yulli M Passos, Marcius S Almeida, Anderson S Pinheiro, and Yraima Cordeiro. In vitro characterization of protein: Nucleic acid liquid–liquid phase separation by microscopy methods and nanoparticle tracking analysis. In *Protein Aggregation: Methods and Protocols*, pages 605–631. Springer, 2022.
- [4] Ariel J Atkinson, Onur G Apul, Orren Schneider, Sergi Garcia-Segura, and Paul Westerhoff. Nanobubble technologies offer opportunities to improve water treatment. *Accounts of chemical research*, 52(5):1196–1205, 2019.
- [5] Jie Zhu, Hongjie An, Muidh Alheshibri, Lvdan Liu, Paul MJ Terpstra, Guangming Liu, and Vincent SJ Craig. Cleaning with bulk nanobubbles. *Langmuir*, 32(43):11203–11211, 2016.
- [6] Fernanda Yumi Ushikubo, Takuro Furukawa, Ryou Nakagawa, Masatoshi Enari, Yoshio Makino, Yoshinori Kawagoe, Takeo Shiina, and Seiichi Oshita. Evidence of the existence and the stability of nano-bubbles in water. *Colloids and Surfaces A: Physicochemical and Engineering Aspects*, 361(1-3):31–37, 2010.
- [7] Marwa Sakr, Mohamed M Mohamed, Munjed A Maraqa, Mohamed A Hamouda, Ashraf Aly Hassan, Jafar Ali, and Jinho Jung. A critical review of the recent developments in micro–nano bubbles applications for domestic and industrial wastewater treatment. *Alexandria Engineering Journal*, 2021.
- [8] Tatek Temesgen, Thi Thuy Bui, Mooyoung Han, Tschung-il Kim, and Hyunju Park. Micro and nanobubble technologies as a new horizon for water-treatment techniques: A review. *Advances in colloid and interface science*, 246:40–51, 2017.
- [9] James RT Seddon, Detlef Lohse, William A Ducker, and Vincent SJ Craig. A deliberation on nanobubbles at surfaces and in bulk. *ChemPhysChem*, 13(8): 2179–2187, 2012.

- [10] Joost H Weijs and Detlef Lohse. Why surface nanobubbles live for hours. *Physical review letters*, 110(5):054501, 2013.
- [11] Minmin Zhang and James RT Seddon. Nanobubble–nanoparticle interactions in bulk solutions. *Langmuir*, 32(43):11280–11286, 2016.
- [12] Binyu Zhao, Xingya Wang, Yang Song, Jun Hu, Junhong Lü, Xingfei Zhou, Renzhong Tai, Xuehua Zhang, and Lijuan Zhang. Stiffness and evolution of interfacial micropancakes revealed by afm quantitative nanomechanical imaging. *Physical Chemistry Chemical Physics*, 17(20):13598–13605, 2015.
- [13] Ali A Paknahad, Liam Kerr, Daniel A Wong, Michael C Kolios, and Scott SH Tsai. Biomedical nanobubbles and opportunities for microfluidics. *RSC advances*, 11(52):32750–32774, 2021.
- [14] Radwa H Abou-Saleh, Fern J Armistead, Damien VB Batchelor, Benjamin RG Johnson, Sally A Peyman, and Stephen D Evans. Horizon: Microfluidic platform for the production of therapeutic microbubbles and nanobubbles. *Review of Scientific Instruments*, 92(7):074105, 2021.
- [15] Milton S Plesset and Satwindar S Sadhal. On the stability of gas bubbles in liquid-gas solutions. In *Mechanics and Physics of Bubbles in Liquids*, pages 133–141. Springer, 1982.
- [16] Limin Zhou, Shuo Wang, Lijuan Zhang, and Jun Hu. Generation and stability of bulk nanobubbles: A review and perspective. *Current Opinion in Colloid & Interface Science*, 53:101439, 2021.
- [17] Neelkanth Nirmalkar, AW Pacek, and Mostafa Barigou. On the existence and stability of bulk nanobubbles. *Langmuir*, 34(37):10964–10973, 2018.
- [18] Zhou Fang, Xingya Wang, Limin Zhou, Lijuan Zhang, and Jun Hu. Formation and stability of bulk nanobubbles by vibration. *Langmuir*, 36(9):2264–2270, 2020.
- [19] Hilman Syaeful Alam, Priyono Sutikno, Tubagus Ahmad Fauzi Soelaiman, and Anto Tri Sugiarto. Bulk nanobubbles: generation using a two-chamber swirling flow nozzle and long-term stability in water. *Journal of Flow Chemistry*, pages 1–13, 2021.
- [20] Khanh Kim Thi Phan, Tuyen Truong, Yong Wang, and Bhesh Bhandari. Nanobubbles: Fundamental characteristics and applications in food processing. *Trends in Food Science & Technology*, 95:118–130, 2020.
- [21] You Tian, Zi Zhang, Zhiwei Zhu, and Da-Wen Sun. Effects of nano-bubbles and constant/variable-frequency ultrasound-assisted freezing on freezing behaviour of viscous food model systems. *Journal of Food Engineering*, 292:110284, 2021.



- [22] Kosuke Ebina, Kenrin Shi, Makoto Hirao, Jun Hashimoto, Yoshitaka Kawato, Shoichi Kaneshiro, Tokimitsu Morimoto, Kota Koizumi, and Hideki Yoshikawa. Oxygen and air nanobubble water solution promote the growth of plants, fishes, and mice. *PLoS One*, 8(6):e65339, 2013.
- [23] S Oshita and S Liu. Nanobubble characteristics and its application to agriculture and food. In *Int. Symp. Agri-Food Health Wealth*, pages 23–32, 2013.
- [24] Janitha Hewa Batagoda, Shaini Dilsha Aluthgun Hewage, and Jay N Meegoda. Remediation of heavy-metal-contaminated sediments in usa using ultrasound and ozone nanobubbles. *Journal of Environmental Engineering and Science*, 14(2):130–138, 2019.
- [25] Hengzhen Li, Liming Hu, Dejun Song, and Fei Lin. Characteristics of micro-nano bubbles and potential application in groundwater bioremediation. *Water Environment Research*, 86(9):844–851, 2014.
- [26] Sae Hayakumo, Shinichi Arakawa, Yoshihiro Mano, and Yuichi Izumi. Clinical and microbiological effects of ozone nano-bubble water irrigation as an adjunct to mechanical subgingival debridement in periodontitis patients in a randomized controlled trial. *Clinical oral investigations*, 17:379–388, 2013.
- [27] Shuxin Shen, Ying Li, Yunbin Xiao, Zonglei Zhao, Chuanxi Zhang, Junfen Wang, Hairui Li, Feng Liu, Nvqin He, Ye Yuan, et al. Folate-conjugated nanobubbles selectively target and kill cancer cells via ultrasound-triggered intracellular explosion. *Biomaterials*, 181:293–306, 2018.
- [28] VB Orel, MA Zabolotny, and VE Orel. Heterogeneity of hypoxia in solid tumours and mechanochemical reactions with oxygen nanobubbles. *Medical Hypotheses*, 102:82–86, 2017.
- [29] Panagiotis E Theodorakis and Zhizhao Che. Surface nanobubbles: Theory, simulation, and experiment. a review. *Advances in colloid and interface science*, 272:101995, 2019.
- [30] Bram M Borkent, Sissi de Beer, Frieder Mugele, and Detlef Lohse. On the shape of surface nanobubbles. *Langmuir*, 26(1):260–268, 2010.
- [31] FA Long and GC Nutting. The relative surface tension of potassium chloride solutions by a differential bubble pressure method1. *Journal of the American Chemical Society*, 64(10):2476–2482, 1942.
- [32] Naoyuki Ishida, Taichi Inoue, Minoru Miyahara, and Ko Higashitani. Nano bubbles on a hydrophobic surface in water observed by tapping-mode atomic force microscopy. *Langmuir*, 16(16):6377–6380, 2000.

- [33] Yawei Liu and Xianren Zhang. Nanobubble stability induced by contact line pinning. *The Journal of chemical physics*, 138(1):014706, 2013.
- [34] Hong Peng, Greg R Birkett, and Anh V Nguyen. Progress on the surface nanobubble story: What is in the bubble? why does it exist? *Advances in colloid and interface science*, 222:573–580, 2015.
- [35] Michael P Brenner and Detlef Lohse. Dynamic equilibrium mechanism for surface nanobubble stabilization. *Physical review letters*, 101(21):214505, 2008.
- [36] Seung Hoon Oh, Jung Guen Han, and Jong-Min Kim. Long-term stability of hydrogen nanobubble fuel. *Fuel*, 158:399–404, 2015.
- [37] Xue Hua Zhang, Anthony Quinn, and William A Ducker. Nanobubbles at the interface between water and a hydrophobic solid. *Langmuir*, 24(9):4756–4764, 2008.
- [38] Kazunari Ohgaki, Nguyen Quoc Khanh, Yasuhiro Joden, Atsushi Tsuji, and Takaharu Nakagawa. Physicochemical approach to nanobubble solutions. *Chemical Engineering Science*, 65(3):1296–1300, 2010.
- [39] Roland Steitz, Thomas Gutberlet, Thomas Hauss, Beate Klösgen, Rumen Krastev, Sebastian Schemmel, Adam C Simonsen, and Gerhard H Findenegg. Nanobubbles and their precursor layer at the interface of water against a hydrophobic substrate. *Langmuir*, 19(6):2409–2418, 2003.
- [40] Philipp Gutfreund, Marco Maccarini, Andrew JC Dennison, and Max Wolff. The search for nanobubbles by using specular and off-specular neutron reflectometry. *Langmuir*, 32(35):9091–9096, 2016.
- [41] Xue Hua Zhang. Quartz crystal microbalance study of the interfacial nanobubbles. *Physical Chemistry Chemical Physics*, 10(45):6842–6848, 2008.
- [42] Beng Hau Tan, Hongjie An, and Claus-Dieter Ohl. Identifying surface-attached nanobubbles. *Current Opinion in Colloid & Interface Science*, 53:101429, 2021.
- [43] Marc A Hampton and Anh V Nguyen. Nanobubbles and the nanobubble bridging capillary force. *Advances in colloid and interface science*, 154(1-2): 30–55, 2010.
- [44] Qianxiang Xiao, Yawei Liu, Zhenjiang Guo, Zhiping Liu, Detlef Lohse, and Xianren Zhang. Solvent exchange leading to nanobubble nucleation: A molecular dynamics study. *Langmuir*, 33(32):8090–8096, 2017.

- [45] Xuehua Zhang, Md Hemayet Uddin, Haijun Yang, Gary Toikka, William Ducker, and Nobuo Maeda. Effects of surfactants on the formation and the stability of interfacial nanobubbles. *Langmuir*, 28(28):10471–10477, 2012.
- [46] Chenwei Li and Haijun Zhang. Surface nanobubbles and their roles in flotation of fine particles—a review. *Journal of Industrial and Engineering Chemistry*, 106:37–51, 2022.
- [47] Ye Wang, Xiang Li, Yan Zhou, Pengyu Huang, and Yuhong Xu. Preparation of nanobubbles for ultrasound imaging and intracellular drug delivery. *International journal of pharmaceutics*, 384(1-2):148–153, 2010.
- [48] Vincent Stuart James Craig. Formation of micronuclei responsible for decompression sickness. *Journal of colloid and interface science*, 183(1):260–268, 1996.
- [49] Elisavet D Michailidi, George Bomis, Athanasios Varoutoglou, George Z Kyzas, George Mitrikas, Athanasios Ch Mitropoulos, Eleni K Efthimiadou, and Evangelos P Favvas. Bulk nanobubbles: Production and investigation of their formation/stability mechanism. *Journal of colloid and interface science*, 564:371–380, 2020.
- [50] Le Sun, Fenghua Zhang, Xiaoming Guo, Zhengming Qiao, Yi Zhu, Nuo Jin, Yan Cui, and Weimin Yang. Research progress on bulk nanobubbles. *Particuology*, 60:99–106, 2022.
- [51] ISO 20480-1. Fine bubble technology—general principles for usage and measurement of fine bubbles—part 1: Terminology, 2017.
- [52] Paul S Epstein and Milton S Plesset. On the stability of gas bubbles in liquid-gas solutions. *The Journal of Chemical Physics*, 18(11):1505–1509, 1950.
- [53] Kyuichi Yasui, Toru Tuziuti, Wataru Kanematsu, and Kazumi Kato. Dynamic equilibrium model for a bulk nanobubble and a microbubble partly covered with hydrophobic material. *Langmuir*, 32(43):11101–11110, 2016.
- [54] Shuo Ke, Wei Xiao, Nannan Quan, Yaming Dong, Lijuan Zhang, and Jun Hu. Formation and stability of bulk nanobubbles in different solutions. *Langmuir*, 35(15):5250–5256, 2019.
- [55] Joost H Weijs, James RT Seddon, and Detlef Lohse. Diffusive shielding stabilizes bulk nanobubble clusters. *ChemPhysChem*, 13(8):2197–2204, 2012.
- [56] Wang Lei, Ming Zhang, Zhenxin Zhang, Ning Zhan, and Rong Fan. Effect of bulk nanobubbles on the entrainment of kaolinite particles in flotation. *Powder Technology*, 362:84–89, 2020.

- [57] Guohui Chang, Yaowen Xing, Fanfan Zhang, Zili Yang, Xiaokang Liu, and Xiahui Gui. Effect of nanobubbles on the flotation performance of oxidized coal. *ACS omega*, 5(32):20283–20290, 2020.
- [58] Ekaterina Y Lukianova-Hleb, Xiaoyang Ren, Rupa R Sawant, Xiangwei Wu, Vladimir P Torchilin, and Dmitri O Lapotko. On-demand intracellular amplification of chemoradiation with cancer-specific plasmonic nanobubbles. *Nature medicine*, 20(7):778–784, 2014.
- [59] Damien VB Batchelor, Radwa H Abou-Saleh, P Louise Coletta, James R McLaughlan, Sally A Peyman, and Stephen D Evans. Nested nanobubbles for ultrasound-triggered drug release. *ACS applied materials & interfaces*, 12(26):29085–29093, 2020.
- [60] Muhammad Saad Khan, Jangsun Hwang, Youngmin Seo, Kyusoon Shin, Kyungwoo Lee, Chanhwi Park, Yonghyun Choi, Jong Wook Hong, and Jonghoon Choi. Engineering oxygen nanobubbles for the effective reversal of hypoxia. *Artificial cells, nanomedicine, and biotechnology*, 46(sup3):318–327, 2018.
- [61] Yuncheng Wu, Tao Lyu, Bin Yue, Elisa Tonoli, Elisabetta AM Verderio, Yan Ma, and Gang Pan. Enhancement of tomato plant growth and productivity in organic farming by agri-nanotechnology using nanobubble oxygation. *Journal of agricultural and food chemistry*, 67(39):10823–10831, 2019.
- [62] Asri Ifani Rahmawati, Rizki Nugraha Saputra, Arief Hidayatullah, Agus Dwiarto, Hardi Junaedi, Dedi Cahyadi, Henry Kasman Hadi Saputra, Wendy Tri Prabowo, Ujang Komarudin Asdani Kartamiharja, Hanny Shafira, et al. Enhancement of penaeus vannamei shrimp growth using nanobubble in indoor raceway pond. *Aquaculture and Fisheries*, 6(3):277–282, 2021.
- [63] Mehmet A Oturan and Jean-Jacques Aaron. Advanced oxidation processes in water/wastewater treatment: principles and applications. a review. *Critical reviews in environmental science and technology*, 44(23):2577–2641, 2014.
- [64] HNP Dayarathne, Sanghyun Jeong, and Am Jang. Chemical-free scale inhibition method for seawater reverse osmosis membrane process: Air micro-nano bubbles. *Desalination*, 461:1–9, 2019.
- [65] Wanyi Fu and Wen Zhang. Microwave-enhanced membrane filtration for water treatment. *Journal of Membrane Science*, 568:97–104, 2018.
- [66] Bruce D Johnson and Robert C Cooke. Generation of stabilized microbubbles in seawater. *Science*, 213(4504):209–211, 1981.

- [67] Nikolai F Bunkin, Alexey V Shkirin, Nikolay V Suyazov, Vladimir A Babenko, Andrey A Sychev, Nikita V Penkov, Konstantin N Belosludtsev, and Sergey V Gudkov. Formation and dynamics of ion-stabilized gas nanobubble phase in the bulk of aqueous nacl solutions. *The Journal of Physical Chemistry B*, 120(7):1291–1303, 2016.
- [68] Tapio Vehmas and Lasse Makkonen. Metastable nanobubbles. *ACS omega*, 6(12):8021–8027, 2021.
- [69] Jong-Yun Kim, Myung-Geun Song, and Jong-Duk Kim. Zeta potential of nanobubbles generated by ultrasonication in aqueous alkyl polyglycoside solutions. *Journal of colloid and interface science*, 223(2):285–291, 2000.
- [70] Shuo Wang, Limin Zhou, and Yongxiang Gao. Can bulk nanobubbles be stabilized by electrostatic interaction? *Physical Chemistry Chemical Physics*, 23(31):16501–16505, 2021.
- [71] Valentin Leroy and Tomohisa Norisuye. Investigating the existence of bulk nanobubbles with ultrasound. *ChemPhysChem*, 17(18):2787–2790, 2016.
- [72] Yi Lu, Lei Yang, Yangmin Kuang, Yongchen Song, Jiafei Zhao, and Amadeu K Sum. Molecular simulations on the stability and dynamics of bulk nanobubbles in aqueous environments. *Physical Chemistry Chemical Physics*, 23(48):27533–27542, 2021.
- [73] H Oliveira, A Azevedo, and J Rubio. Nanobubbles generation in a high-rate hydrodynamic cavitation tube. *Minerals Engineering*, 116:32–34, 2018.
- [74] Z Pourkarimi, B Rezai, M Noaparast, AV Nguyen, and S Chehreh Chelgani. Proving the existence of nanobubbles produced by hydrodynamic cavitation and their significant effects in powder flotation. *Advanced Powder Technology*, 32(5):1810–1818, 2021.
- [75] Parag R Gogate and Aniruddha B Pandit. A review and assessment of hydrodynamic cavitation as a technology for the future. *Ultrasonics sonochemistry*, 12(1-2):21–27, 2005.
- [76] Xiangning Bu and Muidh Alheshibri. The effect of ultrasound on bulk and surface nanobubbles: A review of the current status. *Ultrasonics Sonochemistry*, 76:105629, 2021.
- [77] Neelkanth Nirmalkar, AW Pacek, and Mostafa Barigou. Bulk nanobubbles from acoustically cavitated aqueous organic solvent mixtures. *Langmuir*, 35(6):2188–2195, 2019.

- [78] Ananda J Jadhav and Mostafa Barigou. Electrochemically induced bulk nanobubbles. *Industrial & Engineering Chemistry Research*, 2021.
- [79] Alexander V Postnikov, Ilia V Uvarov, Nikita V Penkov, and Vitaly B Svetovoy. Collective behavior of bulk nanobubbles produced by alternating polarity electrolysis. *Nanoscale*, 10(1):428–435, 2018.
- [80] Y Choquette, H Menard, and L Brossard. Electrocatalytic performance of composite-coated electrodes for alkaline water electrolysis. *International journal of hydrogen energy*, 15(1):21–26, 1990.
- [81] Karol Ulatowski, Paweł Sobieszuk, Andrzej Mróz, and Tomasz Ciach. Stability of nanobubbles generated in water using porous membrane system. *Chemical Engineering and Processing-Process Intensification*, 136:62–71, 2019.
- [82] Ahmed Khaled Abdella Ahmed, Cuizhen Sun, Likun Hua, Zhibin Zhang, Yanhao Zhang, Wen Zhang, and Taha Marhaba. Generation of nanobubbles by ceramic membrane filters: The dependence of bubble size and zeta potential on surface coating, pore size and injected gas pressure. *Chemosphere*, 203: 327–335, 2018.
- [83] Masato Kukizaki and Masahiro Goto. Size control of nanobubbles generated from shirasu-porous-glass (spg) membranes. *Journal of membrane science*, 281 (1-2):386–396, 2006.
- [84] Ahmed Khaled Abdella Ahmed, Cuizhen Sun, Likun Hua, Zhibin Zhang, Yanhao Zhang, Taha Marhaba, and Wen Zhang. Colloidal properties of air, oxygen, and nitrogen nanobubbles in water: Effects of ionic strength, natural organic matters, and surfactants. *Environmental Engineering Science*, 35(7): 720–727, 2018.
- [85] JK Nielsen, C Maus, D Rzesanke, and T Leisner. Charge induced stability of water droplets in subsaturated environment. *Atmospheric Chemistry and Physics*, 11(5):2031–2037, 2011.
- [86] Takafumi Seto, Tetsuya Maekawa, Saho Osone, Kazuki Kawamura, Toshiyuki Yamauchi, and Yoshio Otani. Formation of highly charged nanodroplets by condensation–electrospray device. *Chemical engineering science*, 85:46–49, 2013.
- [87] Beng Hau Tan, Hongjie An, and Claus-Dieter Ohl. How bulk nanobubbles might survive. *Physical review letters*, 124(13):134503, 2020.
- [88] NF Bunkin, AV Kochergin, AV Lobeyev, BW Ninham, and OI Vinogradova. Existence of charged submicrobubble clusters in polar liquids as revealed by

- correlation between optical cavitation and electrical conductivity. *Colloids and Surfaces A: Physicochemical and Engineering Aspects*, 110(2):207–212, 1996.
- [89] Michelle C Barry, Kiril Hristovski, and Paul Westerhoff. Promoting hydroxyl radical production during ozonation of municipal wastewater. *Ozone: Science & Engineering*, 36(3):229–237, 2014.
- [90] Andrew Malloy and Bob Carr. Nanoparticle tracking analysis—the halo™ system. *Particle & Particle Systems Characterization*, 23(2):197–204, 2006.
- [91] Chris Gardiner, Yannick J Ferreira, Rebecca A Dragovic, Christopher WG Redman, and Ian L Sargent. Extracellular vesicle sizing and enumeration by nanoparticle tracking analysis. *Journal of extracellular vesicles*, 2(1):19671, 2013.
- [92] JitKang Lim, Swee Pin Yeap, Hui Xin Che, and Siew Chun Low. Characterization of magnetic nanoparticle by dynamic light scattering. *Nanoscale research letters*, 8:1–14, 2013.
- [93] Marcela Alexander and Douglas G Dalgleish. Dynamic light scattering techniques and their applications in food science. *Food Biophysics*, 1:2–13, 2006.
- [94] D Johnson, DL Oatley-Radcliffe, and N Hilal. Atomic force microscopy (afm). In *Membrane characterization*, pages 115–144. Elsevier, 2017.
- [95] Michael Krieg, Gotthold Fläschner, David Alsteens, Benjamin M Gaub, Wouter H Roos, Gijs JL Wuite, Hermann E Gaub, Christoph Gerber, Yves F Dufrêne, and Daniel J Müller. Atomic force microscopy-based mechanobiology. *Nature Reviews Physics*, 1(1):41–57, 2019.
- [96] Ricardo Garcia. Nanomechanical mapping of soft materials with the atomic force microscope: methods, theory and applications. *Chemical Society Reviews*, 49(16):5850–5884, 2020.
- [97] Yue Lin, Min Zhou, Xiaolin Tai, Hangfei Li, Xiao Han, and Jiaguo Yu. Analytical transmission electron microscopy for emerging advanced materials. *Matter*, 4(7):2309–2339, 2021.
- [98] Pamela E Champness. *Electron diffraction in the transmission electron microscope*. Garland Science, 2020.
- [99] Abraham J Koster and Judith Klumperman. Electron microscopy in cell biology: integrating structure and function. *Nature Reviews Molecular Cell Biology*, 4(9; SUPP):SS6–SS9, 2003.

- [100] Tao Lyu, Shubiao Wu, Robert JG Mortimer, and Gang Pan. Nanobubble technology in environmental engineering: revolutionization potential and challenges, 2019.
- [101] Vanessa N Lima, Carmen SD Rodrigues, Emanuel FS Sampaio, and Luis M Madeira. Insights into real industrial wastewater treatment by fenton’s oxidation in gas bubbling reactors. *Journal of environmental management*, 265:110501, 2020.
- [102] Nicolas Kalogerakis, Georgina Calypso Kalogerakis, and Quartus Paulus Botha. Environmental applications of nanobubble technology: Field testing at industrial scale. *The Canadian Journal of Chemical Engineering*, 99(11): 2345–2354, 2021.
- [103] Xuezhi Wang, Zhongfang Lei, Kazuya Shimizu, Zhenya Zhang, and Duu-Jong Lee. Improved methane production from corn straw using anaerobically digested sludge pre-augmented by nanobubble water. *Bioresource technology*, 311:123479, 2020.
- [104] Klaus Werner Stöckelhuber, Boryan Radoev, Andreas Wenger, and Hans Joachim Schulze. Rupture of wetting films caused by nanobubbles. *Langmuir*, 20(1):164–168, 2004.
- [105] Weiguang Zhou, Ke Liu, Long Wang, Baonan Zhou, Jiaojiao Niu, and Leming Ou. The role of bulk micro-nanobubbles in reagent desorption and potential implication in flotation separation of highly hydrophobized minerals. *Ultrasonics Sonochemistry*, 64:104996, 2020.
- [106] A Sobhy and D Tao. Nanobubble column flotation of fine coal particles and associated fundamentals. *International Journal of Mineral Processing*, 124: 109–116, 2013.
- [107] Karthik Sajith Babu, Dylan Zhe Liu, and Jayendra K Amamcharla. Application of micro-and nano-bubbles as a tool to improve the rheological and microstructural properties of formulated greek-style yogurts. *Foods*, 11(4):619, 2022.
- [108] Heni Dallagi, Piyush Kumar Jha, Christine Faille, LE-Bail Alain, Ashish Rawson, and Thierry Benezech. Removal of biocontamination in the food industry using physical methods; an overview. *Food Control*, page 109645, 2023.
- [109] Shahar Baram, Maya Weinstein, Jacob F Evans, Anna Berezkin, Yael Sade, Meni Ben-Hur, Nirit Bernstein, and Hadas Mamane. Drip irrigation with



- nanobubble oxygenated treated wastewater improves soil aeration. *Scientia Horticulturae*, 291:110550, 2022.
- [110] Zhimin Sha, Zheng Chen, Yanfang Feng, Lihong Xue, Linzhang Yang, Linkui Cao, and Qingnan Chu. Minerals loaded with oxygen nanobubbles mitigate arsenic translocation from paddy soils to rice. *Journal of Hazardous Materials*, 398:122818, 2020.
- [111] Yunpeng Zhou, Felipe Bastida, Yanzheng Liu, Yaxin Liu, Yang Xiao, Peng Song, Tianze Wang, and Yunkai Li. Selenium fertigation with nanobubbles influences soil selenium residual and plant performance by modulation of bacterial community. *Journal of Hazardous Materials*, 423:127114, 2022.
- [112] DP Galang, AK Ashari, L Sulmatiw, G Mahasri, LA Sari, et al. The oxygen content and dissolved oxygen consumption level of white shrimp *litopenaeus vannamei* in the nanobubble cultivation system. In *IOP Conference Series: Earth and Environmental Science*, volume 236, page 012014. IOP Publishing, 2019.
- [113] Chayuda Jhunkeaw, Nareerat Khongcharoen, Naruporn Rungrueng, Pattiya Sangpo, Wattana Panphut, Anat Thapinta, Saengchan Senapin, Sophie St-Hilaire, and Ha Thanh Dong. Ozone nanobubble treatment in freshwater effectively reduced pathogenic fish bacteria and is safe for nile tilapia (*oreochromis niloticus*). *Aquaculture*, 534:736286, 2021.
- [114] Muhammad Usman Farid, Paula Jungwon Choi, Jehad A Kharraz, Jia-Yong Lao, Sophie St-Hilaire, Yuefei Ruan, Paul Kwan Sing Lam, and Alicia Kyoungjin An. Hybrid nanobubble-forward osmosis system for aquaculture wastewater treatment and reuse. *Chemical Engineering Journal*, 435:135164, 2022.
- [115] Nguyen Huu Nghia, Nguyen Thi Nguyen, Phan Trong Binh, Le Thi May, Tong Tran Huy, Pham Thai Giang, Sophie St-Hilaire, Phan Thi Van, et al. Effect of nanobubbles (oxygen, ozone) on the pacific white shrimp (*penaeus vannamei*), *vibrio parahaemolyticus* and water quality under lab conditions. *Fisheries and Aquatic Sciences*, 25(8):429–440, 2022.
- [116] Le Thanh Dien, Thao Phuong Huynh Ngo, Thao V Nguyen, Pattanapon Kayansamruaj, Krishna R Salin, Chadag Vishnumurthy Mohan, Channarong Rodkhum, and Ha Thanh Dong. Non-antibiotic approaches to combat motile aeromonas infections in aquaculture: Current state of knowledge and future perspectives. *Reviews in Aquaculture*, 2023.
- [117] Wen Bin Cai, Heng Li Yang, Jian Zhang, Ji Kai Yin, Yi Lin Yang, Li Jun Yuan, Li Zhang, and Yun You Duan. The optimized fabrication of nanobubbles

- as ultrasound contrast agents for tumor imaging. *Scientific reports*, 5(1):1–11, 2015.
- [118] Ryo Suzuki, Yusuke Oda, Daiki Omata, Norihito Nishiie, Risa Koshima, Yasuyuki Shiono, Yoshikazu Sawaguchi, Johan Unga, Tomoyuki Naoi, Yoichi Negishi, et al. Tumor growth suppression by the combination of nanobubbles and ultrasound. *Cancer science*, 107(3):217–223, 2016.
- [119] Hengli Yang, Wenbin Cai, Lei Xu, Xiuhua Lv, Youbei Qiao, Pan Li, Hong Wu, Yilin Yang, Li Zhang, and Yunyou Duan. Nanobubble–affibody: Novel ultrasound contrast agents for targeted molecular ultrasound imaging of tumor. *Biomaterials*, 37:279–288, 2015.
- [120] Tinghui Yin, Ping Wang, Rongqin Zheng, Bowen Zheng, Du Cheng, Xinling Zhang, and Xintao Shuai. Nanobubbles for enhanced ultrasound imaging of tumors. *International journal of nanomedicine*, pages 895–904, 2012.
- [121] Sachin S Thakur, Ying-Shan Chen, Zachary H Houston, Nicholas Fletcher, Nigel L Barnett, Kristofer J Thurecht, Ilva D Rupenthal, and Harendra S Parekh. Ultrasound-responsive nanobubbles for enhanced intravitreal drug migration: An ex vivo evaluation. *European Journal of Pharmaceutics and Biopharmaceutics*, 136:102–107, 2019.
- [122] Dmitri Lapotko. Plasmonic nanobubbles as tunable cellular probes for cancer theranostics. *Cancers*, 3(1):802–840, 2011.
- [123] Karol Ulatowski, Kamil Wierzbowski, Julia Fiuk, and Paweł Sobieszuk. Effect of nanobubble presence on murine fibroblasts and human leukemia cell cultures. *Langmuir*, 38(28):8575–8584, 2022.
- [124] Gwiwoong Nam, Mohamed M Mohamed, and Jinho Jung. Novel treatment of microcystis aeruginosa using chitosan-modified nanobubbles. *Environmental Pollution*, 292:118458, 2022.
- [125] Hideki Tsuge. *Micro-and nanobubbles*. Pan Stanford Singapore, 2014.
- [126] Wachiranon Chuenchart, Renisha Karki, Ty Shitanaka, Kyle Rafael Marcelino, Hui Lu, and Samir Kumar Khanal. Nanobubble technology in anaerobic digestion: A review. *Bioresource Technology*, 329:124916, 2021.
- [127] Hongguang Zhang, Zhenjiang Guo, and Xianren Zhang. Surface enrichment of ions leads to the stability of bulk nanobubbles. *Soft Matter*, 16(23):5470–5477, 2020.
- [128] Damien VB Batchelor, Fern J Armistead, Nicola Ingram, Sally A Peyman, James R McLaughlan, P Louise Coletta, and Stephen D Evans. Nanobubbles

- for therapeutic delivery: production, stability and current prospects. *Current Opinion in Colloid & Interface Science*, 54:101456, 2021.
- [129] Fredrik Eklund, Muidh Alheshibri, and Jan Swenson. Differentiating bulk nanobubbles from nanodroplets and nanoparticles. *Current Opinion in Colloid & Interface Science*, 53:101427, 2021.
- [130] Juan Jin, Zhenqiang Feng, Fang Yang, and Ning Gu. Bulk nanobubbles fabricated by repeated compression of microbubbles. *Langmuir*, 35(12):4238–4245, 2019.
- [131] Gianluca Ferraro, Ananda J Jadhav, and Mostafa Barigou. A henry’s law method for generating bulk nanobubbles. *Nanoscale*, 12(29):15869–15879, 2020.
- [132] Mohammad Reza Ghaani, Peter G Kusalik, and Niall J English. Massive generation of metastable bulk nanobubbles in water by external electric fields. *Science advances*, 6(14):eaaz0094, 2020.
- [133] Nhi Vu-Y Quach, Ao Li, and James Calvin Earthman. Interaction of calcium carbonate with nanobubbles produced in an alternating magnetic field. *ACS Applied Materials & Interfaces*, 12(39):43714–43719, 2020.
- [134] Neelkanth Nirmalkar, AW Pacek, and Mostafa Barigou. Interpreting the interfacial and colloidal stability of bulk nanobubbles. *Soft matter*, 14(47):9643–9656, 2018.
- [135] NF Bunkin, AV Shkirin, PS Ignatiev, LL Chaikov, IS Burkhanov, and AV Starosvetskij. Nanobubble clusters of dissolved gas in aqueous solutions of electrolyte. i. experimental proof. *The Journal of chemical physics*, 137(5):054706, 2012.
- [136] Daniel Midtvedt, Fredrik Eklund, Erik Olsén, Benjamin Midtvedt, Jan Swenson, and Fredrik Höök. Size and refractive index determination of subwavelength particles and air bubbles by holographic nanoparticle tracking analysis. *Analytical chemistry*, 92(2):1908–1915, 2019.
- [137] Vincent S Craig. Gas solubility of electrolytes. *Encyclopedia of Applied Electrochemistry*, page 927, 2014.
- [138] Werner Lang and Rolf Zander. Salting-out of oxygen from aqueous electrolyte solutions: prediction and measurement. *Industrial & engineering chemistry fundamentals*, 25(4):775–782, 1986.
- [139] A Schumpe, I Adler, and W-D Deckwer. Solubility of oxygen in electrolyte solutions. *Biotechnology and Bioengineering*, 20(1):145–150, 1978.

- [140] Xiaotong Ma, Mingbo Li, Patricia Pfeiffer, Julian Eisener, Claus-Dieter Ohl, and Chao Sun. Ion adsorption stabilizes bulk nanobubbles. *Journal of Colloid and Interface Science*, 606:1380–1394, 2022.
- [141] Pratik A Satpute and James C Earthman. Hydroxyl ion stabilization of bulk nanobubbles resulting from microbubble shrinkage. *Journal of Colloid and Interface Science*, 584:449–455, 2021.
- [142] Mingbo Li, Xiaotong Ma, Julian Eisener, Patricia Pfeiffer, Claus-Dieter Ohl, and Chao Sun. How bulk nanobubbles are stable over a wide range of temperatures. *Journal of Colloid and Interface Science*, 596:184–198, 2021.
- [143] Euna Kim, Jong Kwon Choe, Byung Hyo Kim, Joodeok Kim, Jungwon Park, and Yongju Choi. Unraveling the mystery of ultrafine bubbles: Establishment of thermodynamic equilibrium for sub-micron bubbles and its implications. *Journal of colloid and interface science*, 570:173–181, 2020.
- [144] Xiaonan Shi, Shan Xue, Taha Marhaba, and Wen Zhang. Probing internal pressures and long-term stability of nanobubbles in water. *Langmuir*, 37(7): 2514–2522, 2021.
- [145] Shaini Aluthgun Hewage, Jitendra Kewalramani, and Jay N Meegoda. Stability of nanobubbles in different salts solutions. *Colloids and Surfaces A: Physicochemical and Engineering Aspects*, 609:125669, 2021.
- [146] Craig F Bohren and Donald R Huffman. *Absorption and scattering of light by small particles*. John Wiley & Sons, 2008.
- [147] Rosenberg P. Mieconscat. URL <https://sourceforge.net/projects/mieconscat/>.
- [148] Stefka Nikolova Kasarova, Nina Georgieva Sultanova, Christo Dimitrov Ivanov, and Ivan Dechev Nikolov. Analysis of the dispersion of optical plastic materials. *Optical Materials*, 29(11):1481–1490, 2007.
- [149] L De Rond, SFWM Libregts, LG Rikkert, CM Hau, E Van Der Pol, R Nieuwland, TG Van Leeuwen, and FAW Coumans. Refractive index to evaluate staining specificity of extracellular vesicles by flow cytometry. *Journal of Extracellular Vesicles*, 8(1):1643671, 2019.
- [150] W Chantrapornchai, FM Clydesdale, and DJ McClements. Influence of relative refractive index on optical properties of emulsions. *Food research international*, 34(9):827–835, 2001.
- [151] Stephanie H Jones, Martin D King, and Andrew D Ward. Determining the unique refractive index properties of solid polystyrene aerosol using broadband

- mie scattering from optically trapped beads. *Physical Chemistry Chemical Physics*, 15(47):20735–20741, 2013.
- [152] Shunya Tanaka, Koichi Terasaka, and Satoko Fujioka. Generation and long-term stability of ultrafine bubbles in water. *Chemie Ingenieur Technik*, 93(1-2):168–179, 2021.
- [153] Beng Hau Tan, Hongjie An, and Claus-Dieter Ohl. Stability of surface and bulk nanobubbles. *Current Opinion in Colloid & Interface Science*, 53:101428, 2021.
- [154] Limin Zhou, Shuo Wang, Lijuan Zhang, and Jun Hu. Generation and stability of bulk nanobubbles: A review and perspective. *Current Opinion in Colloid & Interface Science*, page 101439, 2021.
- [155] Zhi-Hong Zhang, Shaomeng Wang, Lina Cheng, Haile Ma, Xianli Gao, Charles S. Brennan, and Jing-Kun Yan. Micro-nano-bubble technology and its applications in food industry: A critical review. *Food Reviews International*, 0(0):1–23, 2022.
- [156] Ali A. Paknahad, Liam Kerr, Daniel A. Wong, Michael C. Kolios, and Scott S. H. Tsai. Biomedical nanobubbles and opportunities for microfluidics. *RSC Adv.*, 11:32750–32774, 2021.
- [157] Chunhong Su, XiaoJun Ren, Fang Nie, Tiangang Li, Wenhao Lv, Hui Li, and Yao Zhang. Current advances in ultrasound-combined nanobubbles for cancer-targeted therapy: a review of the current status and future perspectives. *RSC Adv.*, 11:12915–12928, 2021.
- [158] Damien V. B. Batchelor, Radwa H. Abou-Saleh, P. Louise Coletta, James. R. McLaughlan, Sally A. Peyman, and Stephen D. Evans. Nested nanobubbles for ultrasound-triggered drug release. *ACS Applied Materials & Interfaces*, 12(26):29085–29093, 2020.
- [159] Roberta Cavalli, Marco Soster, and Monica Argenziano. Nanobubbles: A promising efficient tool for therapeutic delivery. *Therapeutic delivery*, 7(2): 117–138, 2016.
- [160] Shan Xue, Yihan Zhang, Taha Marhaba, and Wen Zhang. Aeration and dissolution behavior of oxygen nanobubbles in water. *Journal of Colloid and Interface Science*, 609:584–591, 2022.
- [161] Petroula Seridou and Nicolas Kalogerakis. Disinfection applications of ozone micro- and nanobubbles. *Environ. Sci.: Nano*, 8:3493–3510, 2021.

- [162] Fanfan Zhang, Lijuan Sun, Haichang Yang, Xiahui Gui, Holger Schönherr, Michael Kappl, Yijun Cao, and Yaowen Xing. Recent advances for understanding the role of nanobubbles in particles flotation. *Advances in Colloid and Interface Science*, 291:102403, 2021.
- [163] Christopher Vega-Sánchez, Sam Peppou-Chapman, Liwen Zhu, and Chiara Neto. Nanobubbles explain the large slip observed on lubricant-infused surfaces. *Nature communications*, 13(1):1–11, 2022.
- [164] Mahsa Zahiri, Sahar Taghavi, Khalil Abnous, Seyed Mohammad Taghdisi, Mohammad Ramezani, and Mona Alibolandi. Theranostic nanobubbles towards smart nanomedicines. *Journal of Controlled Release*, 339:164–194, 2021.
- [165] Uday S Kumar, Arutselvan Natarajan, Tarik F Massoud, and Ramasamy Paulmurugan. Fn3 linked nanobubbles as a targeted contrast agent for us imaging of cancer-associated human pd-l1. *Journal of Controlled Release*, 346:317–327, 2022.
- [166] Joshua Owen, Conor McEwan, Heather Nesbitt, Phurit Bovornchutichai, Raymond Averre, Mark Borden, Anthony P McHale, John F Callan, and Eleanor Stride. Reducing tumour hypoxia via oral administration of oxygen nanobubbles. *PLoS One*, 11(12):e0168088, 2016.
- [167] Satoshi Endo, Andrea Pfennigsdorff, and Kai-Uwe Goss. Salting-out effect in aqueous nacl solutions: Trends with size and polarity of solute molecules. *Environmental Science & Technology*, 46(3):1496–1503, 2012.
- [168] Vincent S. Craig. *Gas Solubility of Electrolytes*, pages 927–931. Springer New York, New York, NY, 2014.
- [169] Thomas Delmas, Hélène Piraux, Anne-Claude Couffin, Isabelle Texier, Francoise Vinet, Philippe Poulin, Michael E Cates, and Jérôme Bibette. How to prepare and stabilize very small nanoemulsions. *Langmuir*, 27(5):1683–1692, 2011.
- [170] Rui Feng, Qixiang Wang, Yiming Qiao, Runheng Yang, Shun An, Fanchen Meng, Shengtao Yu, Wei Hao, Benwei Fu, Peng Tao, et al. Light-driven nanodroplet generation using porous membranes. *Nano Letters*, 20(11):7874–7881, 2020.
- [171] Fredrik Eklund and Jan Swenson. Stable air nanobubbles in water: the importance of organic contaminants. *Langmuir*, 34(37):11003–11009, 2018.

- [172] Toru Tuziuti, Kyuichi Yasui, and Wataru Kanematsu. Influence of increase in static pressure on bulk nanobubbles. *Ultrasonics Sonochemistry*, 38:347–350, 2017.
- [173] Toru Tuziuti, Kyuichi Yasui, and Wataru Kanematsu. Influence of addition of degassed water on bulk nanobubbles. *Ultrasonics sonochemistry*, 43:272–274, 2018.
- [174] N. Nirmalkar, A. W. Pacek, and M. Barigou. On the existence and stability of bulk nanobubbles. *Langmuir*, 34(37):10964–10973, 2018.
- [175] Kazunari Ohgaki, Nguyen Quoc Khanh, Yasuhiro Joden, Atsushi Tsuji, and Takaharu Nakagawa. Physicochemical approach to nanobubble solutions. *Chemical Engineering Science*, 65(3):1296–1300, 2010. ISSN 0009-2509.
- [176] Ananda J Jadhav and Mostafa Barigou. Bulk nanobubbles or not nanobubbles: That is the question. *Langmuir*, 36(7):1699–1708, 2020.
- [177] Annette Häbich, William Ducker, Dave E. Dunstan, and Xuehua Zhang. Do stable nanobubbles exist in mixtures of organic solvents and water? *Journal of Physical Chemistry B*, 114(20):6962 – 6967, 2010.
- [178] Kalyani Agarwal, Mohit Trivedi, and Neelkanth Nirmalkar. Does salting-out effect nucleate nanobubbles in water: Spontaneous nucleation? *Ultrasonics sonochemistry*, 82:105860, 2022.
- [179] Edwin van der Pol, Frank AW Coumans, Auguste Sturk, Rienk Nieuwland, and Ton G van Leeuwen. Refractive index determination of nanoparticles in suspension using nanoparticle tracking analysis. *Nano letters*, 14(11):6195–6201, 2014.
- [180] Dmytro Rak, Michaela Ovadová, and Marián Sedlák. (non) existence of bulk nanobubbles: the role of ultrasonic cavitation and organic solutes in water. *The journal of physical chemistry letters*, 10(15):4215–4221, 2019.
- [181] Mathew J Francis. Effect of degassing on the electrical conductivity of pure water and potassium chloride solutions. *The Journal of Physical Chemistry C*, 112(37):14563–14569, 2008.
- [182] Yujin Tong, Tobias Kampfrath, and R Kramer Campen. Experimentally probing the libration of interfacial water: the rotational potential of water is stiffer at the air/water interface than in bulk liquid. *Physical Chemistry Chemical Physics*, 18(27):18424–18430, 2016.
- [183] Hans M Cassel. Jones-ray effect, wettability, and zeta-potential. *The Journal of Chemical Physics*, 14(7):462–462, 1946.

- [184] Xibo Yan, Marco Delgado, Julien Aubry, Olivier Gribelin, Antonio Stocco, Fernande Boisson-Da Cruz, Julien Bernard, and Francois Ganachaud. Central role of bicarbonate anions in charging water/hydrophobic interfaces. *The Journal of Physical Chemistry Letters*, 9(1):96–103, 2018.
- [185] Marcel D Baer, Douglas J Tobias, and Christopher J Mundy. Investigation of interfacial and bulk dissociation of hbr, hcl, and hno<sub>3</sub> using density functional theory-based molecular dynamics simulations. *The Journal of Physical Chemistry C*, 118(50):29412–29420, 2014.
- [186] Kimiko Makino and Hiroyuki Ohshima. Electrophoretic mobility of a colloidal particle with constant surface charge density. *Langmuir*, 26(23):18016–18019, 2010.
- [187] Hiroyuki Ohshima, Thomas W Healy, and Lee R White. Approximate analytic expressions for the electrophoretic mobility of spherical colloidal particles and the conductivity of their dilute suspensions. *Journal of the Chemical Society, Faraday Transactions 2: Molecular and Chemical Physics*, 79(11):1613–1628, 1983.
- [188] Jacob N Israelachvili. *Intermolecular and surface forces*. Academic press, 2011.
- [189] Kalyani Agarwal, Mohit Trivedi, and Neelkanth Nirmalkar. Does salting-out effect nucleate nanobubbles in water: Spontaneous nucleation? *Ultrasonics Sonochemistry*, 82:105860, 2022.
- [190] Jiajia Wu, Kejia Zhang, Cheng Cen, Xiaogang Wu, Ruyin Mao, and Yingying Zheng. Role of bulk nanobubbles in removing organic pollutants in wastewater treatment. *AMB Express*, 11(1):1–13, 2021.
- [191] Gunanti Mahasri, A Saskia, PS Apandi, NN Dewi, NM Usuman, et al. Development of an aquaculture system using nanobubble technology for the optimisation of dissolved oxygen in culture media for nile tilapia (*oreochromis niloticus*). In *IOP Conference Series: Earth and Environmental Science*, volume 137, page 012046. IOP Publishing, 2018.
- [192] Agata A Exner and Michael C Kolios. Bursting microbubbles: How nanobubble contrast agents can enable the future of medical ultrasound molecular imaging and image-guided therapy. *Current Opinion in Colloid & Interface Science*, page 101463, 2021.
- [193] Celeny Vicente and Jhonny Valverde Flores. Removal of lead and zinc from mining effluents by applying air micro-nanobubbles. *Journal of Nanotechnology*, 1(2):73–78, 2017.



- [194] Ahmed Khaled Abdella Ahmed, Xiaonan Shi, Likun Hua, Leidy Manzueta, Weihua Qing, Taha Marhaba, and Wen Zhang. Influences of air, oxygen, nitrogen, and carbon dioxide nanobubbles on seed germination and plant growth. *Journal of agricultural and food chemistry*, 66(20):5117–5124, 2018.
- [195] Pramesh Dhungana and Bhesh Bhandari. Development of a continuous membrane nanobubble generation method applicable in liquid food processing. *International Journal of Food Science & Technology*, 2021.
- [196] G Passoth. Über den jones-ray-effekt und die oberflächenspannung verdünnter elektrolytösungen. *Zeitschrift für Physikalische Chemie*, 211(1):129–147, 1959.
- [197] JEB Randles and DJ Schiffrin. Surface tension of dilute acid solutions. *Transactions of the Faraday Society*, 62:2403–2408, 1966.
- [198] Direct experimental validation of the jones-ray effect. *Chemical Physics Letters*, 397(1):46–50, 2004.
- [199] Yixing Chen, Halil I Okur, Nikolaos Gomopoulos, Carlos Macias-Romero, Paul S Cremer, Poul B Petersen, Gabriele Tocci, David M Wilkins, Chungwen Liang, Michele Ceriotti, et al. Electrolytes induce long-range orientational order and free energy changes in the h-bond network of bulk water. *Science advances*, 2(4):e1501891, 2016.
- [200] Irving Langmuir. Repulsive forces between charged surfaces in water, and the cause of the jones-ray effect. *Science*, 88(2288):430–432, 1938.
- [201] Vasudevan Venkateshwaran, Srivathsan Vembanur, and Shekhar Garde. Water-mediated ion-ion interactions are enhanced at the water vapor-liquid interface. *Proceedings of the National Academy of Sciences*, 111(24):8729–8734, 2014.
- [202] Lars Onsager and Nicholas NT Samaras. The surface tension of debye-hückel electrolytes. *The Journal of Chemical Physics*, 2(8):528–536, 1934.
- [203] Yixing Chen, Halil I Okur, Nikolaos Gomopoulos, Carlos Macias-Romero, Paul S Cremer, Poul B Petersen, Gabriele Tocci, David M Wilkins, Chungwen Liang, Michele Ceriotti, et al. Electrolytes induce long-range orientational order and free energy changes in the h-bond network of bulk water. *Science advances*, 2(4):e1501891, 2016.
- [204] Yan Levin, Alexandre P Dos Santos, and Alexandre Diehl. Ions at the air-water interface: an end to a hundred-year-old mystery? *Physical review letters*, 103(25):257802, 2009.

- [205] Poul B Petersen and Richard J Saykally. On the nature of ions at the liquid water surface. *Annu. Rev. Phys. Chem.*, 57:333–364, 2006.
- [206] Laurel M Pegram and M Thomas Record Jr. Thermodynamic origin of hofmeister ion effects. *The journal of physical chemistry B*, 112(31):9428–9436, 2008.
- [207] Travis P Pollard and Thomas L Beck. Toward a quantitative theory of hofmeister phenomena: From quantum effects to thermodynamics. *Current opinion in colloid & interface science*, 23:110–118, 2016.
- [208] Pierandrea Lo Nostro and Barry W Ninham. Hofmeister phenomena: an update on ion specificity in biology. *Chemical reviews*, 112(4):2286–2322, 2012.
- [209] Dominik Horinek and Roland R Netz. Specific ion adsorption at hydrophobic solid surfaces. *Physical Review Letters*, 99(22):226104, 2007.
- [210] Grinnell Jones and Laurence D Frizzell. A theoretical and experimental analysis of the capillary rise method for measuring the surface tension of solutions of electrolytes. *The Journal of Chemical Physics*, 8(12):986–997, 1940.
- [211] Grinnell Jones and Wendell A Ray. The surface tension of solutions of electrolytes as a function of the concentration. iii. sodium chloride. *Journal of the American Chemical Society*, 63(12):3262–3263, 1941.
- [212] Grinnell Jones and Wendell A Ray. The surface tension of solutions of electrolytes as a function of the concentration. i. a differential method for measuring relative surface tension. *Journal of the American Chemical Society*, 59(1):187–198, 1937.
- [213] Grinnell Jones and Wendell A Ray. The surface tension of solutions of electrolytes as a function of the concentration ii. *Journal of the American Chemical Society*, 63(1):288–294, 1941.
- [214] Poul B Petersen, Justin C Johnson, Kelly P Knutsen, and Richard J Saykally. Direct experimental validation of the jones-ray effect. *Chemical Physics Letters*, 397(1-3):46–50, 2004.
- [215] Poul B Petersen and Richard J Saykally. Adsorption of ions to the surface of dilute electrolyte solutions: The jones- ray effect revisited. *Journal of the American Chemical Society*, 127(44):15446–15452, 2005.
- [216] Malcolm Dole and John A Swartout. A twin-ring surface tensiometer. i. the apparent surface tension of potassium chloride solutions. *Journal of the American Chemical Society*, 62(11):3039–3045, 1940.

- [217] Yixing Chen, Halil I. Okur, Nikolaos Gomopoulos, Carlos Macias-Romero, Paul S. Cremer, Poul B. Petersen, Gabriele Tocci, David M. Wilkins, Chungwen Liang, Michele Ceriotti, and Sylvie Roke. Electrolytes induce long-range orientational order and free energy changes in the h-bond network of bulk water. *Science Advances*, 2(4):e1501891, 2016.
- [218] Malcolm Dole and John A. Swartout. A twin-ring surface tensiometer. i. the apparent surface tension of potassium chloride solutions. *Journal of the American Chemical Society*, 62(11):3039–3045, 1940.
- [219] Timothy T. Duignan, Mengsu Peng, Anh V. Nguyen, X. S. Zhao, Marcel D. Baer, and Christopher J. Mundy. Detecting the undetectable: The role of trace surfactant in the jones-ray effect. *The Journal of Chemical Physics*, 149(19):194702, 2018.
- [220] Halil I. Okur, Chad I. Drexler, Eric Tyrode, Paul S. Cremer, and Sylvie Roke. The jones-ray effect is not caused by surface-active impurities. *The Journal of Physical Chemistry Letters*, 9(23):6739–6743, 2018.
- [221] Xiangning Bu, Shaoqi Zhou, Xiaoling Tian, Chao Ni, Sabereh Nazari, and Muidh Alheshibri. Effect of aging time, airflow rate, and nonionic surfactants on the surface tension of bulk nanobubbles water. *Journal of Molecular Liquids*, 359:119274, 2022.
- [222] Martin Chaplin. Theory vs experiment: what is the surface charge of water. *Water*, 1(1):1–28, 2009.
- [223] Shaoqi Zhou, Sabereh Nazari, Ahmad Hassanzadeh, Xiangning Bu, Chao Ni, Yaoli Peng, Guangyuan Xie, and Yaqun He. The effect of preparation time and aeration rate on the properties of bulk micro-nanobubble water using hydrodynamic cavitation. *Ultrasonics Sonochemistry*, 84:105965, 2022.
- [224] Kyuichi Yasui, Toru Tuziuti, Noriya Izu, and Wataru Kanematsu. Is surface tension reduced by nanobubbles (ultrafine bubbles) generated by cavitation? *Ultrasonics Sonochemistry*, 52:13–18, 2019.
- [225] Akiomi Ushida, Tomiichi Hasegawa, Naoyuki Takahashi, Toshiyuki Nakajima, Shotaro Murao, Takatsune Narumi, and Hiroshige Uchiyama. Effect of mixed nanobubble and microbubble liquids on the washing rate of cloth in an alternating flow. *Journal of Surfactants and Detergents*, 15(6):695–702, 2012.
- [226] HI Okur, Yixing Chen, DM Wilkins, and Sylvie Roke. The jones-ray effect reinterpreted: Surface tension minima of low ionic strength electrolyte solutions are caused by electric field induced water-water correlations. *Chemical Physics Letters*, 684:433–442, 2017.

- [227] Matthew Palmer and Hazel Hatley. The role of surfactants in wastewater treatment: Impact, removal and future techniques: A critical review. *Water research*, 147:60–72, 2018.
- [228] Daniel Prats, F Ruiz, Beatriz Vázquez, and Manuel Rodriguez-Pastor. Removal of anionic and nonionic surfactants in a wastewater treatment plant with anaerobic digestion. a comparative study. *Water Research*, 31(8):1925–1930, 1997.
- [229] Fathi Aloui, Sonia Kchaou, and Sami Sayadi. Physicochemical treatments of anionic surfactants wastewater: Effect on aerobic biodegradability. *Journal of hazardous materials*, 164(1):353–359, 2009.
- [230] Sheng H Lin, Horng G Leu, et al. Operating characteristics and kinetic studies of surfactant wastewater treatment by fenton oxidation. *Water Research*, 33(7):1735–1741, 1999.
- [231] Yinguang Chen, Haizhen Yang, and Guowei Gu. Effect of acid and surfactant treatment on activated sludge dewatering and settling. *Water Research*, 35(11):2615–2620, 2001.
- [232] Craig D Adams and JJ Kuzhikannil. Effects of uv/h<sub>2</sub>O<sub>2</sub> preoxidation on the aerobic biodegradability of quaternary amine surfactants. *Water Research*, 34(2):668–672, 2000.
- [233] Xiang Li, Wenjuan Zhang, Sizhou Lai, Yanfei Gan, Jun Li, Tingting Ye, Jiguang You, Siyu Wang, Hong Chen, Wenyi Deng, et al. Efficient organic pollutants removal from industrial paint wastewater plant employing fenton with integration of oxic/hydrolysis acidification/oxic. *Chemical Engineering Journal*, 332:440–448, 2018.
- [234] Xiaolei Qu, Pedro JJ Alvarez, and Qilin Li. Applications of nanotechnology in water and wastewater treatment. *Water research*, 47(12):3931–3946, 2013.
- [235] Chungsyng Lu and Huantsung Chiu. Adsorption of zinc (ii) from water with purified carbon nanotubes. *Chemical Engineering Science*, 61(4):1138–1145, 2006.
- [236] Qian Gao, Weixiao Chen, Yin Chen, David Werner, Gerard Cornelissen, Baoshan Xing, Shu Tao, and Xilong Wang. Surfactant removal with multiwalled carbon nanotubes. *Water research*, 106:531–538, 2016.
- [237] Arjunan Babuponnusami and Karuppan Muthukumar. A review on fenton and improvements to the fenton process for wastewater treatment. *Journal of Environmental Chemical Engineering*, 2(1):557–572, 2014.

- [238] M López-López, E Bernal, ML Moyá, F Sanchez, and Pilar López-Cornejo. Study of ionic surfactants interactions with carboxylated single-walled carbon nanotubes by using ion-selective electrodes. *Electrochemistry Communications*, 67:31–34, 2016.
- [239] Xiaohong Sun, Jingrao Chen, Wenhong Fan, Shu Liu, and Mohammed Kamruzzaman. Production of reactive oxygen species via nanobubble water improves radish seed water absorption and the expression of aquaporin genes. *Langmuir*, 38(38):11724–11731, 2022.
- [240] Shu Liu, Seiichi Oshita, Dang Quoc Thuyet, Masanao Saito, and Takahiko Yoshimoto. Antioxidant activity of hydrogen nanobubbles in water with different reactive oxygen species both in vivo and in vitro. *Langmuir*, 34(39):11878–11885, 2018.
- [241] Hongguang Zhang, Shan Chen, Zhenjiang Guo, and Xianren Zhang. The fate of bulk nanobubbles under gas dissolution. *Physical Chemistry Chemical Physics*, 24(16):9685–9694, 2022.
- [242] Jeong Il Lee, Jung-Geun Han, and Jong-Min Kim. Formation and stability of bulk nanobubbles generated by gas–liquid mixing. 2022.
- [243] Masayoshi Takahashi, Kaneo Chiba, and Pan Li. Formation of hydroxyl radicals by collapsing ozone microbubbles under strongly acidic conditions. *The Journal of Physical Chemistry B*, 111(39):11443–11446, 2007.
- [244] Elisavet D Michailidi, George Bomis, Athanasios Varoutoglou, Eleni K Efthimiadou, Athanasios C Mitropoulos, and Evangelos P Favvas. Fundamentals and applications of nanobubbles. In *Interface Science and Technology*, volume 30, pages 69–99. Elsevier, 2019.
- [245] SI Koshoridze and Yu K Levin. Conditions of nucleation and stability of bulk nanobubbles. *Russian Physics Journal*, 65(1):99–106, 2022.
- [246] Marcin Odziomek, Karol Ulatowski, Katarzyna Dobrowolska, Izabela Górniak, Paweł Sobieszuk, and Tomasz R Sosnowski. Aqueous dispersions of oxygen nanobubbles for potential application in inhalation therapy. *Scientific Reports*, 12(1):1–10, 2022.
- [247] Damien VB Batchelor, Fern J Armistead, Nicola Ingram, Sally A Peyman, James R McLaughlan, P Louise Coletta, and Stephen D Evans. The influence of nanobubble size and stability on ultrasound enhanced drug delivery. *Langmuir*, 2022.

- [248] Preeti Pal and Harish Anantharaman. Co<sub>2</sub> nanobubbles utility for enhanced plant growth and productivity: Recent advances in agriculture. *Journal of CO<sub>2</sub> Utilization*, 61:102008, 2022.
- [249] Wei Fan, Jingyu Cui, Qi Li, Yang Huo, Dan Xiao, Xia Yang, Hongbin Yu, Chunliang Wang, Peter Jarvis, Tao Lyu, et al. Bactericidal efficiency and photochemical mechanisms of micro/nano bubble-enhanced visible light photocatalytic water disinfection. *Water Research*, 203:117531, 2021.
- [250] Ashutosh Agarwal, Wun Jern Ng, and Yu Liu. Principle and applications of microbubble and nanobubble technology for water treatment. *Chemosphere*, 84(9):1175–1180, 2011.
- [251] A Azevedo, H Oliveira, and J Rubio. Bulk nanobubbles in the mineral and environmental areas: Updating research and applications. *Advances in Colloid and Interface Science*, 271:101992, 2019.
- [252] Dongping Tao. Recent advances in fundamentals and applications of nanobubble enhanced froth flotation: A review. *Minerals Engineering*, 183: 107554, 2022.
- [253] Zhi-Hong Zhang, Shaomeng Wang, Lina Cheng, Haile Ma, Xianli Gao, Charles S Brennan, and Jing-Kun Yan. Micro-nano-bubble technology and its applications in food industry: A critical review. *Food Reviews International*, pages 1–23, 2022.
- [254] Ananda J Jadhav and Mostafa Barigou. On the clustering of bulk nanobubbles and their colloidal stability. *Journal of Colloid and Interface Science*, 601: 816–824, 2021.
- [255] Masayoshi Takahashi, Yasuyuki Shirai, and Shigetoshi Sugawa. Free-radical generation from bulk nanobubbles in aqueous electrolyte solutions: ESR spin-trap observation of microbubble-treated water. *Langmuir*, 37(16): 5005–5011, 2021.
- [256] Masato Yamaguchi, Teng Ma, Daisuke Tadaki, Ayumi Hirano-Iwata, Yoshihiko Watanabe, Hiroyasu Kanetaka, Hiroshi Fujimori, Emiko Takemoto, and Michio Niwano. Bactericidal activity of bulk nanobubbles through active oxygen species generation. *Langmuir*, 37(32):9883–9891, 2021.
- [257] Wei Xiao, Shuo Ke, Nannan Quan, Limin Zhou, Jun Wang, Lijuan Zhang, Yaming Dong, Wenqing Qin, Guanzhou Qiu, and Jun Hu. The role of nanobubbles in the precipitation and recovery of organic-phosphine-containing beneficiation wastewater. *Langmuir*, 34(21):6217–6224, 2018.

- [258] Nurhafizah Mohd Selihin and Meng Guan Tay. A review on future wastewater treatment technologies: micro-nanobubbles, hybrid electro-fenton processes, photocatalytic fuel cells, and microbial fuel cells. *Water Science and Technology*, 85(1):319–341, 2022.
- [259] Emilie Dressaire, Rodney Bee, David C Bell, Alex Lips, and Howard A Stone. Interfacial polygonal nanopatterning of stable microbubbles. *Science*, 320(5880):1198–1201, 2008.
- [260] Nikolai F Bunkin, Alexey V Shkirin, Nikita V Penkov, Mikhail V Goltayev, Pavel S Ignatiev, Sergey V Gudkov, and Andrey Yu Izmailov. Effect of gas type and its pressure on nanobubble generation. *Frontiers in Chemistry*, 9: 630074, 2021.
- [261] Xiaotong Ma, Mingbo Li, Xuefei Xu, and Chao Sun. On the role of surface charge and surface tension tuned by surfactant in stabilizing bulk nanobubbles. *Applied Surface Science*, 608:155232, 2023.
- [262] Xiaotong Ma, Mingbo Li, Patricia Pfeiffer, Julian Eisener, Claus-Dieter Ohl, and Chao Sun. Ion adsorption stabilizes bulk nanobubbles. *Journal of Colloid and Interface Science*, 606:1380–1394, 2022. ISSN 0021-9797. doi: <https://doi.org/10.1016/j.jcis.2021.08.101>. URL <https://www.sciencedirect.com/science/article/pii/S0021979721013382>.
- [263] N. Nirmalkar, A. W. Pacek, and M. Barigou. Interpreting the interfacial and colloidal stability of bulk nanobubbles. *Soft Matter*, 14:9643–9656, 2018. doi: 10.1039/C8SM01949E. URL <http://dx.doi.org/10.1039/C8SM01949E>.
- [264] Katarzyna Hänni-Ciunel, Natascha Schelero, and Regine von Klitzing. Negative charges at the air/water interface and their consequences for aqueous wetting films containing surfactants. *Faraday Discuss.*, 141:41–53, 2009. doi: 10.1039/B809149H. URL <http://dx.doi.org/10.1039/B809149H>.
- [265] Keiji Yasuda, Hodaka Matsushima, and Yoshiyuki Asakura. Generation and reduction of bulk nanobubbles by ultrasonic irradiation. *Chemical Engineering Science*, 195:455–461, 2019.

## Chapter A

### Appendix

---

#### A.1 Zeta potential measurement by DLS

A dynamic light scattering (DLS) technique (Zetasizer Nano ZSP, Malvern Instruments) is used to measure the zeta potential of nanobubbles. The mobility of the bubbles and charge (Zeta potential) is measured by the so-called Electrophoretic Light Scattering (ELS). The motion of a charged particle in a solution gives rise to the frequency shift that depends on the velocity of the particle. The expression for frequency shift is written as follows:

$$\Delta f = 2v_p \frac{\sin(\theta/2)}{\lambda} \quad (\text{A.1})$$

and electrophoretic mobility can be defined as,

$$\mu_e = \frac{v_p}{E} \quad (\text{A.2})$$

where  $v_p$ ,  $\theta$ ,  $\lambda$ , and  $E$  are the drift velocity of the particles, scattering angle, the wavelength of the light beam, and applied electric field, respectively. Zeta potential ( $\zeta$ ), can be estimated from the following expression:

$$\zeta = \frac{3\mu_e\eta}{2\epsilon_r\epsilon_0 f(\kappa a)} \quad (\text{A.3})$$

where  $\epsilon_r$ ,  $\epsilon_0$ ,  $\eta$  and  $f(\kappa a)$  are the relative permittivity, the permittivity of vacuum, the viscosity of the dispersion medium at the experimental temperature, and Henry's function, respectively.

#### A.2 Characterization of nanobubble sample by NTA

Bubble size distribution, mean diameter, and number density of the nanobubbles were characterized using a NanoSight NS300 instrument (Malvern Instruments, UK). The working principle of NS300 is based on the tracking of individual nanobubbles by illuminating laser light in the nanobubble sample. A laser beam (65 mW,  $\lambda = 405$  nm) is passed through the sample chamber through a prism-edged glass flat (optical flat). The Brownian motion of bubbles is visualized by 20x magnification of microscope objective fitted above the liquid cell chamber. A charge-coupled device (CCD), electron multiplied CCD, or high-sensitivity CMOS camera mounted on the microscope objective has been used to record the Brownian motion of the bubbles. The 2D tracking of nanobubbles can be utilized to calculate the diffusion coefficient of Brownian motion using the following form of the well-known Einstein-Stokes



equation:

$$\frac{\overline{(x, y)}^2}{4t} = D_t = \frac{\kappa_B T}{3\pi\mu d} \quad (\text{A.4})$$

where  $\overline{(x, y)}^2$  is the mean square displacement of nanobubbles in two dimensions measured in time  $t$ . The parameters  $D_t, \mu, \kappa_B, T$ , and  $d$  are respectively, diffusion coefficient, Boltzmann constant, temperature, viscosity, and diameter of the bubble. It is to be noted that this technique can simultaneously analyze a population of nanobubbles on an individual basis; it is thus ideally suited for real-time analysis of poly-disperse systems ranging from 10 to 2000 nm in size and  $10^6$  to  $10^9$  bubbles/mL.

### A.3 Mie theory

Consider a plane of electromagnetic waves illuminating spherical nanobubbles of diameter,  $d$ , and the refractive index,  $n_p$ . The plane electromagnetic wave propagates along the  $z$ -direction and polarized in the  $x$ -direction:

$$E_i = E_{0,x} e^{i(kz - \omega t)} \hat{e}_x \quad (\text{A.5})$$

with  $E_{0,x}$  the electric field amplitude,  $\omega$  the angular frequency,  $t$  time,  $\hat{e}_x$  the orthonormal basis vector oriented along the positive  $x$  axis, and  $k = 2\pi n_m / \lambda$  the wave number, and  $\lambda$  is the wavelength of the incident light in vacuum. The scattering cross-section is defined as an imaginary area illustrating the light probability per unit incident irradiance, followed by particle scattering which is stated as

$$C_{sca} = \int_0^{2\pi} \int_0^\pi \frac{|X^2|}{k^2} \sin\theta d\theta d\phi \quad (\text{A.6})$$

with  $\theta$  the polar angle,  $\phi$  the azimuthal angle, and  $X$  the vector scattering amplitude. The Malvern Panalytical NanoSight NS300 instrument parameters including  $\theta$  and  $\phi$  are bounded by the optical numerical aperture of the microscope objective. Thereupon,  $\theta$  is integrated from  $\theta_1 = \theta_0 - \alpha_{max}$  to  $\theta_2 = \theta_0 + \alpha_{max}$ , with  $\theta_0$  the angle between the optical axis of the objective and the wave propagation direction  $\hat{e}_z$ . For NS300,  $\theta_0 = \pi/2$ . Since the objective has a circular geometry,  $\phi_1$  is expressed in terms of  $\theta$  as follows:

$$\phi_1 = \arcsin\left(\frac{\sin\left(\frac{1}{2}\pi - \alpha_{max}\right)}{\sin\left(\frac{1}{2}\pi - \theta_0 + \theta\right)}\right) \quad (\text{A.7})$$

and  $\phi_2 = \pi - \phi_1$ . In total, 50 iterations are computed to integrate  $\theta$  and  $\phi$ . For the study of spherical geometry, vector scattering amplitude,  $X$  is in correlation with amplitude scattering matrix elements  $S_j$  as follows:

$$X = (S_2 \cos\phi) \hat{e}_{||s} + (S_1 \sin\phi) \hat{e}_{\perp s} \quad (\text{A.8})$$

where the vectors,  $\hat{e}_{\parallel s}$  is parallel and  $\hat{e}_{\perp s}$  is perpendicular to the scattering plane, which is exemplified by the scattering direction  $\hat{e}_r$  and the propagation direction of the wave  $\hat{e}_z$ . The parameters  $S_1$  and  $S_2$  rely on  $d$ ,  $n_p$ ,  $n_k$ ,  $k$  and  $\theta$ , and were computed through the MieConScat. Considering  $\hat{e}_{\parallel s}$  and  $\hat{e}_{\perp s}$  is orthogonal, the term  $|X^2|$  can be expressed as follows:

$$|X|^2 = |S_2|^2 \cos^2 \phi + |S_1|^2 \sin^2 \phi \quad (\text{A.9})$$

#### A.4 Steps to estimate refractive index

1. Calculate scattering power from intensity data from NTA using the formula  
Scattering power = sum of all pixel intensities divided by shutter time.
2. Calculate experimental scattering cross-section ( $S_1$ ) experimental scattering cross-section = scaling factor = 0.0673 \*scattering power
3. Calculate theoretical scattering cross-section from Mie theory calculation.
4. Input = mean diameter, the wavelength of the laser, RI of particles
5. Output = theoretical scattering cross-section ( $S_2$ ) at expected input RI of particles value
6. If  $S_1 = S_2 \rightarrow$  expected RI is the final RI else  $S_1 \neq S_2 \rightarrow$  try to match  $S_1$  and  $S_2$  by varying the RI.

Table A.1: List of parameters for Mie Scattering

S.No.	Parameters	Values
1	Diameter of nano entities (nm)	NTA report
2	Diameter resolution	1
3	Real RI	1.633 at 405nm
4	Imaginary RI	0.002
5	Minimum scattering angle	72.5379°
6	Maximum scattering angle	107.4621°
7	Wavelength (nm)	405

## Resume

---

Department of Chemical Engineering, Indian Institute of Technology Ropar, Nangal Road, Rupnagar, Punjab  
140001, INDIA

Email: [2017chz0003@iitrpr.ac.in](mailto:2017chz0003@iitrpr.ac.in), [kalyani1903@gmail.com](mailto:kalyani1903@gmail.com); Phone. +91 97609561919

---

### Education

#### PhD

*Title:* The Unusual Properties of Nanobubbles.

*Advisor:* Dr. Neelkanth Nirmalkar, Assistant Professor, Chemical Engineering, IIT Ropar.

2018 — 2023, Indian Institute of Technology Ropar, India.

**CGPA — 8.25/10, Institute Fellowship**

#### M.Tech (Chemical Engineering)

*Thesis:* Extraction of Essential Oil from Betel leaf (*Piper Betle*) using Different Extraction Process.

*Advisor:* Dr. Sanjiv Kumar Gupta, Professor, Chemical Engineering, HBTU.

Aug 2015- Sept 2017, Harcourt Butler Technical University, Kanpur, India.

**74.8% (Hons.), TEQIP Fellowship**

#### B.Tech (Chemical Engineering)

2010-2014, AKTU, Lucknow, India

**82.36% (Hons.)**

### Research Interests

- Multiphase fluid flow
- Nano fluids
- Mass transfer process

### Teaching Experience

- **Teaching Assistant for Simulation lab (CH 230), IIT Ropar.**

Assisted in lab sessions and guided student teams through all stages of course project.

- **Teaching Assistant for Fluid Flow, Heat and Mass Transfer Laboratory (CH 231), IIT Ropar, Jan- May 2019.**

Assisted in lab sessions and helped students to comprehend the basics of fluid flow, heat and mass transfer (Bernoulli's theorem, plate and frame filter, laminar flow, estimation of diffusivity coefficient, vapor- liquid equilibrium). Graded lab assignments and exams.

- **Teaching Assistant for Microfluidics (CH 503), IIT Ropar.**

## Projects and Achievements

- Worked on “Random verification on annual inventory on hazardous waste management” for Central Pollution Control Board, India, 2021-2022.
- First position in “Technology day, 2022” held at IIT Ropar under the category of Prototype development for nanobubble generator.
- Setup of research lab “Multiphase fluid flow” at IIT Ropar in Department of Chemical Engineering.
- Recognized and felicitated for the Women in IP on “World Intellectual Property Day, 2023” at IIT Ropar.

## Industrial Training Experience

- Birla Tyres, Laksar, Uttarakhand (June – July 2013)
- Himachal Polyolefin Limited, Himachal (June - July 2012)

## Skills

- Microsoft office, Latex
- Origin, Tecplot, Image J (post-processing)

## Personal Details

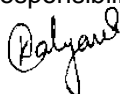
- Date and place of Birth: 19/03/92, Meerut, U.P
- Nationality: Indian
- Languages: Hindi, English

## References

- **Dr. Neelkanth Nirmalkar**  
Assistant Professor, Department of Chemical Engineering, IIT Ropar, India  
Email: [n.nirmalkar@iitrpr.ac.in](mailto:n.nirmalkar@iitrpr.ac.in)
- **Dr. Lipika Kabiraj**  
Assistant Professor, Department of Mechanical Engineering, IIT Ropar, India  
Email: [lipika.kabiraj@iitrpr.ac.in](mailto:lipika.kabiraj@iitrpr.ac.in)
- **Dr. Asad H. Sahir**  
Assistant Professor, Department of Chemical Engineering, IIT Ropar, India  
Email: [asad.sahir@iitrpr.ac.in](mailto:asad.sahir@iitrpr.ac.in)

## Declaration

I hereby declare that the information mentioned above is correct up to my knowledge, and I bear the responsibility for the correctness of the particulars as mentioned above.



Kalyani Agarwal  
IIT Ropar